

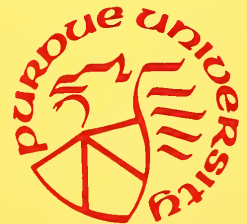


JOINT HIGHWAY RESEARCH PROJECT

JHRP-74-4

PREDICTION OF LONG TERM
DEFORMATION OF A COMPACTED
COHESIVE EMBANKMENT OVER
A SOFT FOUNDATION

Yon-Nein Chen



| | | | | | |
|---|--|--|--|---|-----------|
| 1. Report No. | | 2. Government Accession No. | | 3. Recipient's Catalog No. | |
| 4. Title and Subtitle "PREDICTION OF LONG TERM DEFORMATION OF A COMPACTED COHESIVE SOIL EMBANKMENT OVER A SOFT FOUNDATION" | | | | 5. Report Date May 1974 | |
| | | | | 6. Performing Organization Code C-36-6F | |
| 7. Author(s) Yon-Nein Chen | | | | 8. Performing Organization Report No. JHRP-74-4 | |
| 9. Performing Organization Name and Address Joint Highway Research Project Civil Engineering Building Purdue University West Lafayette, Indiana 47907 | | | | 10. Work Unit No. | |
| | | | | 11. Contract or Grant No. HPR-1(10) Part II | |
| 12. Sponsoring Agency Name and Address* Indiana State Highway Commission 100 North Senate Avenue Indianapolis, Indiana 46204 | | | | 13. Type of Report and Period Covered Final Report | |
| | | | | 14. Sponsoring Agency Code CA 375 | |
| 15. Supplementary Notes Conducted in cooperation with the U.S. Department of Transportation, Federal Highway Administration. Research Study titled "Long Term Deformation of Compacted Cohesive Soil Embankments". | | | | | |
| 16. Abstract The study is concerned with prediction of the long-term deformation of a compacted cohesive soil embankment over a soft foundation. The prediction of embankment performance was made using the finite element method of analysis incorporating a nonlinear viscoelastic model of the fill behavior and a quasi-elastic representation of the foundation. A full-scale test embankment was constructed and instrumented to permit evaluation of the predictive approach. Samples of subsurface and the embankment material were tested in the laboratory to determine numerical values of desired material parameters. The performance of the test embankment was monitored both during and after its construction. Instrumentation included spiral-foot settlement gauges, slope indicators and total pressure plates. These functioned satisfactorily, and the measurements obtained were of sufficient accuracy except for a few instruments. Hydraulic settlement gauges were also used. They have many advantageous features, but these were outweighed by the temperature sensitivity which was a significant problem during cold weather. The observed results were compared with the theoretical predictions. Variations from the predicted behavior were interpreted in light of the relation between the assumptions of the analysis and the real field conditions. Primary emphasis was on predicting those movements resulting from long-term deformations of the compacted clay fill. The calculated results are fairly close to the field measurements. | | | | | |
| 17. Key Words Embankment Stresses and Deformations; Compacted Cohesive Soil Embankments; Long Term Deformation; Embankment Performance; Nonlinear Viscoelastic Model; Finite Element Analysis; Settlement Gauges; Slope Indicators; Total* | | | | 18. Distribution Statement | |
| 19. Security Classif. (of this report) Unclassified | | 20. Security Classif. (of this page) Unclassified | | 21. No. of Pages 185 | 22. Price |

Final Report
PREDICTION OF LONG TERM DEFORMATION OF A COMPACTED
COHESIVE SOIL EMBANKMENT OVER A SOFT FOUNDATION


by
Yon-Nein Chen
Graduate Instructor in Research

Joint Highway Research Project
Project No.: C-36-6F
File No.: 6-6-6

Prepared as Part of an Investigation
Conducted by
Joint Highway Research Project
Engineering Experiment Station
Purdue University
in cooperation with the
Indiana State Highway Commission
and the
U.S. Department of Transportation
Federal Highway Administration

The contents of this report reflect the views of the author who is responsible for the facts and the accuracy of the data presented herein. The contents do not necessarily reflect the official views or policies of the Federal Highway Administration. This report does not constitute a standard, specification or regulation.

Purdue University
West Lafayette, Indiana
May 1, 1974



Digitized by the Internet Archive
in 2011 with funding from
LYRASIS members and Sloan Foundation; Indiana Department of Transportation

ACKNOWLEDGMENTS

The writer is greatly indebted to Dr. W. H. Perloff, the writer's major professor and supervisor of this investigation, for his guidance, encouragement, and constructive criticism during the course of this study and preparation of this thesis.

Special thanks is made to Professor G. A. Leonards for his generous assistance and helpful suggestions during the course of this study, and to Professor M. E. Harr, Professor V. J. Meyers, Professor E. C. Ting for their aid and encouragement in this work.

Appreciative acknowledgment is made to Mr. W. DeGroff for his invaluable assistance during the field measurements and the experimental work.

Financial assistance which made this investigation possible was by the Joint Highway Research Project, to which the writer is deeply appreciative. The assistance of the field engineers involved to this project in ISHC is appreciated.

The writer is particularly grateful to his wife for her patience and encouragement.

In addition, the writer also wishes to express sincere thanks to Dr. K. Y. Lo, Visiting Professor at Purdue University during the 1973-1974 academic year from the University of Western Ontario, London, Canada, for his many helpful suggestions.

TABLE OF CONTENTS

| | Page |
|---|------|
| LIST OF TABLES | v |
| LIST OF FIGURES | vi |
| ABSTRACT | ix |
| CHAPTER I - INTRODUCTION | 1 |
| 1-1. Introduction | 1 |
| 1-2. Review of Previous Work. | 6 |
| 1-3. Objectives | 14 |
| CHAPTER II - ANALYSIS | 16 |
| 2-1. Assumptions. | 16 |
| 2-2. Method of Analysis | 17 |
| 2-2-1. General. | 17 |
| 2-2-2. The Finite Element Method | 18 |
| 2-2-3. Stiffness of a Triangular Element | 23 |
| 2-3. Constitutive Equation for Compacted Clays. | 27 |
| 2-4. Nonlinear Viscoelastic Formulation | 31 |
| 2-5. Material Property Evaluation | 34 |
| 2-6. Determination of Strains | 40 |
| 2-7. Failure Criterion for Compacted Clays. | 43 |
| 2-8. Analysis of Saturated Foundation Clay Soils. | 47 |
| 2-9. Incorporation of Material Characterization into the Finite Element Analysis | 52 |
| CHAPTER III - LABORATORY EXPERIMENTS | 58 |
| 3-1. Material | 58 |
| 3-2. Preparation of Soil Specimen | 63 |
| 3-3. Description of Experimental Apparatus for Creep Tests. | 68 |
| 3-4. Creep Testing Procedures | 73 |
| 3-5. Strength Determination | 76 |
| 3-6. One-Dimensional Consolidation Test | 77 |
| 3-7. Test Results | 77 |
| CHAPTER IV - MEASURED PERFORMANCE OF THE TEST SECTION | 94 |
| 4-1. Field Instrumentation. | 94 |
| 4-2. Measured Stresses in the Embankment Fill | 101 |

| | Page |
|---|------|
| 4-3. Measured Vertical Movements | 117 |
| 4-4. Measured Horizontal Movements | 129 |
| CHAPTER V - PREDICTION OF THE TEST SECTION PERFORMANCE | 151 |
| 5-1. Method of Analysis and Material Parameters. | 151 |
| 5-2. Stresses in the Embankment Fill | 155 |
| 5-3. Vertical Movements. | 161 |
| 5-4. Horizontal Movements | 164 |
| 5-5. Combined Movements Within the Embankment. | 172 |
| CHAPTER VI - SUMMARY, CONCLUSIONS AND RECOMMENDATIONS | 174 |
| 6-1. Summary | 174 |
| 6-2. Conclusions | 175 |
| 6-3. Recommendations | 175 |
| LIST OF REFERENCES. | 177 |
| APPENDICES | |
| Appendix A: Finite Element Computer Program | 185 |
| Appendix B: Mesh Plotter. | 201 |
| Appendix C: Computer Program for Evaluating Lateral Movement. | 212 |
| Appendix D: Creep Test Data | 215 |
| Appendix E: Consolidation Test Data | 225 |
| Appendix F: Field Records of Exploratory Borings. | 226 |
| Appendix G: Field Measurements. | 235 |
| Appendix G-1: Total Pressure Plates | 235 |
| Appendix G-2: Spiral-Foot Settlement Gauges | 262 |
| Appendix G-3: Slope Indicators. | 274 |

LIST OF TABLES

| Table | Page |
|---|------|
| I. Classification Properties of the Soils | 62 |
| II. In-Place Density Test Data | 67 |
| III. Creep Test Results | 80 |
| IV. Consolidation Test Results | 87 |
| V. Comparison of Hydraulic Settlement Gauges and S-3 Measured Settlements Relative to Datum of 7/14/71 | 128 |
| VI. Comparison of Measured and Computed Stresses at the End of Embankment Construction. | 156 |
| Appendix Table | |
| E-1. Consolidation Test Data | 225 |

LIST OF FIGURES

| Figure | Page |
|--|------|
| 1.1 General Plan | 2 |
| 1.2 Profile of Foundation. | 4 |
| 2.1 Element Geometry | 19 |
| 2.2 Assumed Displacement Field | 25 |
| 2.3 Confined Creep Test Results. | 29 |
| 2.4 Effect of Confining Pressure on Creep Parameters for EPK . . | 30 |
| 2.5 Creep and Recovery Test. | 35 |
| 2.6 Cylindrical Test Specimen. | 41 |
| 2.7 Failure Criteria | 44 |
| 2.8 Relation Between Principal Strain Ratio and Time | 54 |
| 3.1 Grain Size Distribution for Foundation Soils | 59 |
| 3.2 Plasticity Chart for Subsoils and Embankment Soils | 60 |
| 3.3 Grain Size Distribution for Embankment Soils | 61 |
| 3.4 Liquid-Solids Twin Shell Blender | 65 |
| 3.5 Standard Compaction Curves for Embankment Soils. | 66 |
| 3.6 Creep Test in Progress | 69 |
| 3.7 Schematic Diagram of Radial Displacement Sensor and Specimen on Triaxial Cell Base. | 71 |
| 3.8 Radial Displacement Sensor and Specimen Mounted on Triaxial Compression Cell Base. | 72 |
| 3.9 Special Former on Triaxial Base. | 75 |
| 3.10 Preparation and Placement of Specimen into Consolidometer. . | 78 |

| Figure | Page |
|--|------|
| 3.11 Effect of Octahedral Normal Stress on Failure Strength. | 81 |
| 3.12 Creep Parameters and Poisson's Ratio. | 83 |
| 3.13 Nonlinear Material Properties C_1 and C_2 | 84 |
| 3.14 Time Scale Factor C_σ | 85 |
| 3.15 Nonlinear Material Properties C_1 , C_2 and C_σ | 86 |
| 3.16 Unconfined Compression Test for Foundation Soil | 88 |
| 3.17 Field Vane Shear Strength | 89 |
| 3.18 Relationship Between Effective Consolidation Pressure and Void Ratio | 90 |
| 3.19 Relationship Between Effective Vertical Pressure and Axial Strain. | 92 |
| 3.20 Effect of Effective Vertical Pressure on Constrained Modulus. | 93 |
| 4.1 Fill Elevation-Time Curve | 95 |
| 4.2 Slope Indicator 3-7 Locations and Pressure Plate Locations. | 97 |
| 4.3 Spiral-Foot Number 13 and Slope Indicators Number 1 and 2 | 98 |
| 4.4 Hydraulic Settlement Gauge Locations. | 99 |
| 4.5 Spiral-Foot Locations | 100 |
| 4.6 The State of Stress for a Group of Plates | 103 |
| 4.7 Total Stresses. | 105 |
| 4.8 Total Pressure and Fill Elevation Diagrams. | 114 |
| 4.9 Fill Elevation For N-S Direction at 70 Days (June 14, 1971) and 90 Days (July 4, 1971). | 116 |
| 4.10 Vertical Movements of Spiral-Foot | 119 |
| 4.11 Vertical Settlements of S-1, S-7 and S-13 | 124 |
| 4.12 Settlements for Hydraulic Settlement Gauges | 126 |
| 4.13 Ground Water Table Change With Time | 130 |
| 4.14 Slope Indicator Movements | 133 |

| Figure | | Page |
|----------|---|------|
| 4.15 | Horizontal Movements at Elevation 504.00 Feet for I-3 & I-5. | 149 |
| 5.1 | Idealized Scheme for Two Dimensional Finite Element Analysis | 152 |
| 5.2 | Vertical Stress at Elevation 505.50 Feet | 158 |
| 5.3 | Distribution of Horizontal Stress Due to Embankment Along Vertical Section | 159 |
| 5.4 | Vertical Settlements at S-7 and S-10 | 162 |
| 5.5 | Vertical Settlements at S-2 and S-4 | 163 |
| 5.6 | Vertical Settlements at S-3 | 165 |
| 5.7 | Vertical Settlements for Hydraulic Settlement Gauges | 166 |
| 5.8 | Lateral Movements at End of Construction | 167 |
| 5.9 | Lateral Movements at Constant Load | 170 |
| 5.10 | Comparison of Computed and Measured Movements (8/5/71-9/8/71) | 173 |
| Appendix | | |
| Figure | | |
| F.1 | Test Boring for Sta. 789+55, 250 RT | 226 |
| F.2 | Test Boring for Sta. 789+45, 125 RT | 227 |
| F.3 | Test Boring for Sta. 789+55, <u>g</u> | 228 |
| F.4 | Test Boring for Sta. 789+45, 125 LT | 229 |
| F.5 | Test Boring for Sta. 789+55, 250 LT | 230 |
| F.6 | Test Boring for Sta. 789+00, <u>g</u> | 231 |
| F.7 | Test Boring for Sta. 790+00, <u>g</u> | 232 |
| F.8 | Test Boring for Sta. 789+50, <u>g</u> | 233 |
| F.9 | Test Boring for Sta. 789+50, Out of Toe on Left | 234 |

ABSTRACT

Chen, Yon-Nein. Ph.D., Purdue University, December 1973.
Prediction of Long Term Deformation of a Compacted Cohesive Soil
Embankment Over a Soft Foundation. Major Professor: Dr. William H.
Perloff.

The study is concerned with prediction of the long-term deformation of a compacted cohesive soil embankment over a soft foundation. The prediction of embankment performance was made using the finite element method of analysis incorporating a nonlinear viscoelastic model of the fill behavior and a quasi-elastic representation of the foundation. A full-scale test embankment was constructed and instrumented to permit evaluation of the predictive approach. Samples of the subsurface and the embankment material were tested in the laboratory to determine numerical values of desired material parameters. The performance of the test embankment was monitored both during and after its construction.

Instrumentation included spiral-foot settlement gauges, slope indicators and total pressure plates. These functioned satisfactorily, and the measurements obtained were of sufficient accuracy except for a few instruments. Hydraulic settlement gauges were also used. They have many advantageous features, but these were outweighed by the temperature sensitivity which was a significant problem during cold weather.

The observed results were compared with the theoretical predictions. Variations from the predicted behavior were interpreted in light of the relation between the assumptions of the analysis and the real field conditions. Primary emphasis was on predicting those movements

resulting from long-term deformations of the compacted clay fill. The calculated results are fairly close to the field measurements.

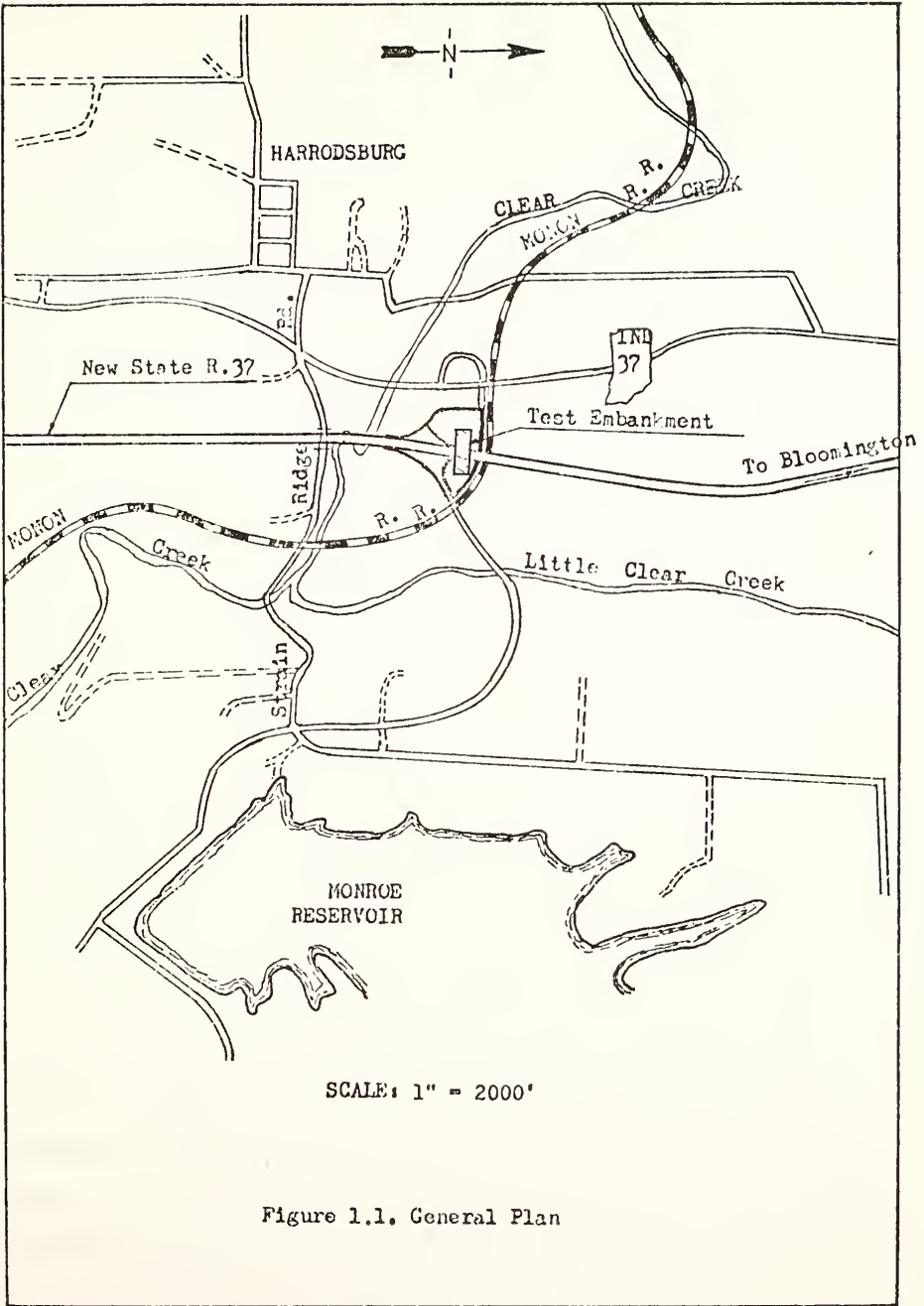
CHAPTER I
INTRODUCTION

1-1. Introduction

This study describes the prediction and measurement of long-term deformations of a compacted cohesive soil embankment overlying a soft foundation. Settlements of such an embankment result from time-dependent deformations of both the foundation soils and the compacted clay fill. Such movements may lead to safety and driver comfort problems in the case of highway embankments. The study extends previous work on development of a constitutive relation for partially saturated cohesive material to a field problem.

An instrumented test embankment was constructed at the Monroe Reservoir interchange on the reconstructed Indiana State Route 37, south of Bloomington, Indiana. The site location, shown in Figure 1.1, was selected jointly by staff of the Purdue University Joint Highway Research Project and the Indiana State Highway Commission. The test section lies between Stations 789+00 and 790+00.

The test embankment is 100 feet long and up to 40 feet in height. In cross-section the test fill is nearly symmetrical about the centerline, with a base width of 440 feet, a top width of 200 feet, and side slopes of 4 on 1. Within the test section, the embankment was composed exclusively of locally available clay. There is a 12-foot thick berm, constructed of clay soil, on both sides of the embankment, and a grade



SCALE: 1" = 2000'

Figure 1.1. General Plan

of 4% on the surface of the pavement.

The cohesive soil available near the site was moved from the borrow area and placed in the test section by scrapers. Clay fill was compacted between limits of 1 percent above, or 2 percent below optimum moisture content, by paddlefoot rollers. Construction took place in the period from April to August, 1971. Construction of the test embankment was supervised by ISHC, with the cooperation of Joint Highway Research Project (JHRP) personnel of Purdue. Field instrumentation was installed partly by contractor personnel and partly by project staff.

Adjacent to the test section, the embankment was constructed of rock fill. A two-foot thick sand blanket was placed beneath the rock fill in the north end of the test section. Vertical sand drains in the foundation had also been installed in this portion.

The general subsurface conditions at the site are typical of the lacustrine deposits in the Clear Creek Valley. As indicated in Figure 1.2, the soil profile consists of stratified deposits of soft silty clay, sandy gravel, medium silty clay, dense sandy gravel and gray shale. The ground water table was usually located about 4 feet below the original ground surface. Bedrock, as determined by a refusal to auger penetration, was typically at a depth of 25.8 feet to 30 feet. A boring program was undertaken in order to determine the stratigraphic profile, to obtain disturbed samples for classification tests, and to obtain relatively undisturbed samples of the soft clays for laboratory testing. Before embankment construction, seven soil borings were made at the test site. Additionally two borings were taken after the embankment was constructed. For each boring, standard 3-inch diameter undisturbed samples of the

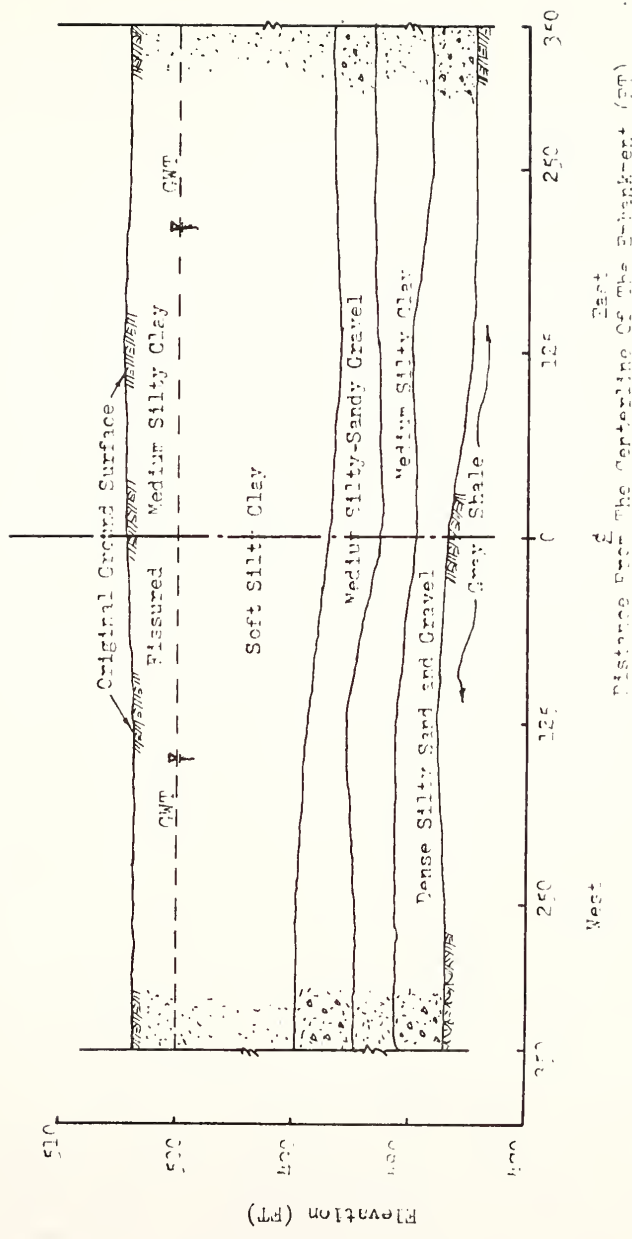


Figure 1.2. Profile of Foundation

clay were obtained. This was accomplished by pressing a thin-wall, 3-inch O.D. shelly tube a distance of 18-24 inches. Numerous field vane tests and standard penetration tests were conducted below the hollow auger at desired depths. The field records of exploratory borings are listed in Appendix F.

It is convenient to consider this investigation as consisting of 3 parts. One part included the performance of test soil borings, as described in the previous paragraph, and in carrying out the installation of the field instrumentation. There were 7 slope indicators, 12 spiral-foot settlement gauges, 4 hydraulic settlement gauges, and 27 total pressure plates installed in and under the fill to monitor stresses and movements. Details of the instrumentation and its installation are given by DeGroot (1973). Field measurements have been taken regularly since embankment construction started.

In the second part of the investigation, samples of the subsurface and embankment materials were tested in the laboratory to determine the values of the pertinent material parameters required for the predictive phase. As discussed in subsequent sections, stress-dependent nonlinear viscoelastic parameters were determined from triaxial creep test for the compacted clay fill. For the foundation clays an effective stress dependent equivalent constrained modulus was found from one-dimensional consolidation test results.

The third part of the study consisted of establishing a prediction of embankment performance based on the results of the laboratory tests, using the finite element method. The computed values for movements and stresses were then compared with those observed in the field. Primary

emphasis was on predicting those movements resulting from long-term deformations of the compacted clay fill.

1-2. Review of Previous Work

In the case of a compacted clay embankment overlying a soft clay foundation, the behavior of the embankment and foundation soils are viewed in different ways, mainly due to differences the degree of saturation and to compaction condition. The performance of the compacted embankment soils is essentially dependent on the behavior of soil skeleton; while for the saturated foundation clays the response is profoundly affected by the rate of dissipation of excess pore water pressure. Therefore, the review of previous work presented in this section, is grouped into two broad categories: partially saturated soils and fully saturated soils. An attempt has been made to discuss only those aspects of the topics which have a direct bearing on this investigation.

Before 1960, most investigators concerned with compacted clays [Hvorslev, 1936; Casagrande and Wilson, 1951; Osterberg and Perloff, 1960; Seed et al, 1960] were primarily interested in the ultimate strength of such materials, and in the effect which time-rate of loading would have on their strength.

In 1961, Folque prepared test specimens by kneading compaction, and carried out constant rate of strain tests, relaxation tests, and constant stress tests. A rheological model was used to interpret creep deformations of compacted cohesive soils subjected to low constant stress levels.

Alpan (1961) applied Terzaghi's equation for partly saturated soils, introducing a modified time factor ρT instead of T , in which ρ was a function of degree of saturation, volume change of pore air, and volume change of a sample. As Alpan did not take into account the compressibility of pore fluid and the change of soil properties during consolidation, his method is inadequate for the consolidation equation of partly saturated soils.

Lara-Thomas (1962) performed torsional shear creep tests on hollow compacted clay cylinders, and measured the shear deformation with time. He plotted the logarithm of strain rate against the logarithm of time, and found that the relation between strain rate and time was a straight line, and that the rate of strain decreased with time. He concluded that the great part of the time-dependent deformation on compacted clay soils was due to shear deformation, and not to volume flow. His experimental data can be fitted by a suitable rheological model.

Yoshimi and Osterberg (1963) studied the deformation characteristics of Vicksburg silty clay, compacted on the dry side of the optimum water content. From one-dimensional compression tests, they found that there was virtually no outflow of pore water, that the pore air formed interconnected channels, and that the compression-time relations were independent of sample thickness or drainage conditions. They concluded that the pore water movement was negligible and that the time-dependent compression was controlled by the rheological characteristics of the soil structure.

Barden (1965) developed an equation describing the consolidation behavior of compacted clays, with degree of saturation from zero to one-hundred percent. However, he could not obtain the solution to the

equation, because the equation was in actuality a system of simultaneous nonlinear partial differential equations and contained unknown functions. To simplify the equation, he classified the degree of saturation in five cases, and obtained solutions for soils compacted wet of optimum and soils compacted slightly dry of optimum. In the process of simplification, Barden assumed linear relations between pore pressure u and permeability, between u and density of pore fluid, and between u and porosity, without regard to physical properties of compacted soils. Thus, his solution did not explain the effects of such properties as initial pore pressure, degree of saturation, and coefficient of volume change.

Tsyrovich et al. (1965) obtained an equation for consolidation of compacted clays taking into account the compressibility of pore fluid and the effect of secondary compression, but without considering a change in permeability.

Perloff (1966) used a triaxial compression creep test on compacted cohesive soils, and found a relationship between the maximum shear strain and time within the creep loading as follows:

$$(\epsilon_1 - \epsilon_3)(t) = at^b \quad (1-1)$$

where

$(\epsilon_1 - \epsilon_3)(t)$ = maximum shear strain at time t ;

$\epsilon_1(t)$ = axial strain at time t ;

$\epsilon_3(t)$ = lateral strain at time t ;

t = elapsed time;

a, b = constants.

He concluded that creep strains were found to be a nonlinear function of the stress level, and that when applied stresses were expressed as a fraction of the failure stress the creep response was independent of confining pressure and initial water content, but dependent upon the type of compaction, and upon compaction energy.

Sankaran (1966) found that when compacted clay soil experienced creep deformations, there was virtually no outflow of pore water. The time-dependent deformation of compacted clays in a triaxial test was very similar to that in a one-dimensional consolidation test, when drainage was permitted. The ratio ϵ_3/ϵ_1 appeared to serve as a measure of the ratio of imposed shear stress to the shearing resistance of both compacted and saturated soils during creep, provided there were drainage. If that were the case, he suggested that ϵ_3/ϵ_1 might provide a criterion for creep failure.

Pagen and Jagannath (1967, 1968) showed that compacted soils behaved as linear viscoelastic materials within a given range of stress or strain, depending on the environmental conditions and compaction methods. The strain-time response in a creep test indicated that strain and time were related by a power function of the following form in the initial stages of the mechanical response of the soil:

$$\epsilon = ct^m \quad (1-2)$$

where c and m are constants, and

ϵ = axial strain;

t = time in minutes.

During the steady-state flow portion of creep response, the strain-time function was described as:

$$\epsilon = c' + m't \quad (1-3)$$

where c' and m' are constants.

Toriyama and Sawada (1968) studied the one-dimensional characteristics of partly saturated soils compacted wet of optimum. The pore pressure set up by the loading under undrained condition was dependent on the compressibility and the degree of saturation of the soils. A consolidation equation of partly saturated soils compacted wet of optimum was obtained by taking into account the compressibility of the pore fluid, the change in permeability with degree of saturation, and the change in compressibility m_v and permeability k with effective stress. Numerical solution of the equation led to the conclusion that the consolidation progresses more rapidly as the degree of saturation before loading, the initial pore pressure, and/or the coefficient of volume change increased.

Ramaswamy (1971) extended Perloff's work (1966) and developed a generalized model to describe time-dependent deformations of compacted clays. He found that the relation between maximum shear strain and time could be expressed in a power law form, and that the nonlinear viscoelastic constitutive equations, developed by Schapery (1966, 1969) from the principles of irreversible thermodynamics, could be applied to the prediction of the creep and recovery response of the compacted cohesive soil as observed in the laboratory. The model developed, which is described in detail in the next chapter, is consistent with the earlier

efforts discussed herein, but is a more general formulation, suitable for incorporation into a boundary value problem analysis. He also showed that clays compacted in the laboratory exhibited anisotropic mechanical behavior.

The conventional means for predicting the time-rate of settlement of structures founded on a fully saturated clay has been based on the Terzaghi's consolidation theory (1923). Terzaghi's theory was concerned only with one-dimensional consolidation. Terzaghi made a number of simplifying assumptions in order to derive and solve the equation of consolidation. Two of the important assumptions were that the relationship between void ratio and effective stress was independent of time, and that changes in void ratio were caused only by changes in effective stress. The part of the volume change accounted for by the theory of consolidation has been referred to as primary consolidation.

Biot (1941, 1956, 1957) extended Terzaghi's theory of one-dimensional consolidation to a general linear three-dimensional theory of consolidation of a porous elastic material in a saturated condition. He did not take into account the effects of included air on the process as a physical problem. Also, the secondary compression effects, or viscoelastic characteristics of the soil skeleton, were neglected.

Tan (1961) assumed a general theory of consolidation for a homogeneous, orthotropic and anisotropic (with respect to permeability) layer of clay soil. He formulated equations for the three-dimensional and the plane strain cases. Parameters in the rheological properties of the soil were evaluated by experimental procedures. Solutions to these equations had a wider range of validity than did Biot's equations.

Leonards and Altschaeffl (1964) experimented on artificially sedimented clays, and showed that the compressibility of sedimented clay was much smaller during deposition than when measured in the conventional oedometer test. They found that normally consolidated clays subjected to long periods of secondary compression would not compress along the virgin curve until a substantial pressure increment had been added. This pressure increment was found to be approximately 40 percent of the effective overburden pressure. This effect of precompression, first noticed by Leonards and Ramiah (1959), was termed the "quasi-preconsolidation pressure." The effect could be due to the fact that in a given time after being consolidated, a cohesive soil may develop an interparticle strength, capable of supporting some small increment of load with little compression. This interparticle strength may be due to physical-chemical bonds, which develop with time between clay sized particles. Leonards and Altschaeffl (1964) suggested that the relative amount of secondary compression taking place in the field (where the drainage paths are long) may be much less than that predicted from laboratory tests).

The time-dependent behavior of saturated cohesive soils has been examined using the theory of rate-processes. The rate-process theory [Glasstone, et al., 1941] postulates that an energy barrier, called activation energy, must be overcome if the particles are to move from their positions of equilibrium to new equilibrium positions from time to time. Murayama and Shibata (1961) were the first investigators to apply the rate-process theory to analyze the results of a number of triaxial creep tests, taking into account the effect of temperature.

Later on, the rate-process theory has been developed and adapted for use in the study of time-dependent deformation of soils by several investigators [Mitchell and Campanella, 1963; Christensen and Wu, 1964; Mitchell, 1964; Mitchell et al., 1968]. In general, the theory of rate-process shows that a straight-line relationship exists between logarithm of strain rate and deviator stress, and that the creep behavior of clay soil can be explained by hyperbolic sine function.

Singh and Mitchell (1968) developed a single three-parameter phenomenological equation which they used to describe the strain rate versus time and strain versus time response of clays subjected to constant stress loading. The proposed relationships were valid over a range of creep stresses varying from 30 percent to 90 percent or more of the initial soil strength. Walker (1969) suggested that the three parameters were likely to be functions of the testing conditions. He considered that any generalized relationship should include all of the variables involved in the deformation process, i.e., volumetric and shearing strains, pore water pressure, and their variations with applied stress and time.

Soydemir and Schmid (1967, 1970) proposed a linear viscoelastic model for the solution of time-dependent displacement and stress fields. The linear viscoelastic model was incorporated in terms of volumetric (a single Kelvin unit) and deviatoric (a single Maxwell unit) components. They had difficulty retransforming the Laplace domain solution into the real time domain.

Solutions to boundary value problems involving consolidation with even simple constitutive relations are difficult to obtain. For

instance, the linear three-dimensional theory of consolidation, developed by Biot (1941), has been applied to the simple diffusion solutions for one-dimensional problems, and for some two-dimensional problems with finite boundaries, provided that homogeneous elastic constants exist.

Recently the finite element method has become a powerful tool for solving problems in the whole range of solid and continuum mechanics. The method has been employed to circumvent the great mathematical complexity of consolidation theory. Christian and Boehmer (1970) used the finite element technique to give the solution of the consolidation problems of a linearly elastic material in plane strain with finite boundaries.

Thus, there presently appears to be no better method for predicting the long-term deformation of a compacted cohesive soil embankment over a soft foundation. This applies especially in the area of prediction of time-dependent deformation of the compacted cohesive soils using a nonlinear constitutive relation.

1-3. Objectives

The overall objectives of this investigation are to develop a model for predicting stresses and deformations of compacted cohesive soil embankments, and to test the predictive capability of the model in the field. In order to accomplish the broad objectives of this investigation, the following steps are indicated:

- (1) Combine the previously developed nonlinear viscoelastic representation for compacted clay with an equivalent elastic model for the foundation materials, and incorporate them in a finite element analysis of the field problem to be analyzed.

(2) Using laboratory tests, determine numerical values for the appropriate material parameters.

(3) Carry out the analysis of the field problem using the parameters determined in the laboratory.

(4) Construct and monitor the performance of a full-scale field embankment.

(5) Compare the analytical predictions with the field observation.

CHAPTER II

ANALYSIS

2-1. Assumptions

It is necessary to make certain simplifying assumptions to evolve a mathematical treatment of the problem. The assumptions made for this investigation are as follows:

- (1) The embankment soil exhibits nonlinear viscoelastic behavior. Its material properties are dependent upon the stress state and time. Strains are "small," and no time-independent plastic strains are considered.
- (2) The failure criterion for compacted cohesive soil is equivalent to an extended von Mises yield criterion, in which the failure stress depends on the octahedral normal stress.
- (3) The foundation is a layered soil system of limited depth, bounded at the top by a limited surface of compacted cohesive soil. The soil for each layer in the foundation is assumed to be an elastic, isotropic, and homogeneous material, in which the equivalent elastic constants may be functions of both stress and time.
- (4) Consolidation of the saturated foundation clays is assumed to be one-dimensional.
- (5) The whole system is assumed to deform continuously at constant external loads or its own body forces; unloading is not included.

2-2. Method of Analysis

2-2-1. General

The approach used in this investigation is the finite element method, which is a general and powerful technique for solving boundary value problems in the field of continuum mechanics.

Many investigators have contributed to the development of matrix methods for structural analysis. The matrix method was originally applied to the finite element method in the aircraft industry [Turner, et al., 1956; Argyris, 1957]. Zienkiewicz and Holister (1965), Zienkiewicz and Cheung (1967), Przemieniecki (1968), Zienkiewicz (1971), and Desai and Abel (1972) have described the details in the finite element method in book form. Theoretical justification for the finite element method has been given by Melosh (1963), Jones (1964), and Zienkiewicz and Cheung (1965), using energy principles, and by Oliveira (1968), using functional analysis. These methods are based on a variational principle. The books by Mikhlin (1965) and Vainberg (1964) contributed to this approach.

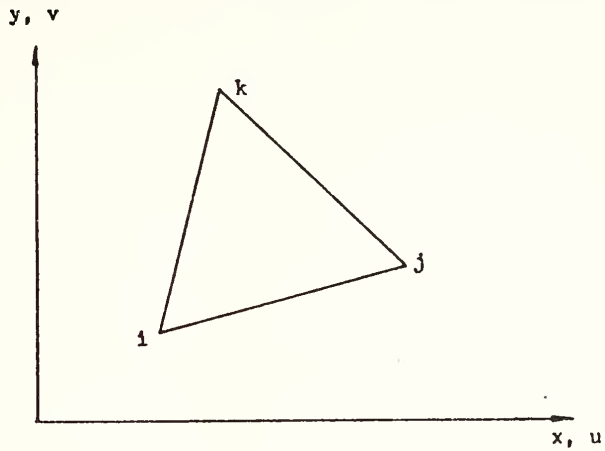
The application of the finite element method to soil engineering problems has been reported by many investigators (Clough and Woodward, 1967; Girijavallabhan and Reese, 1968; Duncan, et al., 1968; Westmann, 1968; Perloff and Pombo, 1969; Christian and Boehmer, 1970; Chen, 1970; to mention just a few). Specially, the finite element approach used previously for analyses of embankments has been described by Brown and King (1966), Finn (1967), Clough and Woodward (1967), and Duncan and Dunlop (1969).

2-2-2. The Finite Element Method

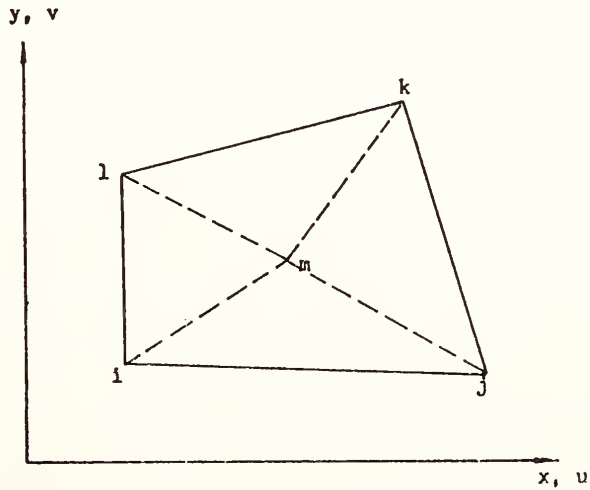
The finite element method described in this study may be used to solve plane strain, plane stress, and axisymmetric problems. A more general formulation is, of course, possible. The plane can be divided into a finite number of small polyhedral elements interconnected at the nodal points. In the plane problem, two element shapes, triangles and quadrilaterals (Fig. 2.1), are considered most commonly. Forces acting on the elements are equivalently replaced by the concentrated forces acting at the nodes of the assemblage of elements. In doing this, the problem becomes similar to the problem of solving for the forces at the points at which bars are joined by pins in structural problems. In general, the equivalent forces which are at the nodal points of one element can be recognized as follows:

- (1) Initial forces: These may be due to either residual stresses or temperature changes.
- (2) Body forces: These forces may result from gravity, or from other accelerations to which the element is subjected (D'Alembert forces).
- (3) External surface tractions: Applied loads acting on the boundary of the certain elements may be treated most conveniently by resolving them into two components: the horizontal component per unit of vertical surface area, and the vertical component per unit of horizontal surface area.
- (4) Concentrated forces: This may be due to any other external forces, directly applied at the nodes on the boundary.

An isotropic elastic continuum under the action of certain forces, p , characterized by some function $f(p)$, acquires a corresponding



(a). Triangular Element



(b). Quadrilateral Element

Figure 2.1. Element Geometry

displacement function $u(p)$. These two functions are connected by the following relation:

$$[K] \{u\} = \{f\} \quad (2-1)$$

where

K = a linear operator, and is symmetric and positive definite;

u = the sought function;

f = a known function with a finite dimension.

Equation (2-1) is used to determine the function u which the operator K transforms into f .

In a physical sense, K is the stiffness matrix of the element, u represents the displacements of the nodes of the element, which in the stiffness method satisfy the strain compatibility conditions within and along the boundary of the adjacent elements, and f represents the forces at the nodal points of the element. In matrix form, K must be a square matrix, u and f are the column matrices.

The matrix K in equation (2-1) is usually referred to as the transformation matrix of the system. The transformation given by equation (2-1) is a linear, single-valued transformation, since only one f corresponds to a given u , and only one u to a given f . This matrix depends on the material properties and nodal point geometries of the system. The following is a brief description of the development of the stiffness matrix.

There are three kinds of parameters involved in elastic theories: displacements, strains, and stresses. Their matrix forms will be denoted by $\{u(t)\}$, $\{\epsilon(t)\}$, and $\{\sigma(t)\}$, respectively. Their magnitudes are related

by three kinds of field equations, which can be expressed as follows:

- (1) For a designated displacement function, strain-displacement relationships in rectangular cartesian coordinates are:

$$[B] \{u(t)\} = \{\varepsilon(t)\} \quad (2-2)$$

- (2) Equilibrium equations for quasi-static problems are:

$$[E] \{\sigma(t)\} = \{X(t)\} \quad (2-3)$$

- (3) Stress-strain relationships for isotropic, linear elastic material are:

$$\{\sigma(t)\} = [C] \{\varepsilon(t)\} \quad (2-4a)$$

or

$$\{\sigma(t)\} = [C] [B] \{u(t)\} \quad (2-4b)$$

Where B and E are differential operators, X is the body forces per unit volume, and C is a symmetric positive definite matrix.

Equations (2-2), (2-3) and (2-4) are valid in the material of the system. The analysis of the isotropic, quasi-static, viscoelastic boundary value problem reduces to finding the solution of the system of field equations (2-2), (2-3), and (2-4) which satisfies certain boundary conditions and initial conditions. The initial conditions appropriate to an initial stress free state of rest are given by :

$$u_i(t) = \varepsilon_{ij}(t) = \sigma_{ij}(t) = 0, \quad -\infty < t < 0 \quad (2-5)$$

The simplest and most important types of boundary conditions can be directly expressed in terms of displacements or stresses (or forces)

applied on the boundary. Let S_1 and S_2 denote the parts of the boundary over which the components of the stresses (or forces) or displacements are respectively prescribed. Then the boundary conditions are described as:

$$\sigma_{ij}(t) n_j = T_i(t) \quad \text{on } S_1 \quad (2-6)$$

and

$$u_i(t) = u_i^0(t) \quad \text{on } S_2 \quad (2-7)$$

where n_j represents the components of the unit outward normal to the boundary of the body. S_1 and S_2 are required to remain constant with time. This means that the kind of the boundary condition at a point, whether it be prescribed traction (or force) or displacement, is not allowed to change.

The application of the method of virtual displacements [Wang, 1953] gives the relations between the nodal point forces and nodal point displacements. Internal strain energy, stored due to the virtual strains, is shown in matrix form as:

$$\delta U = \int_V \{\delta \epsilon(t)\}^T \{\sigma(t)\} dV \quad (2-8)$$

where δ expresses the variations of strains and displacements about the state of equilibrium of the element and corresponding variations of internal strain energy due to a set of virtual nodal point displacements, T denotes the transpose of the matrix.

External work done through the virtual nodal point displacements is :

$$\delta W = \{\delta u(t)\}^T \{f(t)\} \quad (2-9)$$

where $f(t)$ is externally applied loads and body forces.

For stable equilibrium,

$$\delta U = \delta W \quad (2-10)$$

This equation leads to

$$f(t) = \int_V [B]^T [C] [B] \{u(t)\} dV \quad (2-11)$$

The stiffness matrix of the element can be found as

$$K = \int_V [B]^T [C] [B] dV \quad (2-12)$$

Once K is generated for each element, the over-all stiffness matrix for a continuum can be obtained by suitable summation of the elemental stiffness matrices.

2-2-3. Stiffness of a Triangular Element

The stiffness analysis of any arbitrary finite element can be carried out by first assuming displacement functions. Before the assumed displacement functions have to be chosen, the choice of the element shape has to be made. In this study, both triangular and quadrilateral elements are used. The following development of the element stiffness matrix is restricted to triangular elements, since a quadrilateral element can be divided into four triangular subelements, with an additional point in the center of the quadrilateral. Each triangle can be analyzed separately, and the stiffness matrices added algebraically to give the stiffness matrix of the quadrilateral. The equations for the displacements of the central point are eliminated and transformed

into the four corner points. The procedure was first developed by Wilson (1965).

In general, straight lines connecting nodal points in the undeformed element become curved lines in the deformed element. However, if the nodal points are selected sufficiently close to one another, nodal lines in the deformed element are closely approximated by a system of straight line segments. This is equivalent to assuming that the displacement fields corresponding to a given element are linear functions of the local coordinates of that element. This assumption is used by many investigators [Clough, 1960; Oden, 1967]. This linear displacement field (Figure 2.2) is defined in terms of displacement components $u(x,y)$ and $v(x,y)$ by equations of the following form:

$$\begin{aligned} u &= \beta_1 x + \beta_2 y + \beta_3 \\ v &= \beta_4 x + \beta_5 y + \beta_6 \end{aligned} \tag{2-13}$$

In the element shown in Figure 2.2, where the nodal points are i , j , k ,

$$\{u\} = [T_{\delta\beta}] \{\beta\} \tag{2-14}$$

The constants β_i can be written in terms of the corner displacements and the geometry of the element:

$$\{\beta\} = [T_{\beta\delta}] \{u\} \tag{2-15}$$

Assuming small deformations, the strains within the element are, from equation (2-13):

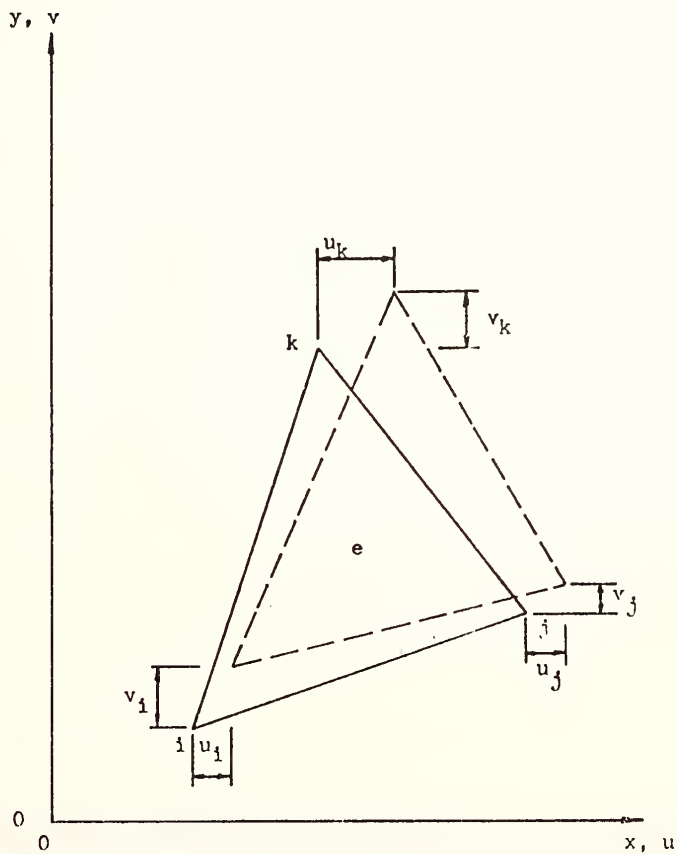


Figure 2.2. Assumed Displacement Field

$$\epsilon_x = \frac{\partial u}{\partial x} = \beta_1$$

$$\epsilon_y = \frac{\partial v}{\partial y} = \beta_5 \quad (2-16)$$

$$\gamma_{xy} = \frac{\partial u}{\partial y} + \frac{\partial v}{\partial x} = \beta_2 + \beta_4$$

in which ϵ_x and ϵ_y are the normal strains in the x- and y-directions, respectively; γ_{xy} is the shearing strain in the xy plane. Equation (2-16) can be rewritten as:

$$\begin{Bmatrix} \epsilon_x \\ \epsilon_y \\ \gamma_{xy} \end{Bmatrix} = \begin{bmatrix} 1 & 0 & 0 & 0 & 0 & 0 \\ 0 & 0 & 0 & 0 & 1 & 0 \\ 0 & 1 & 0 & 1 & 0 & 0 \end{bmatrix} \begin{Bmatrix} \beta_1 \\ \beta_2 \\ \beta_3 \\ \beta_4 \\ \beta_5 \\ \beta_6 \end{Bmatrix} \quad (2-17a)$$

or, symbolically

$$\{\epsilon\} = [M] \{\beta\} \quad (2-17b)$$

The strains are expressed in terms of the nodal point displacement by substituting equation (2-15) into equation (2-17a):

$$\begin{aligned} \{\epsilon\} &= [M] [T_{\beta\delta}] \{u\} \\ &= [B] \{u\} \end{aligned} \quad (2-18)$$

For a plane strain problem, the constitutive relation for a linear elastic material has the form:

$$\begin{Bmatrix} \sigma_x \\ \sigma_y \\ \tau_{xy} \end{Bmatrix} = \frac{E}{(1+\nu)(1-2\nu)} \begin{bmatrix} 1-\nu & \nu & 0 \\ \nu & 1-\nu & 0 \\ 0 & 0 & \frac{1-2\nu}{2} \end{bmatrix} \begin{Bmatrix} \epsilon_x \\ \epsilon_y \\ \gamma_{xy} \end{Bmatrix} \quad (2-19a)$$

or, symbolically

$$\{\sigma\} = [C] \{\epsilon\} \quad (2-19b)$$

in which E and ν are the Young's modulus, and Poisson's ratio, respectively.

Once we have the values of $[B]$ and $[C]$, the stiffness matrix for the element can be expressed from equation (2-12) as:

$$[K] = [B]^T [D] [B] \quad (2-20)$$

where

$$[D] = \int_V [C] dV \quad (2-21)$$

By matrix superposition of the individual element stiffness and force matrices, a set of simultaneous linear equations are obtained for the total system. The solution of this set of algebraic equations represents the solution of the problem.

2-3. Constitutive Equation for Compacted Clays

The development in numerical methods for predicting movements and stresses in soils has been accompanied by corresponding development of rheological models of soil behavior. The parameters involved in the mathematical expressions can then be obtained from laboratory test

results. The model used herein for the compacted clay fill is that developed by Ramaswamy (1971). The creep law for the relation between maximum shear strain and time for a given applied deviator stress can be expressed as a power function of time [Perloff, 1966]:

$$(\epsilon_1 - \epsilon_3) (t) = at^b \quad (2-22)$$

where

$(\epsilon_1 - \epsilon_3) (t)$ = maximum shear strain at time t ;

$\epsilon_1 (t)$ = axial strain at time t ;

$\epsilon_3 (t)$ = lateral strain at time t ;

t = time elapsed after additional axial load applied;

a, b = constants.

Equation (2-22), implies a linear relation between creep strain and time on logarithmic scales. Typical creep curves, plotted to the logarithmic scales, are shown in Figure 2.3. Equation (2-22) implies that the initial value of creep compliance is equal to zero.

From laboratory creep tests on compacted clay, Perloff (1966) concluded that:

(1) The creep parameter a increases nonlinearly as stress increases, and b is independent of the stress level within the range of additional axial load applied, as shown in Figure 2.4.

(2) The power law is independent of drainage conditions, and whether the tested sample is confined or unconfined.

(3) When the applied stresses are expressed as a ratio of soil strength, the creep response is independent of confining pressure and initial water content, and dependent upon compaction type and energy.

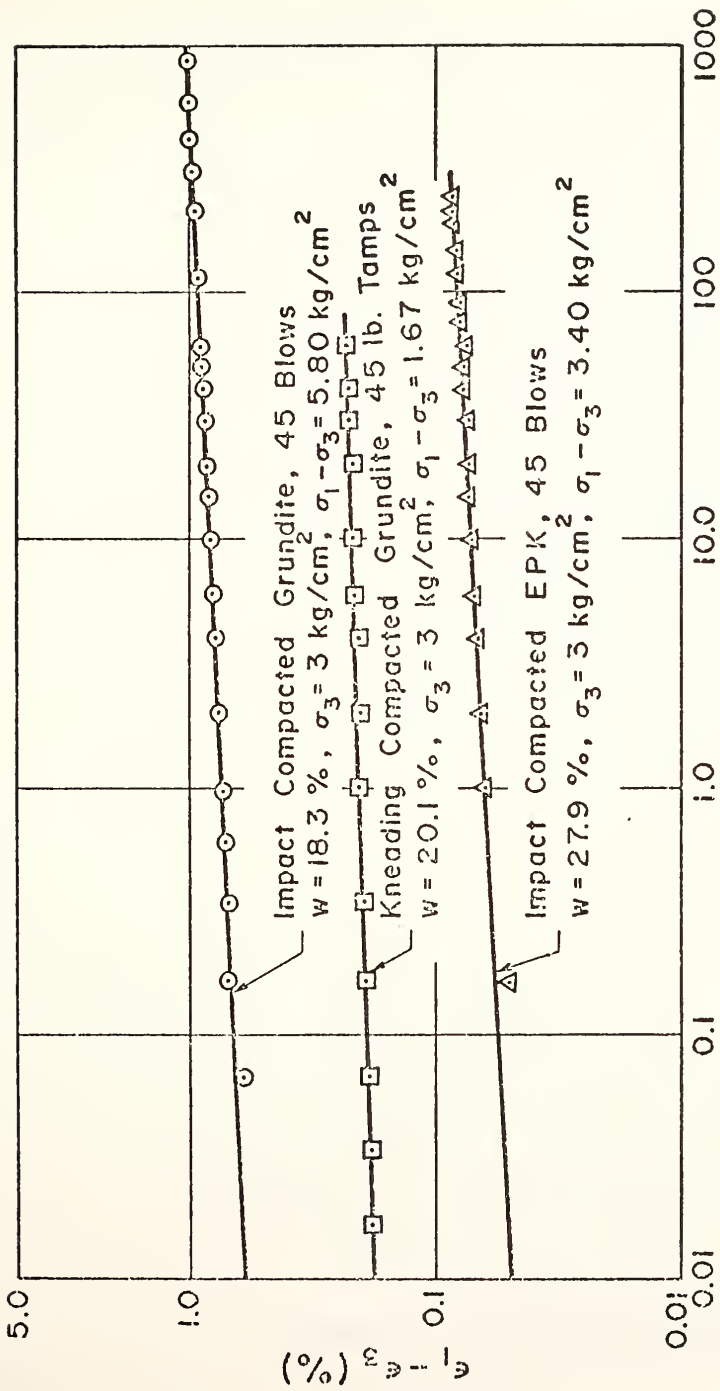


Figure 2.3. Confined Creep Test Results (Perloff, 1966)

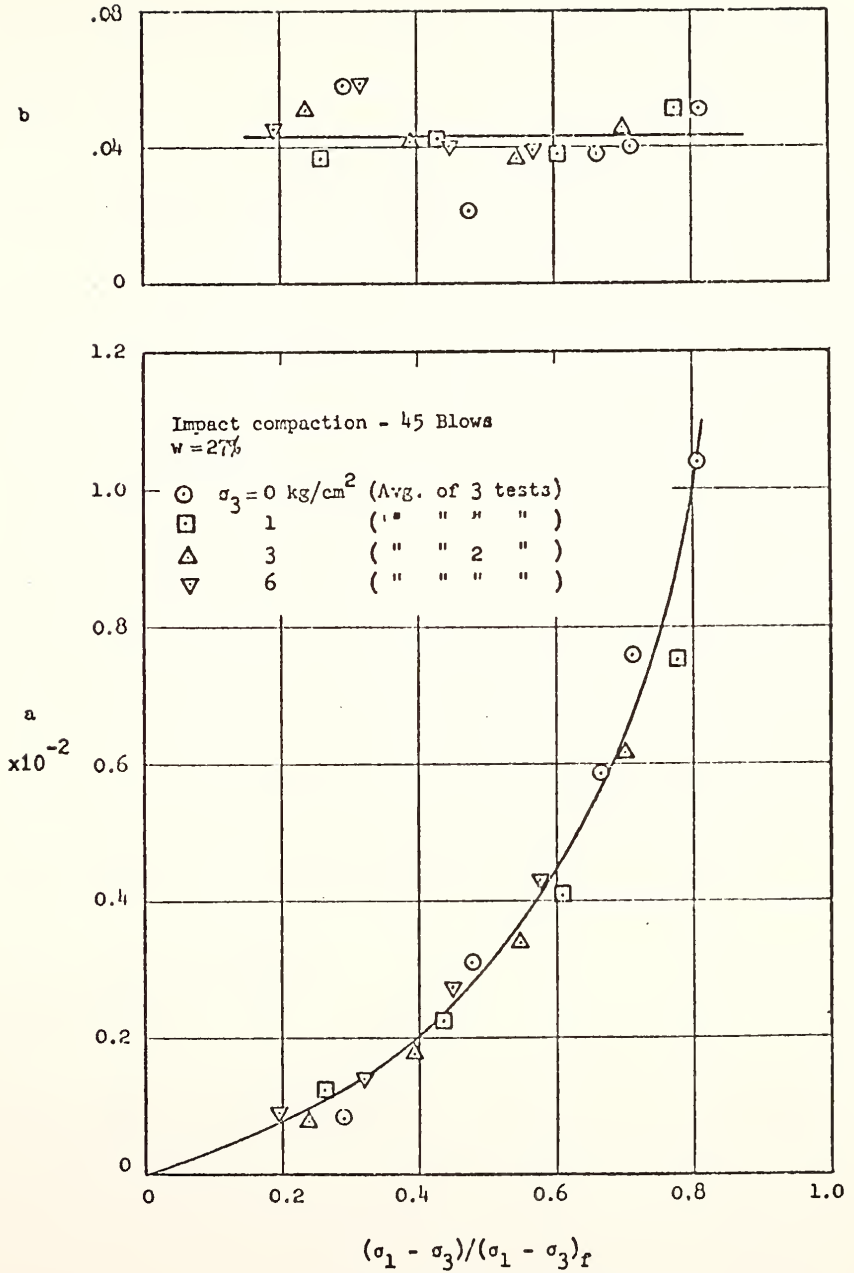


Figure 2.4. Effect of Confining Pressure on Creep Parameters for EPK (Perloff, 1966)

(4) The creep strain is independent of the number of repetitions after the initial loading. Therefore, the soil does not remember previous stress applications after the first application of a load.

2-4. Nonlinear Viscoelastic Formulation

The creep parameters a and b for each deviator stress input can be obtained from creep test data by solving equation (2-22). Then the relation between creep strain and time is easily established. For the finite element analysis, stress-strain relations at a given time, t , have to be chosen in order to define the stresses in terms of strains.

The nonlinear constitutive equation used here has been derived from thermodynamic theory [Schapery, 1966, 1969], and is similar to the Boltzmann superposition integral of linear viscoelastic theory. This is developed below, for simplicity of notation, in terms of uniaxial stress and strain.

If $\sigma(t)$ is the uniaxial stress, and $\epsilon(t)$ is the corresponding strain, then for a linear isotropic viscoelastic material the stress-strain-time relation can be written in terms of integral operators:

$$\epsilon(t) = \int_0^t J(t-\tau) \frac{d\sigma(\tau)}{d\tau} d\tau \quad (2-23a)$$

or, equivalently

$$\epsilon(t) = J(0)\sigma + \int_0^t \Delta J(t-\tau) \frac{d\sigma(\tau)}{d\tau} d\tau \quad (2-23b)$$

where

$J(t)$ = the creep compliance

$J(0)$ = the initial value of creep compliance

$\Delta J(t) = J(t) - J(0)$

= the transient component of creep compliance.

When a unit step stress input $\sigma = \sigma_0 H(\tau)$ is substituted into equation (2-23b), where σ_0 is constant, and

$$H(\tau) = \begin{cases} 0 & , \tau < 0 \\ 1 & , \tau > 0 \end{cases} \quad (2-24)$$

then

$$\varepsilon(t) = J(0)\sigma + \Delta J(t)\sigma \quad (2-25)$$

Equation (2-23) has a step stress discontinuity that occurs at $t=0$ in a creep test. Equation (2-23) is one form of the Boltzmann superposition integral, and is the general linear viscoelastic constitutive relation for creep behavior of materials.

Schapery (1966, 1969) used the principles of irreversible thermodynamics to show that the form of equation (2-23) could be used for certain nonlinear response:

$$\varepsilon(t) = C_0' J(0)\sigma + C_1 \int_0^t \Delta J(\psi-\psi') \frac{dC_2\sigma}{d\tau} d\tau \quad (2-26)$$

where $J(0)$ and $\Delta J(\psi)$ still represent the linear creep compliance defined previously, and ψ represents the so-called reduced-time defined by:

$$\psi = \int_0^t \frac{dt'}{C_\sigma} \quad (C_\sigma > 0) \quad (2-27a)$$

and

$$\psi' = \psi(\tau) = \int_0^\tau \frac{dt'}{C_\sigma} \quad (C_\sigma > 0) \quad (2-27b)$$

C'_0 , C_1 , C_2 and C_σ are the material properties which depend the stress-strength ratio only. By comparing equations (2-23b) and (2-26), it is evident that the stress is sufficiently small, the material is linearly viscoelastic, and $C'_0 = C_1 = C_2 = C_\sigma = 1$.

Similarly, the analogous relation between maximum shear strain and maximum shear stress is

$$(\epsilon_1 - \epsilon_3)(t) = C'_0 J(0)(\sigma_1 - \sigma_3) + C_1 \int_0^t \Delta J(\psi - \psi') \frac{dC_2(\sigma_1 - \sigma_3)}{d\tau} d\tau \quad (2-28)$$

For a constant maximum shear stress, equation (2-28) reduces to:

$$(\epsilon_1 - \epsilon_3)(t) = [C'_0 J(0) + C_1 C_2 \Delta J(\psi)] (\sigma_1 - \sigma_3) \quad (2-29)$$

Since $J(0)$ is equal to zero for the compacted clay soils mentioned previously, equation (2-29) becomes

$$(\epsilon_1 - \epsilon_3)(t) = C_1 C_2 \Delta J(\psi) (\sigma_1 - \sigma_3) \quad (2-30)$$

The nonlinear deviatoric creep compliance, J_n , is defined in the same way as the linear viscoelastic compliance; i.e., is the ratio of strain to stress in a creep test:

$$J_n = \frac{(\epsilon_1 - \epsilon_3)(t)}{(\sigma_1 - \sigma_3)} = C_1 C_2 \Delta J(\psi) \quad (2-31)$$

2-5. Material Property Evaluation

The form of the nonlinear deviatoric creep compliance, J_n , shown in equation (2-31), is such that a simple graphical method can be employed to evaluate some properties from laboratory tests, and partially verify the theory. This may be seen by rewriting J_n as:

$$\log J_n = \log C_1 C_2 + \log \Delta J \left(\frac{t}{C_\sigma} \right) \quad (2-32)$$

If J_n is plotted against t on full logarithmic paper, curves at different stress levels can be superposed by translating them along the two axes. If the curves are shifted to the one for zero stress, the amount of horizontal (t) shift and vertical (J_n) shift equals, respectively, $\log C_1 C_2$ and $\log C_\sigma$. It is seen that creep data are not sufficient for evaluating C_1 and C_2 respectively. However, strain data measured during a recovery period, t_1 at which $(\sigma_1 - \sigma_3)$ is removed, will provide enough additional information to conveniently evaluate all material properties.

When the step-stress input, $(\sigma_1 - \sigma_3)(H(t) - H(t - t_1))$, shown in Figure 2.5, is applied, equation (2-30) yields the creep strain:

$$(\epsilon_1 - \epsilon_3)(t) = C_1 C_2 \Delta J \left(\frac{t}{C_\sigma} \right) (\sigma_1 - \sigma_3) \quad 0 < t < t_1 \quad (2-33)$$

and the recovery strain:

$$(\epsilon_1 - \epsilon_3)_r(t) = (\epsilon_1 - \epsilon_3)(t) - (\epsilon_1 - \epsilon_3)(t - t_1) \quad t > t_1 \quad (2-34a)$$

or, equivalently,

$$(\epsilon_1 - \epsilon_3)_r(t) = C_2 [\Delta J(\psi) - \Delta J(\psi - \psi')] (\sigma_1 - \sigma_3), t > t_1 \quad (2-34b)$$

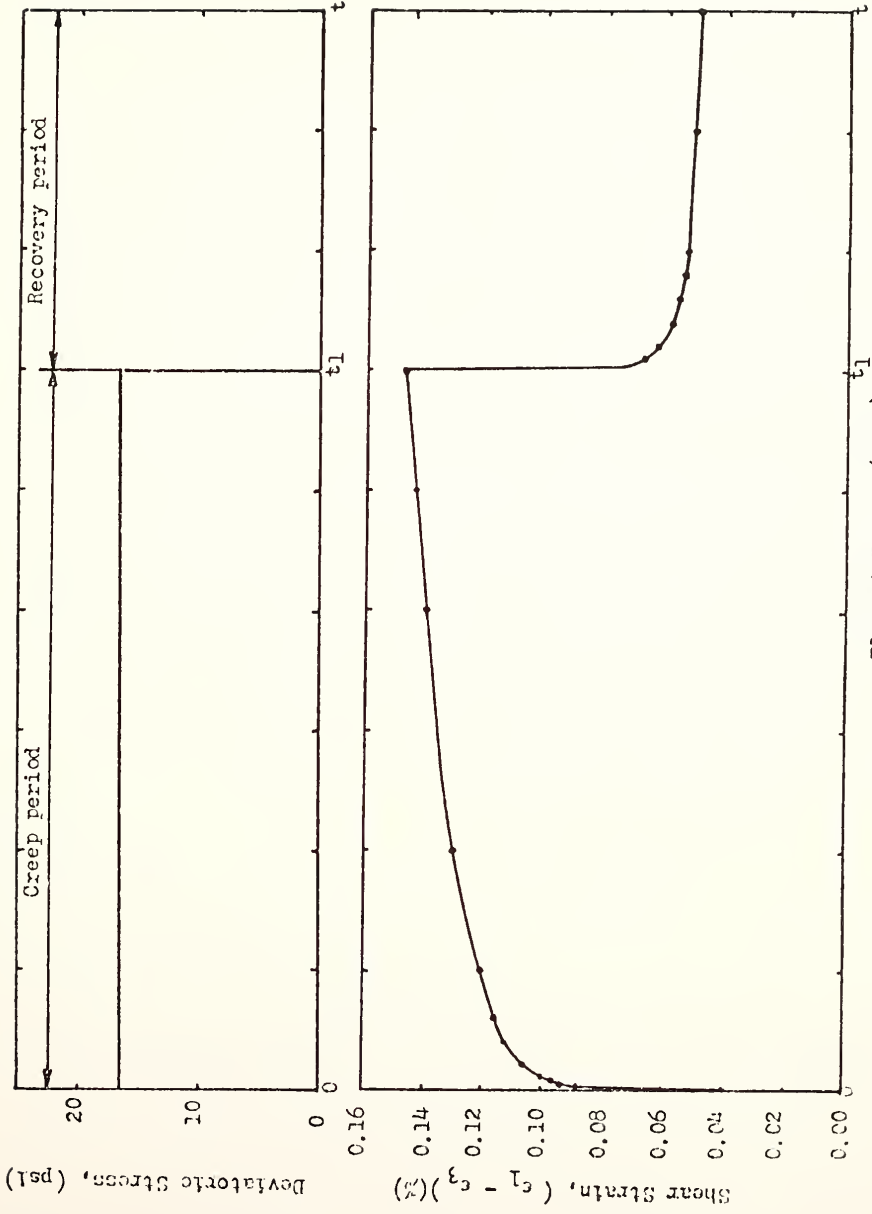


Figure 2.5. Creep and Recovery Test

where

$$\psi_1 = \frac{t_1}{C_\sigma} \quad (2-35a)$$

$$\psi = \frac{t_1}{C_\sigma} + (t - t_1) \quad (2-35b)$$

The creep strain of compacted soils obeys a power law in time (Equation 2-22). In terms of the transient component of the linear viscoelastic creep compliance this is

$$\Delta J(\psi) = C \psi^b \quad (2-36)$$

where the constant C is stress-dependent, and b independent of stress level and time.

Substitution of the power law (2-36) into the recovery equation (2-34) leads to an expression, after some rearrangement, that will be useful for evaluating material properties [Ramaswamy, 1971]:

$$\frac{(\epsilon_1 - \epsilon_3)_r}{\Delta \epsilon_C} = \frac{1}{C_1} [(1 + C_\sigma \lambda)^b - (C_\sigma \lambda)^b] \quad (2-37)$$

where

$$\lambda = \frac{t - t_1}{t_1} \quad (2-38)$$

$$\begin{aligned} \Delta \epsilon_C &= (\epsilon_1 - \epsilon_3)(t_1) - (\epsilon_1 - \epsilon_3)(0) \\ &= C_1 C_2 C \psi_1^b (\sigma_1 - \sigma_3) \end{aligned} \quad (2-39)$$

Equation (2-38) is called the reduced recovery time. And equation (2-39) represents the transient component of strain existing immediately before the stress is removed.

From equation (2-37), C_1 and C_σ can be determined for different stress levels. This can be done either graphically or by a regression procedure. For graphical shifting, a master curve is drawn for $C_\sigma = C_1 = 1$. Then the magnitude of the vertical translation is $\log C_1$, and that of the horizontal translation is $\log C_\sigma$. If, for example, the experimental curve lies above and to the right of the master curve, then $C_\sigma < 1$ and $C_1 < 1$. In this investigation, however, the regression procedure was used.

In order to apply the above nonlinear viscoelastic formulation to the behavior of compacted clays, the effect of confining pressure and the moisture content can be accounted for, provided the creep strain in equation (2-30) is expressed as a function of the stress-strength ratio in the octahedral plane. Under conditions assumed to act in the triaxial compression test,

$$(\epsilon_1 - \epsilon_3)(t) = \frac{3}{2\sqrt{2}} \gamma_{\text{oct}}(t) \quad (2-40)$$

$$(\sigma_1 - \sigma_3)(t) = \frac{3}{\sqrt{2}} \tau_{\text{oct}}(t) \quad (2-41)$$

where

$$\begin{aligned} \gamma_{\text{oct}} &= \text{octahedral shearing strain} \\ &= \frac{2}{3} \sqrt{(\epsilon_1 - \epsilon_2)^2 + (\epsilon_2 - \epsilon_3)^2 + (\epsilon_3 - \epsilon_1)^2} \end{aligned} \quad (2-42)$$

$$\begin{aligned}\tau_{\text{oct}} &= \text{octahedral shearing stress} \\ &= \frac{1}{3} \sqrt{(\sigma_1 - \sigma_2)^2 + (\sigma_2 - \sigma_3)^2 + (\sigma_3 - \sigma_1)^2}\end{aligned}\quad (2-43)$$

The use of equation (2-31) and the power law (2-36) yields:

$$J_n(t) = \Delta J(t) = C \frac{C_1 C_2}{C_\sigma^b} t^b \quad (2-44)$$

For determining the coefficients in equation (2-44), a dimensionless parameter is introduced:

$$R = \frac{\tau_{\text{oct}}}{(\tau_{\text{oct}})_f}$$

where $(\tau_{\text{oct}})_f$ is the octahedral shearing stress at failure. This term will be defined in a later section.

Ramaswamy (1971) studied time-dependent shear strain characteristics of two compacted cohesive soils, and found that for equation (2-44) the following expression obtained:

$$\frac{C_1 C_2}{C_\sigma^b} = \frac{\sinh(C_o R)}{C_o R} \quad (2-45)$$

in which C_o is constant for the particular material. This hyperbolic sine dependence has been explained using Eyring's theory of rate-processes and a simple molecular model [Thorkildsen, 1964]. The same model has been used to explain the creep rate of clays observed by Mitchell, et al., (1968).

Substituting equation (2-45) into equation (2-44) gives

$$\gamma_{\text{oct}} = \frac{\sinh(C_o R)}{C_o R} [2C(\tau_{\text{oct}})_f] t^b R \quad (2-46a)$$

or

$$\gamma_{\text{oct}} = \frac{\sinh(C_o R)}{C_o R} J'_o t^b R \quad (2-46b)$$

where

$$\begin{aligned} J'_o &= \text{constant} \\ &= 2C(\tau_{\text{oct}})_f \end{aligned} \quad (2-47)$$

Determination of the constants C_o and J'_o is easily accomplished by evaluating equation (2-46) at $t=1$ minute and then rewriting it:

$$\gamma_{\text{oct}} \Big|_{t=1} = \frac{\sinh(C_o R)}{C_o} J'_o \quad (2-48)$$

Having determined C_o and J'_o , it is now possible to evaluate $\frac{C_1 C_2}{C_\sigma^b}$ by using equation (2-45).

The material property C_2 is calculated from the following equation:

$$C_2 = \frac{\sinh(C_o R)}{C_o R} \frac{C_\sigma^b}{C_1} \quad (2-49)$$

The constant a in equation (2-22) can be obtained by:

$$a = K' \sinh(C_o R) \quad (2-50)$$

where

$$K' = \text{constant} = \frac{3C(\tau_{\text{oct}})_f}{\sqrt{2} C_o} \quad (2-51)$$

Substituting equations (2-45) and (2-46) into equation (2-40), equation (2-40) reduces to the form:

$$\gamma_{oct}(t) = C_1 C_2 J'_o \left(\frac{t}{C_g}\right)^{b_R} \quad (2-52)$$

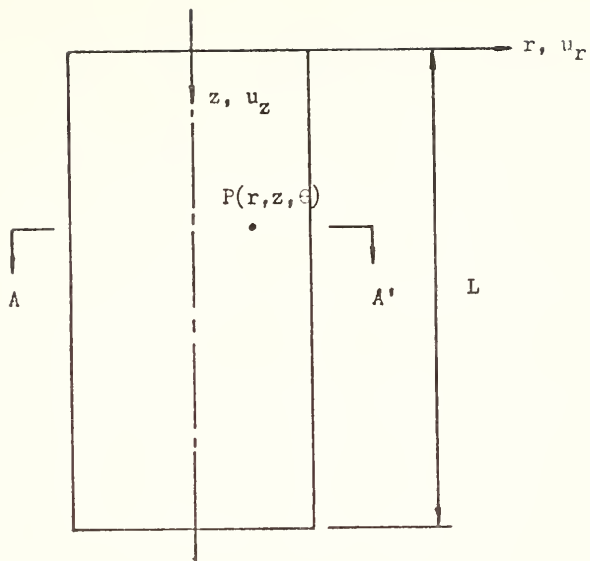
Therefore, all material properties are interpreted from experimental data by the above-mentioned procedures.

2-6. Determination of Strains

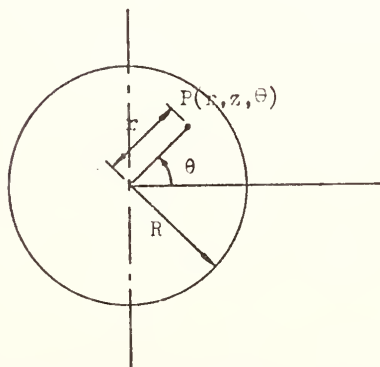
Material property evaluation is based on experimental creep test data. From the triaxial compression creep tests, the measurements permit determination of the total axial and radial movements of the test specimen. These quantities can be used to calculate the average axial and radial strains, as well as the shearing strains, for any desired orientation.

The test specimen used in a triaxial compression creep test is a right circular cylinder, with its axis vertical. The top and bottom surfaces of the test specimen communicate with rigid loading plates. The axial force is applied on the upper loading plate, along the center line of the test specimen. A cylindrical test specimen is shown schematically in Figure 2.6. For axisymmetric stress conditions and a homogeneous test specimen, the principal infinitesimal strains at any point P (z, r, θ) [Love, 1944] are:

$$\begin{aligned} \epsilon'_z &= \frac{\partial u_z}{\partial z} \\ \epsilon'_r &= \frac{\partial u_r}{\partial r} \\ \epsilon'_\theta &= \frac{u_r}{r} \end{aligned} \quad (2-53)$$



(a). Elevation View



(b). Cross Section A-A'

Figure 2.6. Cylindrical Test Specimen

where u_z and u_r are the displacements of the point P in the z and r directions, respectively, and ϵ'_z , ϵ'_r , and ϵ'_θ , are the axial, radial and tangential strains, respectively.

The average principal strains at the outer surface are:

$$\begin{aligned}\epsilon_z &= \frac{1}{L} \int_0^L \epsilon'_z dz = \frac{\Delta L}{L} \\ \epsilon_r &= \frac{1}{R} \int_0^R \epsilon'_r dr = \frac{\Delta R}{R} \\ \epsilon_\theta &= \epsilon'_\theta \Big|_{r=R} = \frac{\Delta R}{R}\end{aligned}\tag{2-54}$$

where L and R represent the axial and radial movements of the outside of the test specimen.

The strain can then be separated into a dilatational component:

$$\epsilon_V = \frac{\Delta V}{V} = \epsilon_z + \epsilon_r + \epsilon_\theta\tag{2-55}$$

in which ΔV stands for volume change and V is the total volume of the test specimen, and a distortional component, which can be expressed by the maximum shear strain:

$$\frac{1}{2} (\epsilon_1 - \epsilon_3) = \frac{1}{2} (\epsilon_z - \epsilon_r)\tag{2-56}$$

It is useful theoretical basis if the material is assumed to be nondilatant and isotropic. These assumptions are used in this investigation, as in other analytical studies [Clough and Woodward, 1967; Girijavallaban and Reese, 1968]. The maximum shear strain, produced in response to an applied deviatoric stress, can be obtained by measuring

the axial and radial displacements of the outer surface of a test specimen.

2-7. Failure Criterion for Compacted Clays

It has been shown by Ramaswamy (1971) that the creep response, as characterized by the parameters a , C_1 , C_2 and C_σ , could be usefully described as a function of the stress-strength ratio. Thus, the question of the most appropriate failure criterion arises.

Three failure criteria often considered for application to soils are those proposed by Tresca (1868), von Mises (1913), and Mohr (1914) - Coulomb (1776). The Tresca failure criterion, appearing as a regular hexagon on the deviatoric plane ($\sigma_1 + \sigma_2 + \sigma_3 = 0$), is a one-parameter failure theory, in which yielding is assumed to occur when the maximum shear stress reaches a certain limiting value. The von Mises failure criterion, a circle on the deviatoric plane, is also a one-parameter failure theory, which states that yielding occurs when τ_{oct} reaches a certain limiting value. The Mohr-Coulomb failure criterion is a two-parameter failure theory, in which the parameters are called the "cohesion" and "angle of shearing resistance" of the soil. The failure loci of the three criteria on the deviatoric plane are given in Figure 2.7.

The determination of a strength criterion appropriate for soils over a wide range of stress and strain has been the objective of many experimental and theoretical investigations. Some of these are discussed below:

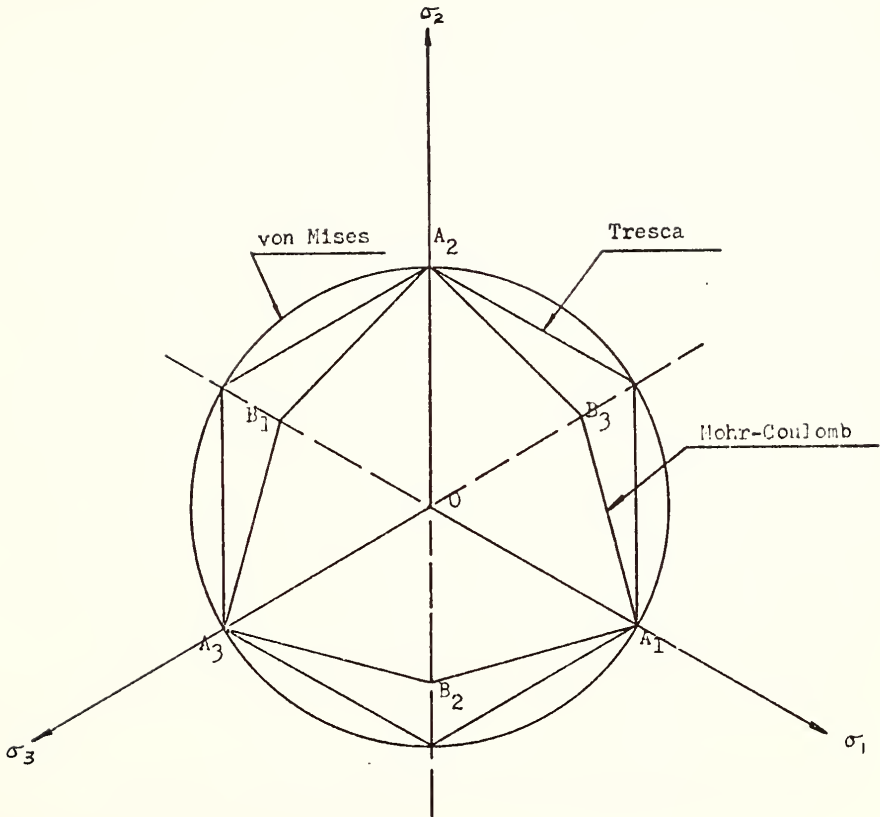


Figure 2.7 . Failure Criteria

(a) The applicability of the Mohr-Coulomb failure criterion for clays has been suggested by Taylor (1951), Hvorslev (1960), Parry (1960), and Roscoe and Burland (1968).

(b) Wu, et al. (1963), have obtained experimental results on clays which agree well with the Mohr-Coulomb failure theory, expressed in terms of the Hvorslev (1937) strength parameters, and indicate that the strength is independent of the intermediate principal stress and the stress path during loading. But for sand, they found that the strength depends on the intermediate principal stress.

(c) Kirkpatrick (1957) suggested that the yield function obtained from sands is consistent with the Mohr-Coulomb criterion. But subsequently Kirkpatrick and Belshaw (1968), using an X-ray technique to measure strains in a triaxial compression specimen, found that the results did not support the use of the Mohr-Coulomb yield function as a plastic potential.

(d) Bell (1965) found experimentally that for cohesionless soils the yield surface is midway between those proposed by Mohr-Coulomb and von Mises.

(e) According to Bishop (1966), the Mohr-Coulomb theory seems to be satisfactory for cohesionless soils.

(f) Drucker, et al. (1957), have applied a generalized Mohr-Coulomb criterion as the yield limit and plastic potential for an approach on the basis of the work-hardening theory of plasticity. Although a qualitative agreement was obtained with the behavior of soils in triaxial tests, the Mohr-Coulomb relation implies volumetric expansion during plastic flow.

The above-mentioned studies suggest that the Mohr-Coulomb failure theory is currently favored for soils, although Habib (1953), Peltier (1957), Haythornthwaite (1960), and Ko & Scott (1968) dispute its applicability to sands. However, the evidence presently available to indicate the effect of an independently controlled intermediate principal stress is still inconclusive.

It has been indicated previously [Perloff, 1966; Ramaswamy, 1971] that the creep parameters a and b are independent of confining pressure and initial water content as the applied deviator stress expressed by a fraction of principal stress difference at failure. The principal stress difference at failure, $(\sigma_1 - \sigma_3)_f$, is that corresponding to the confining pressure, σ_3 , at which the test was performed. Its magnitude, however, is a function of the type of testing. This means that the confining pressure is equal to the octahedral normal stress at the equal all around pressure in the triaxial test. However, the octahedral normal stress increases as the applied deviator loads are increased. If the shearing resistance is a function of confinement, there will be a concurrent increase in the failure strength as the octahedral normal stress increases. So, using the shear strength corresponding to the normal stress acting at the moment of failure seems more realistic than using the failure stress corresponding to the initial normal stress. In a continuous medium, the material is subjected to three principal stresses; hence, the failure criterion should be expressed as a function of all three principal stresses. It is reasonable to expect that each of the three principal stresses would contribute toward failure. For this reason, it will be convenient to describe stress states by using the

octahedral plane in principal stress space, as suggested by Newmark (1960).

Thus, for this study, the failure strength criterion assumed is:

$$(\tau_{\text{oct}})_f = c_{\text{oct}} + \sigma_{\text{oct}} \tan \phi_{\text{oct}} \quad (2-57)$$

where

$(\tau_{\text{oct}})_f$ = octahedral shear stress at failure

σ_{oct} = octahedral normal stress at failure

$$= \frac{1}{3} (\sigma_1 + \sigma_2 + \sigma_3) \quad (2-58)$$

c_{oct} = intercept on τ_{oct} - axis.

ϕ_{oct} = slope of the failure envelope in $\sigma_{\text{oct}} \tau_{\text{oct}}$ -plane.

Equation (2-58) is equivalent to an extended von Mises criterion, with a circular projection on the octahedral plane. This form of failure strength criterion has been used for clays, in studies by Perloff and Pombo (1969), Chen (1970), and Ramaswamy (1971). It is to be noted that $(\tau_{\text{oct}})_f$ is proportional to $(\sigma_1 - \sigma_3)_f$ in the triaxial compression creep tests (Equation (2-41)).

2-8. Analysis of Saturated Foundation Clays

Although concerned primarily with the behavior of the compacted clay fill, the analysis requires consideration of the saturated foundation clays. This has been done by developing equivalent elastic moduli corresponding to the effective stress level and the degree of consolidation. This is done by using the results of one-dimensional consolidation tests on undisturbed samples of the foundation clays.

The one-dimensional consolidation test introduced by Terzaghi (1923) is the classical test for the determination of compressibility and consolidation. In this test, a small cylindrical specimen, as a whole, can consolidate only in the direction of its vertical axis, and only in this direction can the pore water be squeezed out. There is no radial displacement.

Under the conditions of this one-dimensional consolidation test, the axial linear strain, ϵ_1 , equals the dilatational strain, ϵ_V :

$$\epsilon_1 = \epsilon_V = 3\epsilon_{\text{oct}} \quad (2-59)$$

For a homogeneous isotropic specimen, the equivalent bulk modulus, K_b , can be expressed by

$$\begin{aligned} K_b &= \frac{d\sigma'_{\text{oct}}}{d\epsilon_V} \\ &= \frac{d\sigma'_{\text{oct}}}{d\epsilon_1} \end{aligned} \quad (2-60)$$

and the shear modulus, G , has the form:

$$G = \frac{d\tau_{\text{oct}}}{d\gamma_{\text{oct}}} \quad (2-61a)$$

or

$$G = \frac{\frac{\sqrt{2}}{2} (d\sigma'_1 - d\sigma'_{\text{oct}})}{\frac{2\sqrt{2}}{3} d\epsilon_1} \quad (2-61b)$$

The stress-strain relation is expressed:

$$a_v = \frac{d\epsilon_1}{d\sigma'_1} (1 + e_o) \quad (2-62)$$

Substituting equations (2-60) and (2-61) into equation (2-62), the following relation holds:

$$a_v = (1+e_o) / (K_b + \frac{4}{3} G) \quad (2-63)$$

From the theory of elasticity [Wang, 1953], one has:

$$K_b = \frac{E}{3(1-2\nu)} \quad (2-64)$$

and

$$G = \frac{E}{2(1+\nu)} \quad (2-65)$$

Here, E and ν are the Young's modulus and Poisson's ratio, respectively.

By inserting equations (2-64) and (2-65) into equation (2-63), equation (2-63) becomes:

$$a_v = \frac{(1+e_o)(1+\nu)(1-2\nu)}{E(1-\nu)} \quad (2-66)$$

The general differential equation of one-dimensional consolidation as expressed by Terzaghi (1923) is

$$\frac{\partial u}{\partial t} = \frac{\partial \sigma_1}{\partial t} + \frac{k(1+e_o)}{\gamma_w a_v} \frac{\partial^2 u}{\partial z^2} \quad (2-67)$$

Assuming a sudden load application without further total stress increase, and substituting

$$\frac{k(1+e_o)}{\gamma_w a_v} = c_v \quad (2-68)$$

the equation (2-67) reduces to:

$$\frac{\partial u}{\partial t} = c_v \frac{\partial^2 u}{\partial z^2} \quad (2-69)$$

c_v is here called the coefficient of consolidation.

Substituting equation (2-66) into equation (2-68), we have:

$$c_v = \frac{kE(1-\nu)}{\gamma_w(1+\nu)(1-2\nu)} \quad (2-70)$$

By applying initial condition, $u(z,0)=u_0=\text{constant}$, and boundary condition, $u(0,t)=u(2H,t)=0$ for $t > 0$, the solution for equation (2-69) is [Taylor, 1948]:

$$u(z,t) = \sum_{m=0}^{m=\infty} \frac{2u_0}{M} (\sin MZ) \exp(-M^2 T) \quad (2-71)$$

where

u_0 = initial excess pore water pressure

$$Z = \frac{z}{H} \quad (2-72)$$

$$T = \frac{c_v t}{H^2} \quad (2-73)$$

$$M = \pi(2m+1)/2 \quad (2-74)$$

H = effective thickness of consolidation stratum

and m is a dummy variable taking on value 1, 2, 3,

With these values in equation (2-71), the ratio of the change in deformation, at any depth and any time, to the ultimate change at that depth, can be obtained from

$$U_z(t) = 1 - \frac{u(z,t)}{u_0} \quad (2-75)$$

Then the change in vertical effective stress at that depth is

$$\Delta\sigma'_z(t) = u_o U_z \quad (2-76)$$

When lateral stresses are not measured in a one-dimensional consolidation test, they can be estimated from the value of K_o , the coefficient of earth pressure at rest. The coefficient K_o is defined as the ratio of the minor and the major principal effective stresses, under the conditions of complete lateral confinement (zero strain):

$$K_o = \left. \frac{\sigma'_x}{\sigma'_z} \right| \varepsilon_x = 0 \quad (2-77)$$

Under the conditions of the one-dimensional consolidation test, equations (2-42) and (2-43) reduce to

$$\gamma_{\text{oct}} = \frac{2\sqrt{2}}{3} \varepsilon_z \quad (2-78)$$

$$\tau_{\text{oct}} = \frac{\sqrt{2}}{3} (\sigma'_z - \sigma'_x) \quad (2-79)$$

Substituting equation (2-77) into equation (2-79), we have

$$\tau_{\text{oct}} = \frac{\sqrt{2}}{3} (1-K_o) \sigma'_z \quad (2-80)$$

Substituting equations (2-78) and (2-80) into (2-61a), gives

$$G = \frac{1}{2} (1 - K_o - \sigma'_z \frac{dK_o}{d\sigma'_z}) \frac{d\sigma'_z}{d\varepsilon_z} \quad (2-81)$$

Here $\frac{d\sigma'_z}{d\varepsilon_z}$ is called the constrained modulus.

The K_o value appears to be governed by the soil strength, and by the degree of over-consolidation. Samsloe (1953) was the first to recognize the increase in K_o as a result of over-consolidation. Brooker and Ireland (1965) have found that the value of K_o is dependent upon the effective angle of shearing resistance, the plasticity index of the soil, and the over-consolidation ratio. Sherif and Koch (1970) concluded that the K_o value appears to be dependent mainly on the liquid limit and the over-consolidation ratio of the soil.

The constrained modulus can be calculated from the one-dimensional consolidation test e - $\log \sigma'_z$ curve, which permits determination of G . Then the equivalent elastic constants, E and ν , can be determined at a particular time during the consolidation process from the following equations:

$$\nu = \frac{K_o}{1+K_o} \quad (2-82)$$

$$E = 2G(1+\nu) \quad (2-83)$$

2-9. Incorporation of Material Characterization into the Finite Element Analysis

Two approaches are currently employed to incorporate nonlinear and/or time-dependent material characterization into the finite element analysis: (1) An iterative procedure, with the final solution obtained by iterative solution of the nonlinear equations; (2) An incremental procedure, wherein a final solution is obtained from solving a number of linearized problems distributed between the initial and final configurations. The iterative procedure was selected for use in this investigation.

In the finite element analysis each discrete element within the idealized assemblage was considered as a homogeneous, isotropic and different elastic material. Each element was characterized by two equivalent elastic constants, Young's modulus E and Poisson's ratio ν , both of which depend on the state of stress within the element and the elapsed time after loading. The equivalent E and ν are assumed to be constant within an element for a given stress level and time. Poisson's ratio for the compacted cohesive soil is found to be approximately independent of time. From a compressive creep test, the relation between the principal strain ratio, which is equivalent to Poisson's ratio, and time for various stress levels is given in Figure 2.8. A conclusion which can be drawn from this figure is that at lower stress levels the principal strain ratio decreases with an increase in time. At higher stress levels the opposite is true, that is the principal strain ratio increases with an increase in time. This tendency appears to be true for all tests conducted during this investigation, irrespective of test conditions. However, the variation in the principal strain ratio with time, whether it be an increase or a decrease is always comparatively small. Therefore it is reasonable to assume that the average principal strain ratio as an equivalent Poisson's ratio is independent of time. For this study, the equivalent Poisson's ratio, ν , used to analyze compacted clay is

$$\nu = k_0 + k_1 \frac{\tau_{oct}}{(\tau_{oct})_f} \quad (2-84)$$

where k_0 and k_1 are constants obtained from compression creep tests.

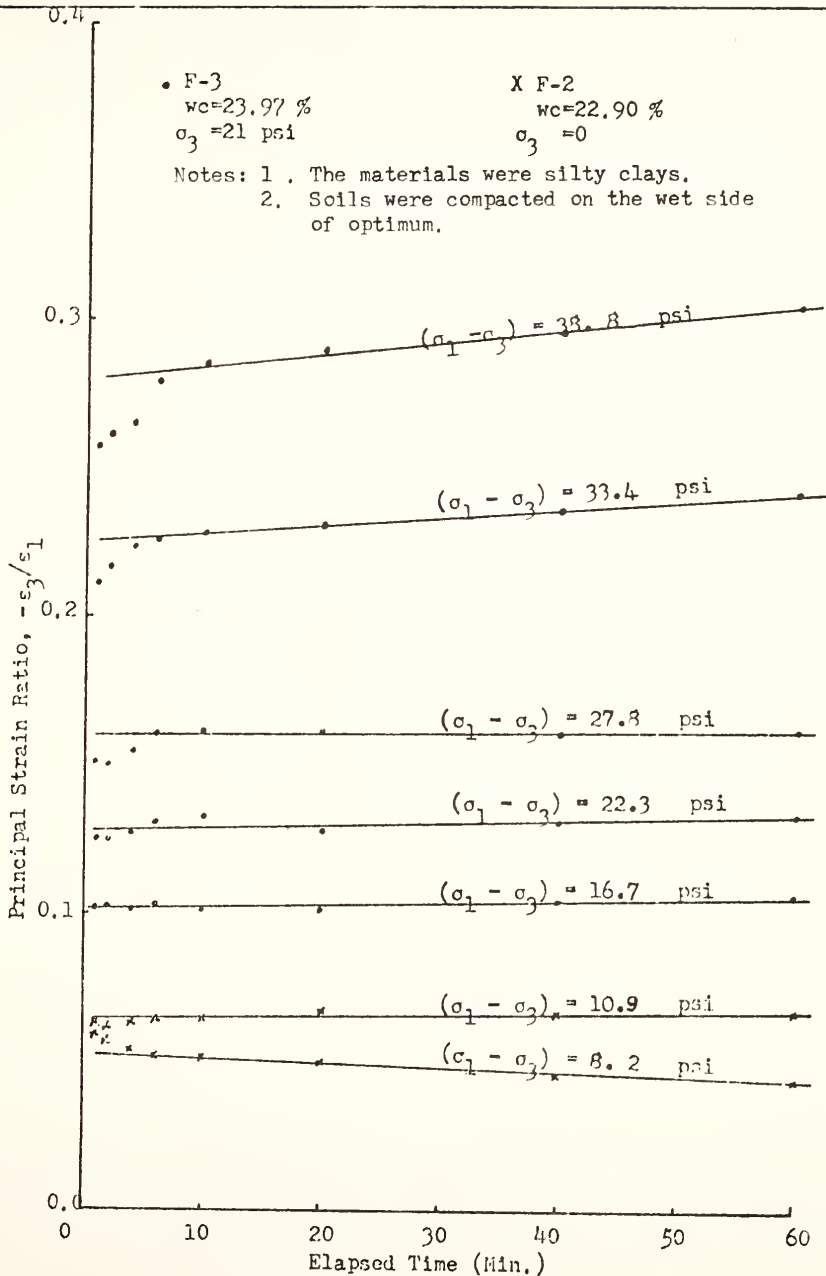


Figure 2.8. Relation Between Principal Strain Ratio and Time

The soil is assumed to be an isotropic, homogeneous and elastic material which obeys Hooke's law of proportionality between stress and strain at a particular time and stress level. If an element of the soil mass is subjected to principal stresses σ_1 , σ_2 and σ_3 in the x, y, z directions. The following relations then hold:

$$\epsilon_1 = \frac{1}{E} [\sigma_1 - \nu(\sigma_2 + \sigma_3)] \quad (2-85a)$$

$$\epsilon_2 = \frac{1}{E} [\sigma_2 - \nu(\sigma_3 + \sigma_1)] \quad (2-85b)$$

$$\epsilon_3 = \frac{1}{E} [\sigma_3 - \nu(\sigma_1 + \sigma_2)] \quad (2-85c)$$

In the triaxial compression creep test, σ_2 is equal to σ_3 . The principal strain difference can then be written as:

$$(\epsilon_1 - \epsilon_3) = \frac{1+\nu}{E} (\sigma_1 - \sigma_3) \quad (2-86a)$$

or

$$\frac{(\epsilon_1 - \epsilon_3)}{(\sigma_1 - \sigma_3)} = \frac{1+\nu}{E} = \frac{1}{2G} \quad (2-86b)$$

Comparing this equation with equation (2-31), yields

$$J_n(t) = \frac{1}{2G(t)} \quad (2-87a)$$

or

$$\frac{1}{G(t)} = C_1 C_2 J'_o \left(\frac{t}{C_\sigma}\right)^b \frac{1}{(\tau_{oct})_f} \quad (2-87b)$$

where $G(t)$ is the equivalent elastic shear modulus at the particular time and particular stress level.

The equivalent Young's modulus for this case is

$$E(t) = 2G(t)(1+\nu) \quad (2-88)$$

In the consideration of the foundation clay soil, two equivalent elastic constants E and ν are required for the finite element analysis in this study. Since E , G and ν are related as indicated in equation (2-88), the determination of any two of the constants allows for calculation of the third. Hence the procedure for determining the equivalent elastic constants E and ν can be briefly described as follows.

It has been found that the shear modulus of any soil is, as a first approximation, related mainly to the void ratio and effective stress and is independent of drainage conditions [Lambe and Whitman, 1969]. This is due to the fact that the shear stress is not changed by changes in pore pressure. From equation (2-82), the value of ν is known for the drained case as obtained from K_o . This value lies between .52 and .95 over the range of over consolidation ratio examined in this study. The shear modulus is then calculated from equation (2-81). The undrained condition is equivalent to the use of $\nu = 0.5$ since this corresponds to no change in volume [Lambe and Whitman, 1969; Boehmer and Christian, 1969]. For the partially drained case, ν is allowed to vary linearly with the degree of drainage. Then using G and new ν , the new E can be evaluated for the partially drained case.

As a first step in the iterative process equivalent elastic constants E and ν are guessed and used to determine the displacements

and stresses in the soil mass at a particular time and stress level. A new set of equivalent elastic constants E and ν are then obtained using the stress state calculated in the first iteration. The new displacements and stresses in the soil mass are calculated using the previously calculated elastic constants E and ν . This iterative procedure is repeated until the differences between the new and previous values of elastic constants E and ν are less than the specified tolerance. When the proper convergence on the values of elastic constants E and ν is obtained for the whole system. The iterative process is stopped and the time increases to a new desired value.

The elastic constants E and ν are assumed to be constant for the sandy gravel layers. Therefore, during the iterative process it is not necessary to calculate the new values of E and ν for these layers.

In summary, the steps taken to determine E and ν are as follows:

(1) For embankment compacted clay: The equivalent Young's modulus for this case is

$$E(t) = 2G(t)(1 + \nu) \quad (2-88)$$

in which $G(t)$ is determined by the following equation

$$\frac{1}{G(t)} = C_1 C_2 J_0 \left(\frac{t}{C_s} \right)^b \left(\frac{1}{\tau_{act}} \right)_f \quad (2-87b)$$

and the equivalent Poisson's ratio is

$$\nu = k_0 + k_1 \frac{\tau_{act}}{(\tau_{act})_f} \quad (2-84)$$

(2) For foundation silty clay: The equivalent elastic constants are determined at a particular time during the consolidation process from the following equations

$$\nu = \frac{K_0}{1 + K_0} \quad (2-82)$$

$$E = 2G(1 + \nu) \quad (2-83)$$

where

$$G = \frac{1}{2} \left(1 - K_0 - \sigma'_x \frac{dK_0}{d\sigma'_x} \right) \frac{d\sigma'_x}{d\varepsilon_x} \quad (2-81)$$

CHAPTER III
LABORATORY EXPERIMENTS

3-1. Material

For experimental purposes, the soils at the study site were considered to be of two types: the undisturbed saturated foundation clays, and the partially saturated compacted clay fill.

The foundation clay soils are the lacustrine deposits resulting from past flooding of the Clear Creek. Typical grain size distribution curves for these soils are given in Figure 3.1. Plasticity characteristics are given in Figure 3.2. It is observed that the underlying soils are more highly plastic under the center of the embankment, and of medium plasticity nearer the outside of the fill.

The soils used to build the embankment were locally available limestone residual silty clays consisting of reddish brown and greyish clays. Grain size distribution curves for the soils are shown in Figure 3.3; plasticity characteristics are given in Figure 3.2. Both soils are highly plastic silty clays.

Classification data for foundation and embankment soils are given in Table I. It seems that greyish clay in embankment is the same classification as foundation clay soil.

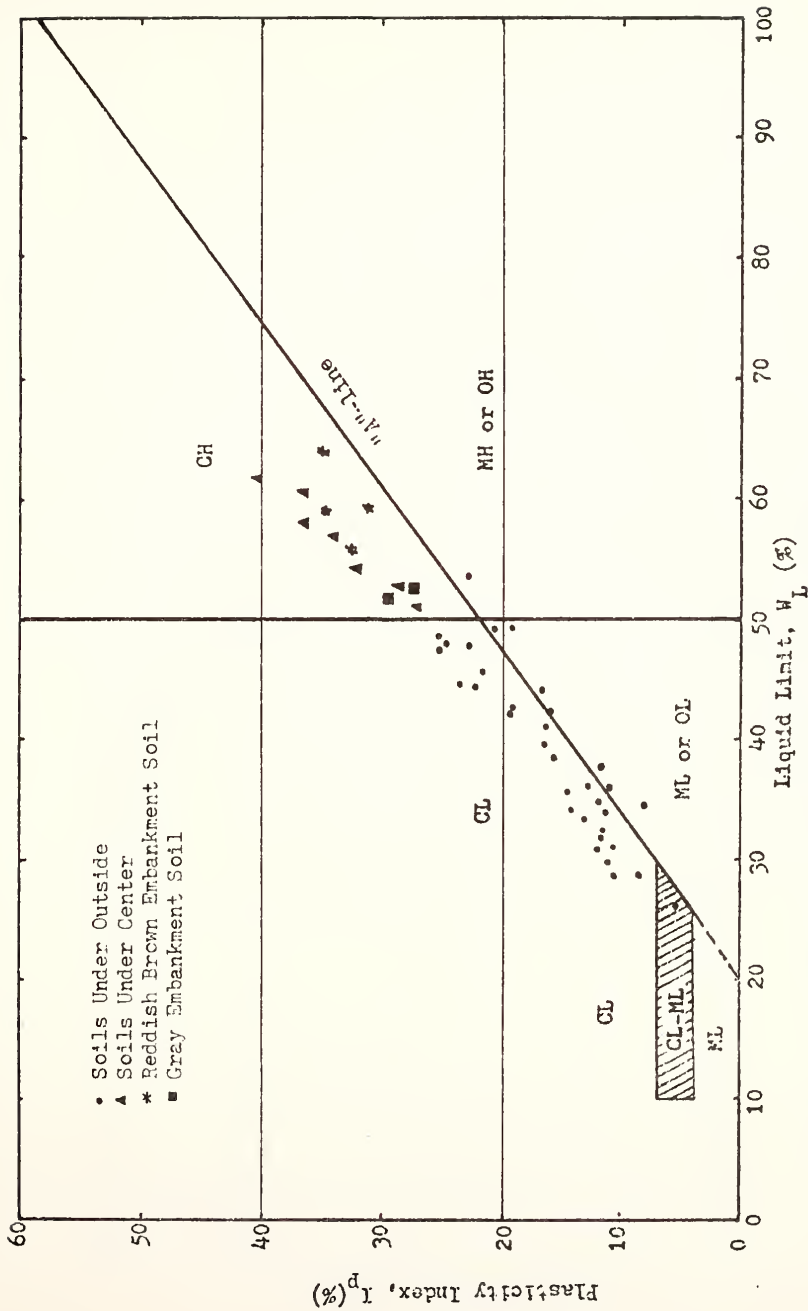


Figure 3.2. Plasticity Chart for Subcells and Embankment Soils

Table I

Classification Properties of the Soils

| Elevation | Color | Specific Gravity | Liquid Limit % | Plastic Limit % | Plastic Index % | Clay Fraction (< 2 μ) % | Remarks |
|-------------------------------|---------------|------------------|-----------------|-----------------|-----------------|------------------------------|--|
| 489.50 (789+55 \bar{c}) | Gray | 2.70 | 51.0 | 24.06 | 26.94 | 28 | Foundation Soil from Shelby Tube (Before Construction) |
| 492.95 (789+50 \bar{c}) | Gray & Brown | 2.71 | 52.6 | 24.56 | 28.04 | 35 | Foundation Soil from Shelby Tube (After Construction) |
| 510.00 | Reddish Brown | 2.76 | 59.3 | 28.1 | 31.2 | 58 | Embankment Soil from Borrow Area |
| 520.00 | Gray | 2.68 | 51.8 | 22.8 | 29.0 | 36.5 | Embankment Soil from Borrow Area |
| 530.00 | Reddish Brown | 2.78 | 64.0 | 29.8 | 34.2 | 45 | Embankment Soil from Borrow Area |
| 520.00 | Reddish Brown | / | 57.4 | 23.7 | 33.7 | / | Embankment Soil from Shelby Tube (After Construction) |
| Foundation Soils | | / | 26.20 -61.80 | 18.07 -30.66 | 5.63 -40.33 | / / | Samples from Split Spoon (Details Shown in Appendix F) |

3-2. Preparation of Soil Specimens

Samples of the foundation clays were obtained from 3-inch diameter shelly tubes taken in seven borings before embankment construction, and two borings after embankment construction. Specimens were cut to the desired length and extruded from shelly tube for one-dimensional consolidation tests. The extruded specimens were trimmed to the desired diameter and height and placed in a teflon-lined 2.5-inch diameter consolidation ring.

Two kinds of samples of the compacted cohesive soils selected for this study were tested: one type was trimmed from block samples of the field compacted material; the other was cut from laboratory Standard Proctor compaction test samples. Specimens used for creep tests were approximately 1.4 inches in diameter and 2.8 inches in height. After being cut from the block sample, specimens were trimmed to the desired dimension and wrapped in "P.V.C. film" which was coated with paraffin wax. The waxed specimens were stored for testing in a desiccator jar whose bottom was filled with water to ensure hundred percent humidity. The soils used in the Standard Proctor compaction test were brought from the field and then allowed to air dry. The material passing No. 4 sieve was separated from larger soil clods. Next these clods were crushed into small size by wood hammer. This procedure was continued until all the material passed No. 4 sieve. Approximate moisture content of the stored reddish brown clay was five percent, and that of the gray-colored clay about four percent. For each desired moisture content, four pounds of soil was mixed with the required amount of water in a "liquid-solids twin shell blender" manufactured by the Patterson Kelley company for

about twenty minutes (Figure 3.4). The blender is composed of three major parts: twin shells, graduated cylinder, and electric motors.

The procedure for mixing embankment soils is briefly described as follows:

- (1) Four pounds of soil was placed in the blender and blender sealed.
- (2) Started blender. After few seconds, intensifier was turned on.
- (3) The water valve was opened, allowing a predetermined amount of water to enter into the blender at approximately 50cc per minute.
- (4) The mixing process was periodically stopped every two minutes in order to scrape material from the interior walls of the blender with a knife.
- (5) After all water was added, intensifier and blender were used for one minute. Then the blender was opened and scraped. Finally, the blender was used only for a few minutes (say five to ten minutes).

The mixed soil was then moved from the blender and placed in the plastic sandwich bag. The end of the bag was sealed by twisting, folding over, and wrapping with a rubber band. The soil was then stored in hundred percent humidity room and allowed to cure for at least twenty four hours before being compacted.

Standard Proctor compaction was used in the testing program. The compaction characteristics of the soils are shown in Figure 3.5. The in-place density test data are listed in Table II. The data were taken by ISHC engineers. From the table, it is observed that the in-place earth fill was compacted on the wet side of optimum.

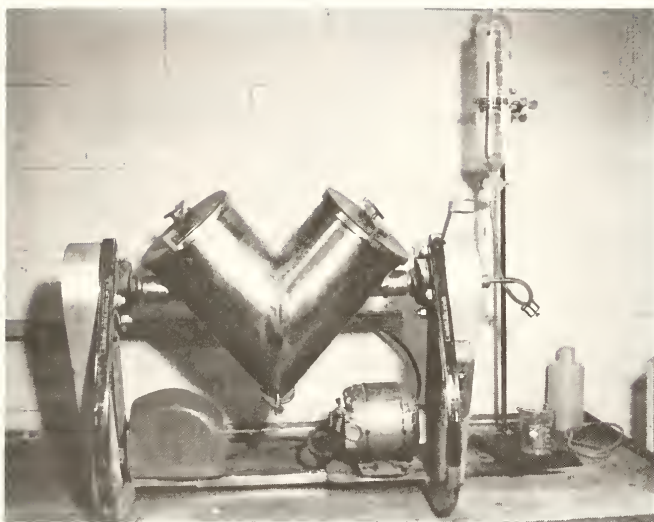


Figure 3.4. Liquid-Solids Twin Shell Blender

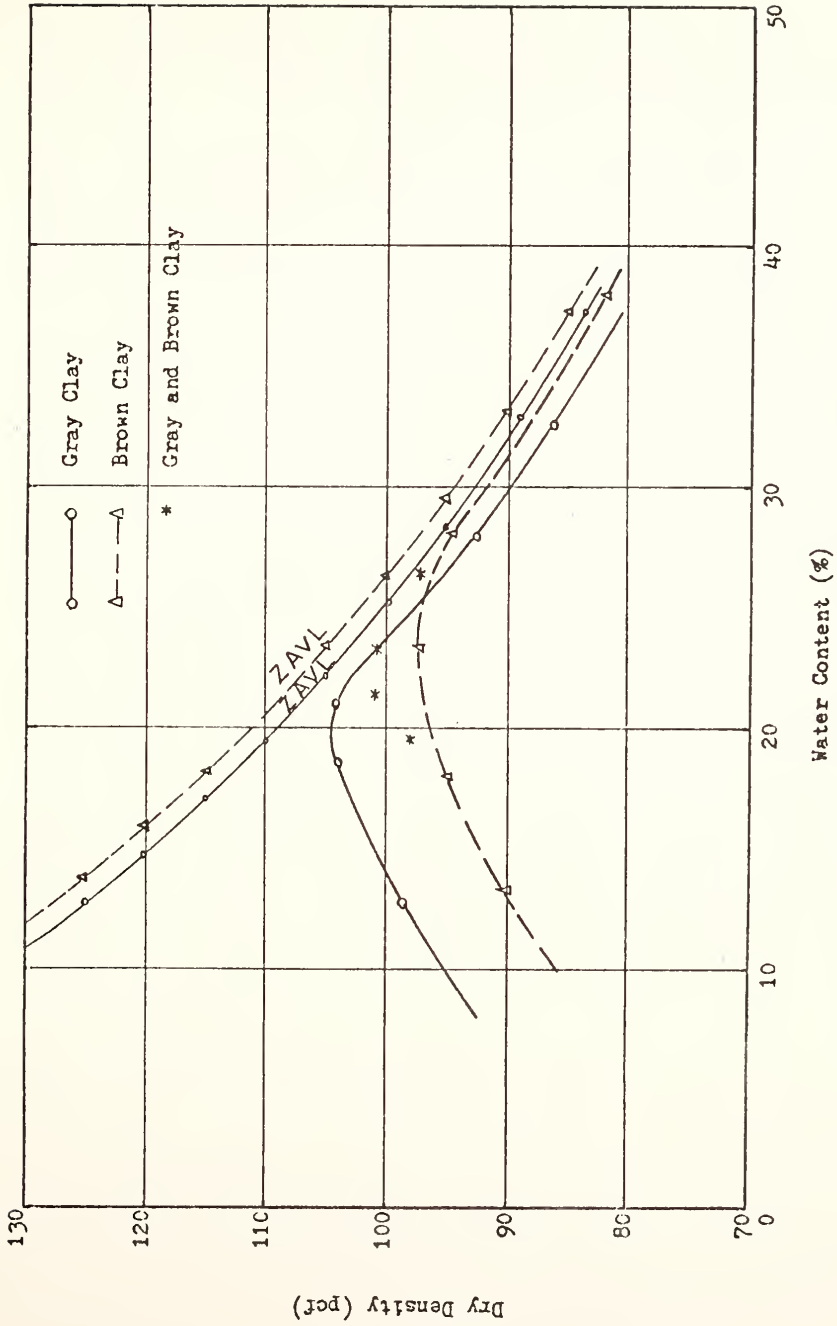


Figure 3.5. Standard Compaction Curves for Embankment Soils

Table II

In-Place Density Test Data (From ISHC)

| Date | Elevation* (ft.) | In-place unit weight (pcf) | Laboratory Compaction Results | | |
|---------|---------------------|----------------------------------|----------------------------------|--------|------------------|
| | | | γ_{OMC} (pcf) | OMC(%) | γ_d (pcf) |
| 4/28/71 | 511.60 | 116.5 | 105.2 | 25.4 | 83.5 |
| 4/29/71 | 514.06 | 111.1 | 105.2 | 25.4 | 83.5 |
| " | " | 124.1 | 123.9 | 18.6 | 104.0 |
| " | " | 121.6 | " | " | " |
| " | " | 117.3 | 105.2 | 25.4 | 83.5 |
| 5/ 3/71 | 514.06 516.00 | 109.2 | " | 25.4 | " |
| " | " | 124.3 | 123.9 | 18.6 | 104.0 |
| " | " | 120.3 | " | " | " |
| " | " | 121.1 | " | " | " |
| 5/ 4/71 | 516.00 | 121.5 | " | " | " |
| 5/14/71 | 516.00 | 124.9 | " | " | " |
| " | " | 125.3 | " | " | " |
| 5/15/71 | 518.00 | 114.3 | 105.2 | 25.4 | 83.5 |
| " | " | 121.3 | 123.9 | 18.6 | 104.0 |
| 5/17/71 | 520.94 | 114.9 | 105.2 | 25.4 | 83.5 |
| " | " | 129.0 | 123.9 | 18.6 | 104.0 |
| " | " | 130.0 | " | " | " |
| " | " | 120.2 | " | " | " |
| 5/22/71 | 520.94 | 116.4 | 120.0 | 23.4 | 97.2 |
| " | " | 121.6 | " | " | " |
| " | " | 123.1 | " | " | " |
| " | " | 124.2 | " | " | " |
| " | " | 117.6 | " | " | " |
| 6/21/71 | 521.44 | 105.2 | 105.2 | 25.4 | 83.5 |
| 6/22/71 | 527.44 | 113.6 | 117.3 | 18.1 | 99.3 |
| " | " | 115.5 | " | " | " |
| 7/ 1/71 | 527.44 | 120.8 | 123.9 | 18.6 | 104.0 |
| 7/ 2/71 | 529.93 | 118.2 | 120.0 | 23.4 | 97.2 |
| 7/ 6/71 | 533.15 | 120.8 | " | " | " |
| 8/12/71 | 536.16 | 116.9 | / | / | / |

*Elevation is approximately determined by writer.

After being extruded from the compaction mold the specimen was trimmed to the desired dimension and placed in a "P.V.C. film" which was then coated with paraffin wax. The compacted specimen was stored on the shelf in a desiccator jar with water in the bottom of the jar for at least one week before doing creep test.

3-3. Description of Experimental Apparatus for Creep Tests

The apparatus for conducting creep tests on the compacted cohesive soil specimens was developed by Perloff (1965). It has the capacity to measure and record both axial and radial displacements of the specimen as continuous functions of time. Figure 3.6 shows the setup of the apparatus. The discussion of apparatus used in this study is divided into five parts as follows: triaxial compression chambers, loading system, axial displacement sensor, radial displacement sensor, and excitation and recording equipment.

(1) Triaxial compression chambers. The triaxial compression chambers which were used in this investigation were of the "Norwegian" variety, manufactured by Geonor, and described in detail by Andresen and Simons (1960). The confining pressure was applied to the chamber fluid, water, by a small piston loaded constant pressure cell shown in Figure 3.6, or applied by air pressure through pressure regulator. The dark color of the chamber water was due to a dye which was used in the pressure fluid to facilitate detection of leakage. An approximately one-half inch deep layer of oil was maintained at the top of the cell in order to lubricate the vertical piston with which the axial load was applied to the specimen. The piston was lapped in a rotating ball

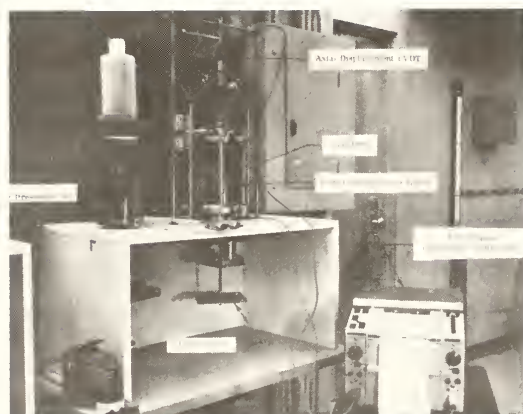


Figure 3.6. Creep Test in Progress

bearing bushing being continuously driven with a flexible cable by the small motor.

(2) Loading system. The triaxial compression cell was mounted in a loading frame in such a manner that axial load could be applied to the piston by placing weights on the load hanger. This permitted compensating the upward force on the piston due to the chamber pressure as well as applying additional axial load for creep testing. In order to apply the load rapidly, and yet smoothly without impact, a pressure regulator was connected on the load hanger. At the instant of loading the air pressure release valve was opened and the forces contacted the load hanger, applying load through the piston to the specimen.

(3) Axial (vertical) displacement sensor. Axial (vertical) displacement of the specimen was determined by measuring the vertical movement of the crossbar which applied loads to the piston of the triaxial compression chamber. The sensor utilized was a Daytronic Model 103C-200 linear variable differential transformer (LVDT). This device converted displacement into an electrical signal which could be continuously recorded.

(4) Radial displacement sensor. In order to directly measure radial movement in a specimen, a device which was a modification of one suggested by Bishop and Henkel (1962), had been designed and constructed (Perloff, 1965). A schematic diagram of this radial displacement sensor is shown in Figure 3.7. A photograph of the device mounted on the base of the triaxial compression cell prior to placing the outer chamber is shown in Figure 3.8. The radial displacement was measured by two curved metal pads which bore lightly on the surface near in the mid-height of

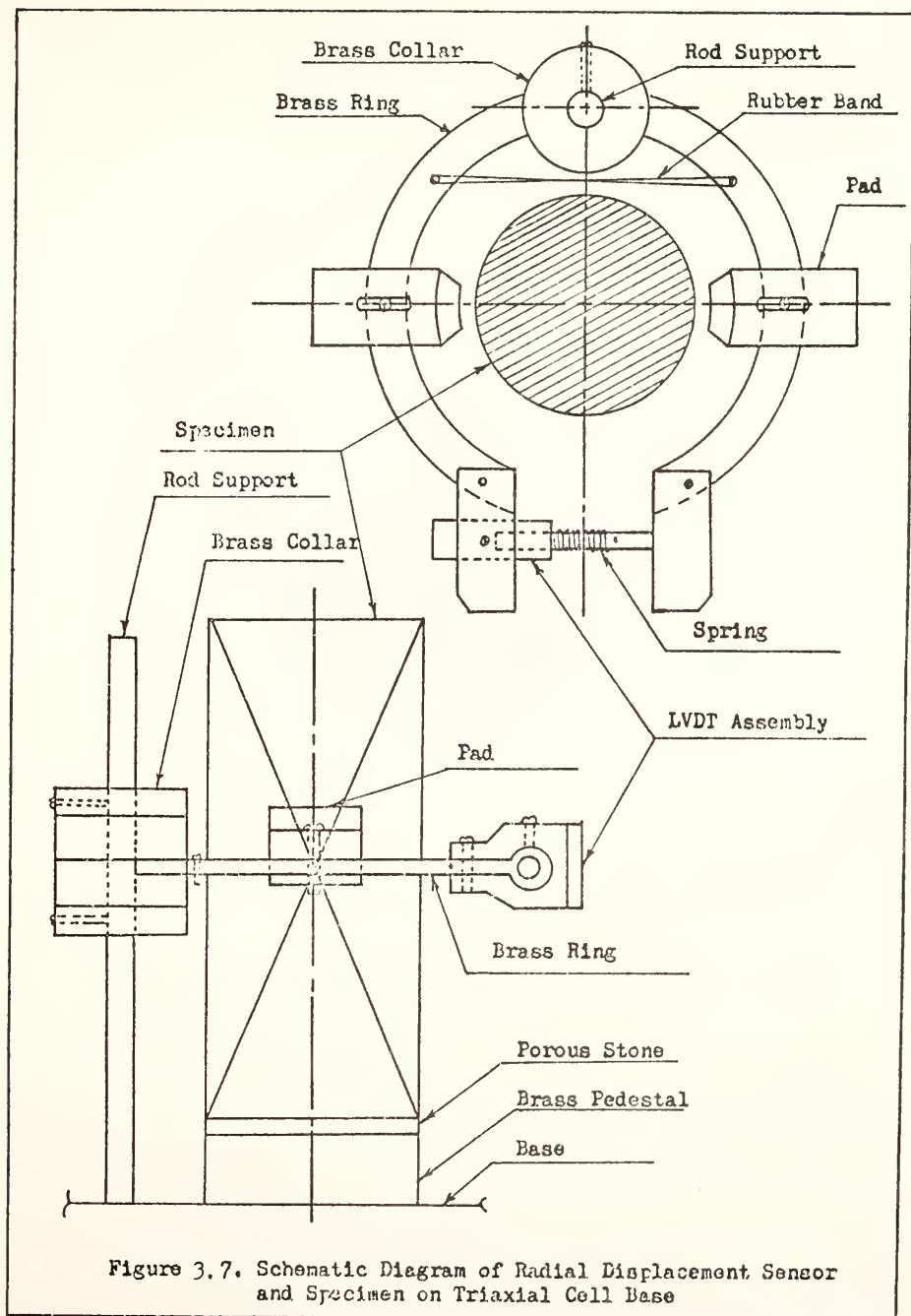


Figure 3.7. Schematic Diagram of Radial Displacement Sensor and Specimen on Triaxial Cell Base

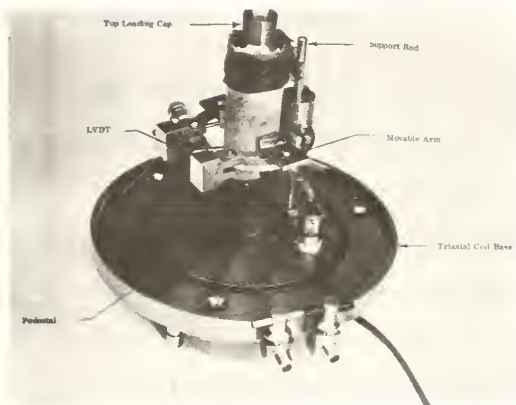


Figure 3.8. Radial Displacement Sensor and Specimen Mounted on Triaxial Compression Cell Base

specimen. The key feature of this device was the International Resistance Company miniature LVDT which converted movement of the two arms in contact with the specimen into an electrical output signal. The stiffness of the spring in the LVDT assembly as well as the tension of the rubber bands could be adjusted so that pressure exerted by the pads on the specimen was sufficient to maintain contact during the testing. All hinges at the junction of the supporting rod and brass collars were lubricated with a thin machine oil to ensure the free movement of the movable arm.

(5) Excitation and recording equipment. A two channel, oscillographic, carrier amplifier recorder manufactured by Texas Instruments, Inc. was utilized in the tests. The recorder served a dual function: the carrier amplifiers on the recorder acted as excitation for both the axial and radial displacement LVDT, and demodulated the signals which were transmitted; the demodulated signal was then recorded on a two-channel strip chart, so that a continuous record of both axial and radial displacements was obtained.

3-4. Creep Testing Procedure

The procedure adopted for creep testing of a compacted specimen was as follows:

(1) Calibration of the LVDT's. Both the axial displacement LVDT and the radial displacement sensor were calibrated before the start of each creep test.

(2) The compacted specimen was then removed from the dessicator, stripped of the protective plastic cover and placed on a dry porous stone resting on the pedestal of the triaxial cell base (Figure 3.8).

(3) A latex protective membrane, 0.06mm thick, was placed around the specimen with a special former (Figure 3.9) designed for using to fix the membrane. After a top loading cap was placed on the specimen, the rubber membrane was firmly attached to the cap and the bottom pedestal with rubber tie strips and silicone grease.

(4) The radial displacement sensor was then mounted on the base of the cell. Figure 3.8 is a photograph of the specimen and the radial displacement sensor in place on the cell base. The LVDT assembly was so adjusted that the radial deformation occurring during the test could be recorded on the "Recording Permapaper," since it could not be adjusted after the application of the confining pressure to the triaxial compression chamber.

(5) The outer chamber was carefully attached to the base of the cell, filled with distilled water (not necessary if using air pressure) and centered on the loading frame.

(6) The axial displacement sensor was mounted on the chamber, and all electrical leads were connected to the oscillographic recorder. Its position was adjusted so that the deformation occurring during the test could be recorded on the "Recording Permapaper."

(7) The desired confining pressure was applied by air pressure through a pressure regulator directly to the triaxial compression chamber. Simultaneously, sufficient axial load was placed on the triaxial chamber load hanger to counteract the uplift pressure on the piston. Volume change was permitted through the open valve connected to the pedestal at the base of the specimen.

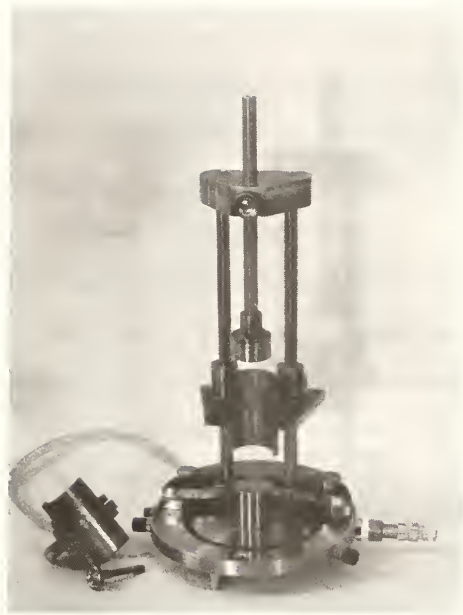


Figure 3.9. Special Former on Triaxial Base

(8) When the deformation due to the confining pressure has almost ceased, the additional desired axial stress was applied to the piston. Two load cycles of creep and relaxation were usually applied for each stress level. The duration of the first cycle of loading was limited to one minute. The specimen was then allowed to relax for fifteen minutes and reload. The second cycle load was left on for one hour, and then removed. The specimen was then allowed to relax for half an hour, by which time essentially all rebound following load removal was completed. These tests were all performed in the undrained conditions. The rationale for this procedure is discussed by Ramaswamy (1971).

(9) When the test was completed, the axial load and confining pressure were removed, the triaxial chamber was moved to another loading frame for determination of the strength of sample.

(10) After each specimen was tested to failure, the triaxial chamber was dismantled, and the specimen was weighed, dried, and re-weighed to determine the moisture content.

3-5. Strength Determination

For determining the strength of compacted samples, a loading device manufactured by Engineering Laboratory Equipment Ltd. was used. The 500 pound capacity U3G1 load cell made by BLH Electronics, in which load was applied at a constant rate of ram movement, was connected to the Sanborn Dual Channel Carrier Amplifier Recorder Model 321 to measure the axial load. The axial displacement was measured with a Federal Dial Gage, Model C8IS graduated to 0.001 inch. The axial displacement rate generally used in testing was 0.02 inches per minute, giving an average axial strain rate about 0.7 percent per minute. Time to failure varied

from about 4 minutes to about 30 minutes, depending upon the compaction conditions and confining pressures.

3-6. One-Dimensional Consolidation Test

The consolidometer used herein is the Anteus consolidometer manufactured by the Anteus Corporation, Mt. Vernon, New York. The operation of the Anteus consolidometer is described in detail by Parker and Miller (1970). The soil specimen was placed between two porous stones whose permeability is greater than that of the soil. Drainage is permitted at the top and at the bottom.

The method of transferring sample from cutting ring to consolidation ring is shown in Figure 3.10. Loads were applied in increments and the load was brought to the level such that the stress in the specimen was larger than the preconsolidation pressure. Further consolidation of the specimen was accomplished by applying the next constant incremental load so that various load increment ratios were applied to the specimen. The maximum load should be great enough to establish the straight line portion of the void ratio-pressure curve in semi-logarithmic scale.

3-7. Test Results

The calculation of the stresses and strains resulting from the application of loads to a soil mass is based on continuum theory. Thus in evaluating experimental test data, it has been assumed that a soil specimen has point like character. By this attribute it is implied that the soil specimen is isotropic and homogeneous, and the measured strains in the experimental test are homogeneous throughout the specimen.

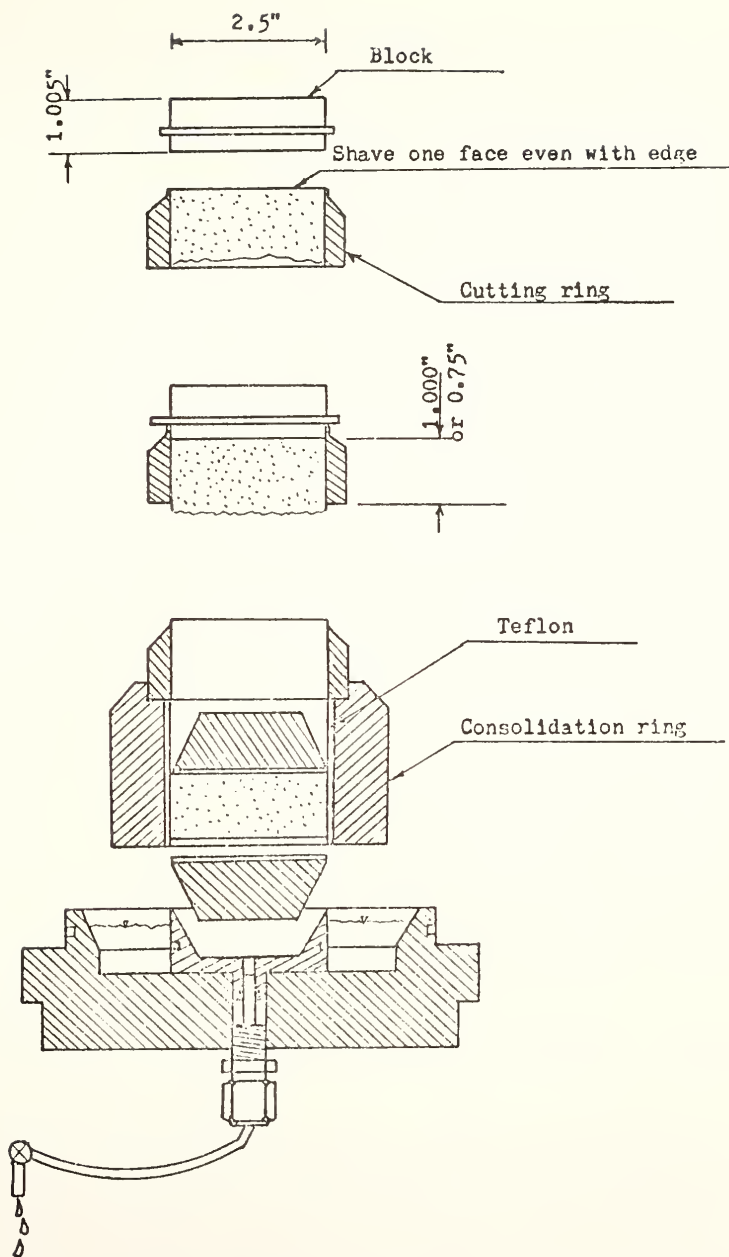


Figure 3.10. Preparation and Placement of Specimen into Consolidometer

Actually the end planes are restrained against radial expansion of the ends and as a consequence, inhomogeneity in stress and strain conditions within the soil specimen will be introduced. Experimental results indicate that the end restraint affects triaxial compression tests on both of cohesive soil (Crawford, 1963; Blight, 1965; Bardon and McDermott, 1965) and cohesionless soil (Shockley and Ahlvin, 1960; Roscoe et al, 1963; Kirkpatrick and Belshaw, 1968). It can be reasonably assumed, however, that homogeneous stress and strain conditions obtain within the sample for compression creep tests if: (1) a sufficiently large length to diameter ratio is used (Bishop and Green, 1965; Duncan and Dunlop, 1968; Perloff and Pombo, 1969); (2) the strains are small (Rowe and Barden, 1964; Duncan and Dunlop, 1968); (3) the end plates are larger than soil specimen (Rowe and Barden, 1964; Januskevicius and Vey, 1965; Kirkpatrick and Belshaw, 1968).

In the compression creep tests used for the study, the length to diameter ratio was approximately equal to two, the strains were always less than one percent, and the diameter for both top loading cap and bottom plate was 1.45 inches while the diameter of the specimen was 1.40 inches. It is believed to assist in eliminating end restraint effects on the observed results.

A summary of creep test results are given in Table III. The test data are listed in Appendix D.

Figure 3.11 indicates the variation in strength with octahedral normal stress for the compacted clays tested. The tested specimens were obtained from both block samples and from Standard Proctor compaction samples. The failure envelope shown, however, was obtained from field

Table III

Creep Test Results

| Specimen No. | Moisture Content % | σ_3 psi | $(\sigma_1 - \sigma_3)$ psi | $(\sigma_1 - \sigma_3)_f$ psi | a $\times 10^{-2}$ | b | Equivalent Poisson's Ratio |
|--------------|--------------------|-------------------|--------------------------------|----------------------------------|-----------------------|---------|----------------------------|
| LG1 | 17.54 | 7 | 16.802 | 81.66 | 0.10000 | 0.11230 | 0.1382 |
| " | " | " | 22.399 | " | 0.13132 | 0.10808 | 0.1536 |
| " | " | " | 27.995 | " | 0.19186 | 0.08837 | 0.1671 |
| F2 | 22.90 | 0 | 8.245 | 55.80 | 0.10815 | 0.09074 | 0.0509 |
| " | " | " | 10.994 | " | 0.13298 | 0.08728 | 0.0648 |
| " | " | " | 16.491 | " | 0.19780 | 0.08602 | 0.0981 |
| F3 | 23.97 | 21 | 16.753 | 59.10 | 0.13334 | 0.09896 | 0.1032 |
| " | " | " | 22.322 | " | 0.16640 | 0.10583 | 0.1295 |
| " | " | " | 27.873 | " | 0.22966 | 0.10370 | 0.1585 |
| " | " | " | 33.410 | " | 0.30201 | 0.10598 | 0.2279 |
| " | " | " | 38.882 | " | 0.44028 | 0.11119 | 0.2818 |
| F4 | 22.54 | 14 | 16.502 | 58.46 | 0.10003 | 0.08989 | 0.0468 |
| " | " | " | 27.504 | " | 0.18876 | 0.10246 | 0.0982 |
| " | " | " | 44.000 | " | 0.39897 | 0.09770 | 0.1646 |
| F6 | 24.26 | 7 | / | 56.49 | / | / | / |
| LR2 | 23.69 | 7 | 22.411 | 64.86 | 0.16885 | 0.08465 | 0.0383 |
| " | " | " | 33.615 | " | 0.29978 | 0.10030 | 0.0658 |
| " | " | " | 44.794 | " | 0.48154 | 0.11286 | 0.1351 |
| " | " | " | 50.285 | " | 0.66319 | 0.08643 | 0.1981 |
| LGR1 | 19.50 | 0 | 16.944 | 58.47 | 0.19628 | 0.10149 | 0.0411 |
| " | " | " | 22.578 | " | 0.21283 | 0.11518 | 0.0820 |
| LGR2 | 21.44 | 21 | 27.904 | 64.25 | 0.32497 | 0.08361 | 0.1168 |
| " | " | " | 39.056 | " | 0.52200 | 0.08865 | 0.1835 |
| LGR3 | 23.10 | 0 | 22.336 | 35.20 | 0.35019 | 0.08623 | 0.1555 |
| " | " | " | 27.893 | " | 0.80048 | 0.10187 | 0.1762 |
| LGR4 | 25.50 | 14 | 5.650 | 33.60 | 0.06870 | 0.10825 | 0.0846 |
| " | " | " | 11.254 | " | 0.21278 | 0.11436 | 0.1766 |

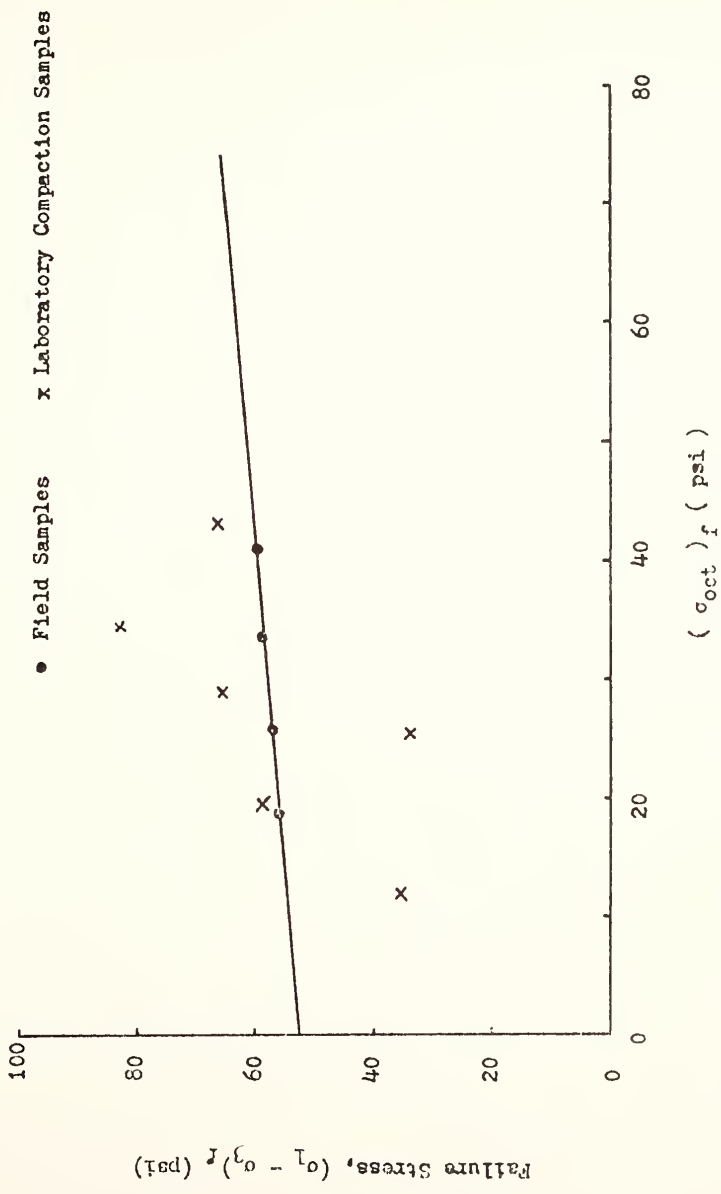


Figure 3.11 . Effect of Octahedral Normal Stress on Failure Strength

sample only. The material for the field sample was a mixture of the gray and reddish brown clays, and was probably more representative of whole embankment material. The apparent scatter in the figure arises because of the variation in moisture content of the laboratory compacted specimens shown. For a given water content, the appropriate envelope, parallel to that for the block sample can be constructed.

Figure 3.12 indicates the stress-strength ratio dependence of creep parameters and Poisson's ratio for embankment soils. In summary, the nonlinear material properties, C_1 , C_2 , and C_σ are plotted in Figures 3.13 and 3.14 respectively. When the applied stress is sufficiently small, C_1 and C_2 are approximately equal to one (Figure 3.13). This implies that the soil behaves as a linear viscoelastic material for this case, as indicated previously. Since the values of time factor, C_σ , decreases to very small value when the stress increases to high stress. It is more convenient to plot $-\ln(C_\sigma)$ against the stress-strength ratio, R , on a logarithmic scale. Figure 3.15 gives the three nonlinear material properties, C_1 , C_2 , and C_σ to logarithmic scales.

The parameters for the compacted embankment soils are obtained from the triaxial compression creep tests conducted on small specimens. The question then arises whether they can be directly applied to the analysis of the actual soil mass. Ramaswamy showed that there seems to be no scaling effect for compacted clay, at least for water contents and stress levels in the range of engineering practice.

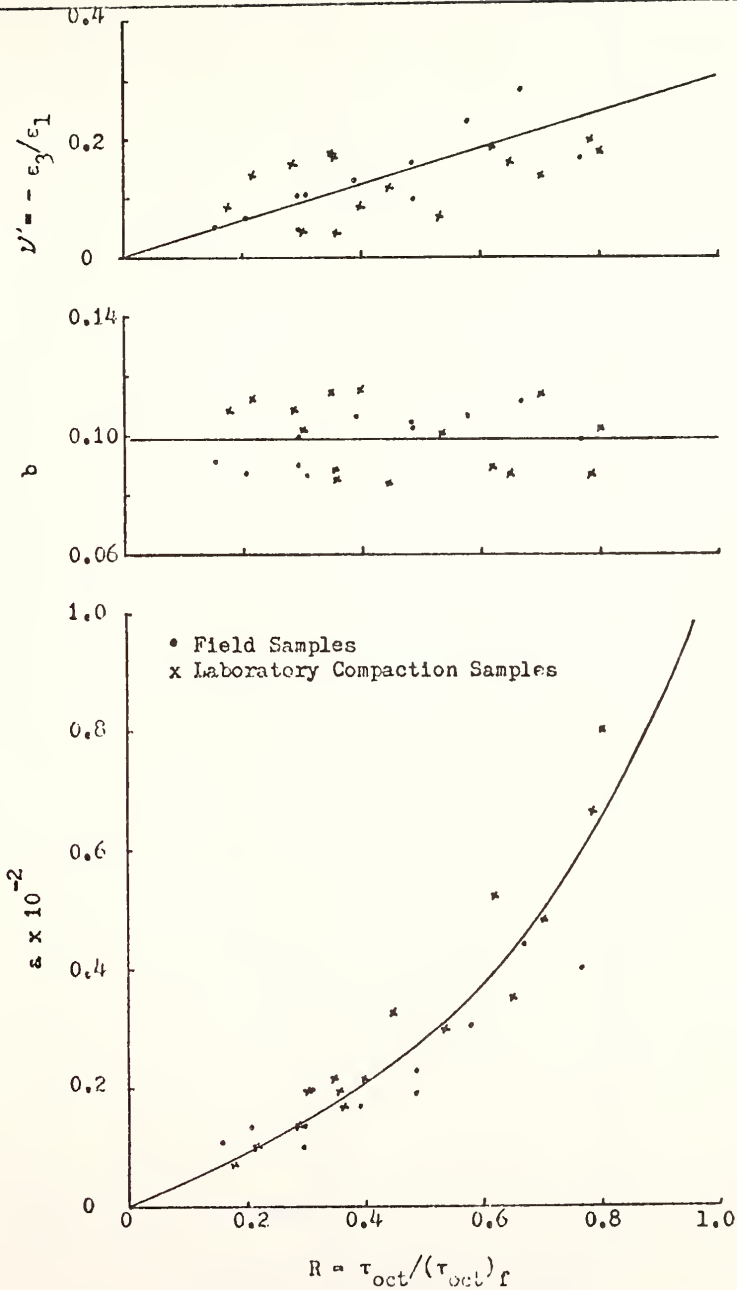
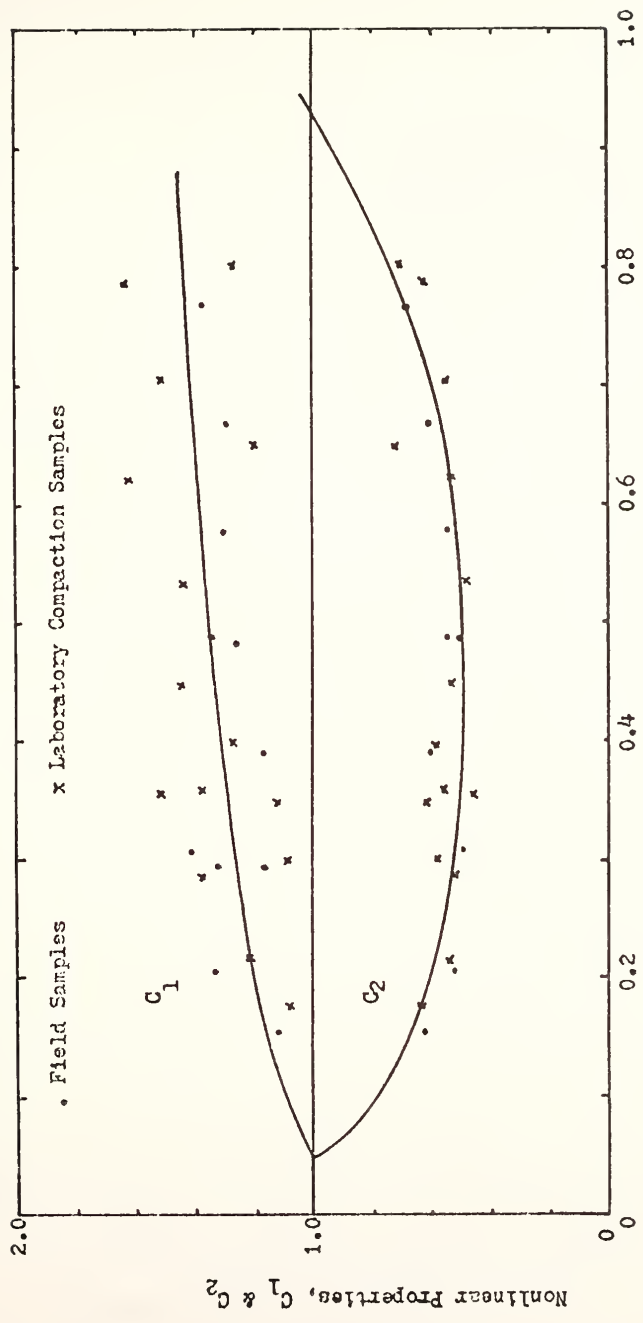
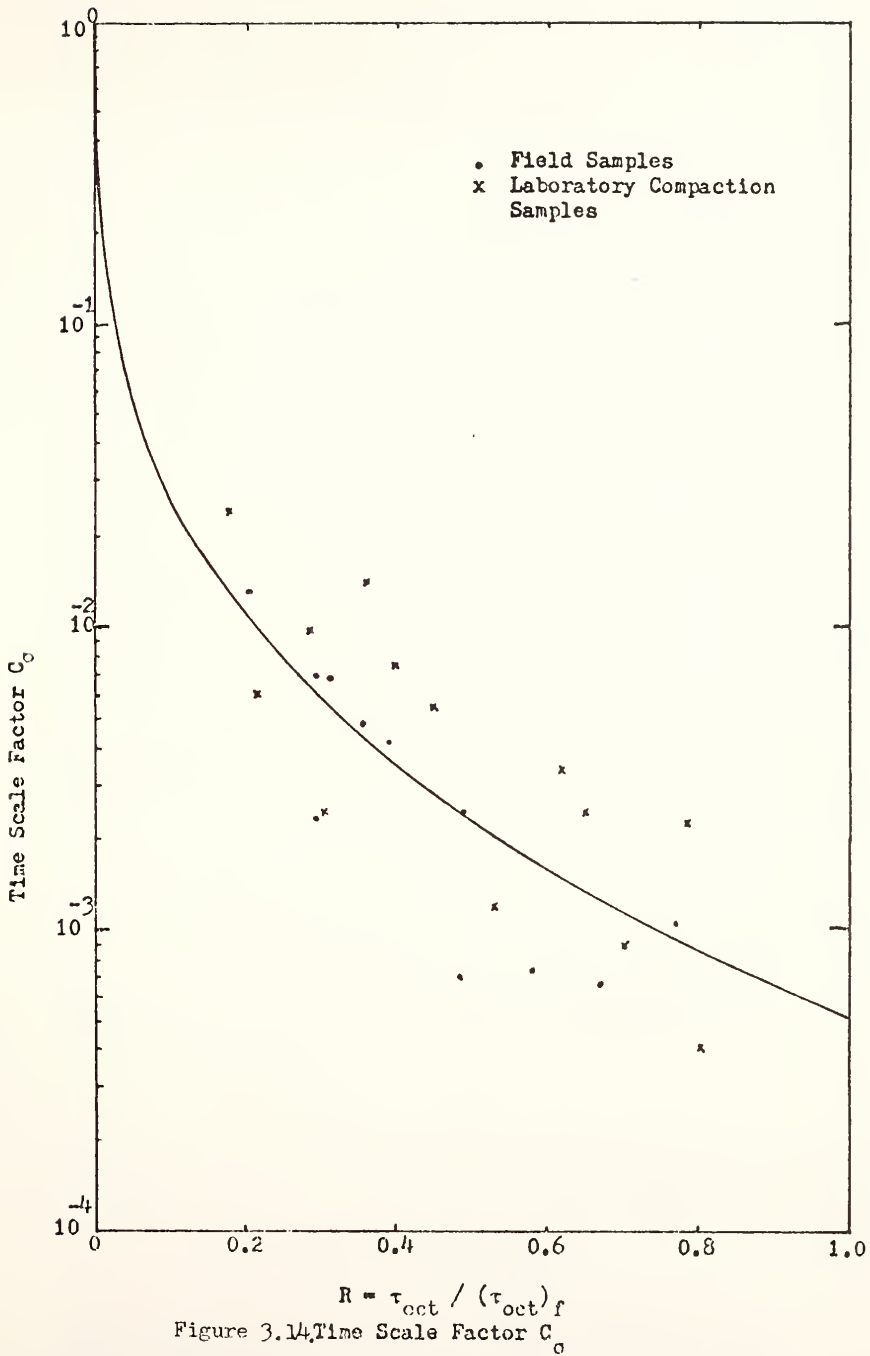


Figure 3.12 . Creep Parameters and Poisson's Ratio



$$R = \tau_{oct} / (\tau_{oct})_f$$

Figure 3.13, Nonlinear Material Properties C_1 and C_2



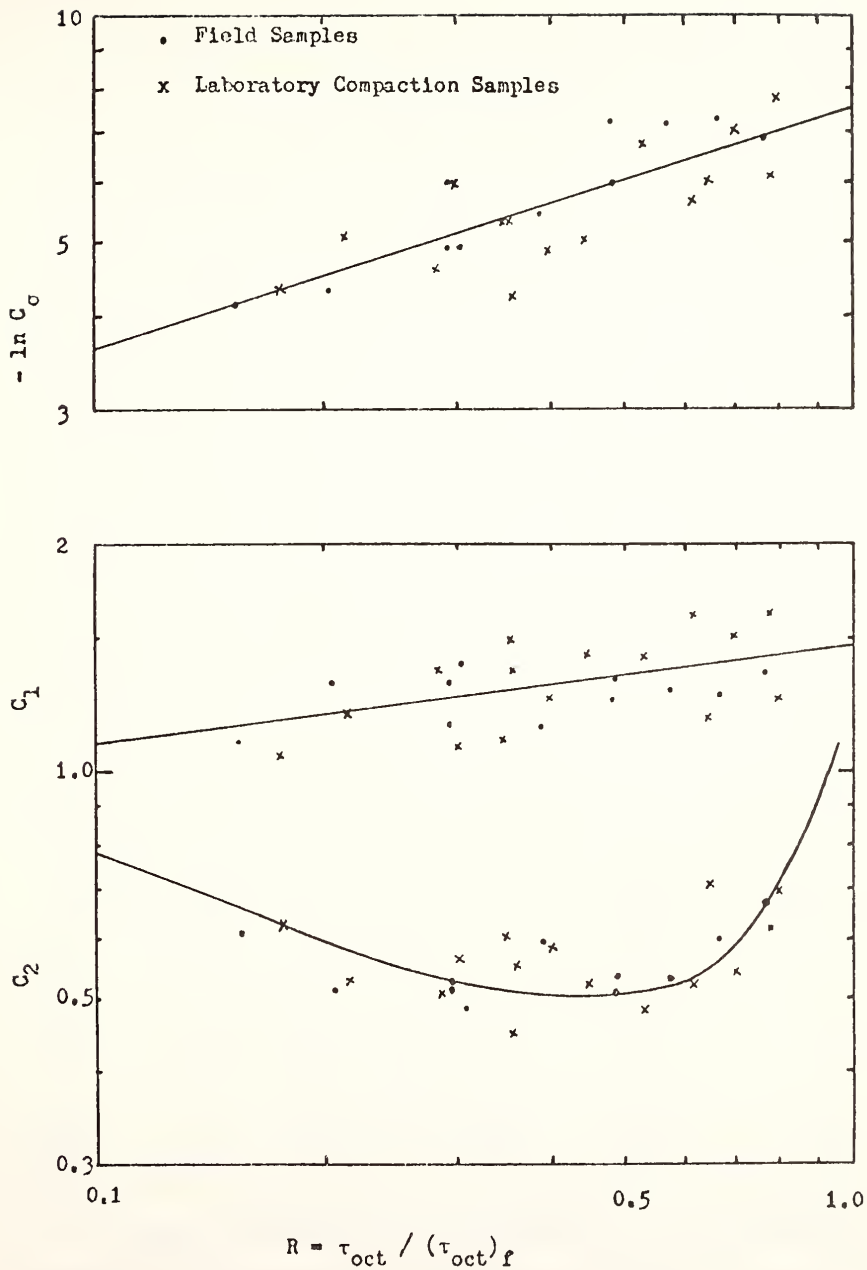


Figure 3.15. Nonlinear Material Properties C_1 & C_2 , and C_σ

The results of one-dimensional consolidation tests for foundation soils located at the center line of the embankment are shown in Table IV. In Table IV, the symbol FSB and FSA represent foundation soil samples taken before and after embankment construction, respectively. The shear strength shown in Table IV is obtained by using a CL-600 Torvane, developed by the Slope Indicator Co. and manufactured by Soiltest, Inc., Evanston, Illinois, at the end of the shelly tube samples. A typical unconfined compression curve is given in Figure 3.16. The field vane test results are shown in Figure 3.17. A comparison between Figures 3.16 and 3.17 shows that the average field vane strength is very nearly equal the value obtained in the laboratory test. It can be seen from Table IV that the strength of the soil at the center line of the embankment is greater than the average field vane strength, almost twice that value. It should be noted that the sensitivity of foundation silty clay was between 2 and 3.

Table IV Results of One-Dimensional Consolidation Test (At The Center)

| Specimen No. | σ_{vo}' (TSF) | P_c' (TSF) | C_c | C_r | Shear Strength (TSF) | C_v $\times 10^{-4}$ cm ² /sec |
|--------------|----------------------|--------------|-------|-------|----------------------|---|
| FSB-1 | 0.55 | 2.2 -2.7 | 0.344 | / | 0.45 | 4.2 |
| FSB-2 | 0.55 | 2.2 -2.7 | 0.340 | 0.025 | 0.45 | 4.0 |
| FSA-1 | 2.71 | 3.10 | 0.314 | 0.043 | 0.90 | 2.2 |
| FSA-2 | 2.71 | 3.00 | 0.319 | 0.040 | 0.90 | 2.4 |

A summary of one-dimensional consolidation test data is listed in Appendix E. The results of one-dimensional consolidation tests plotted on the arithmetic scale are given in Figure 3.18. The curves seem to be parallel after the effective stress exceeds the precompression pressure.

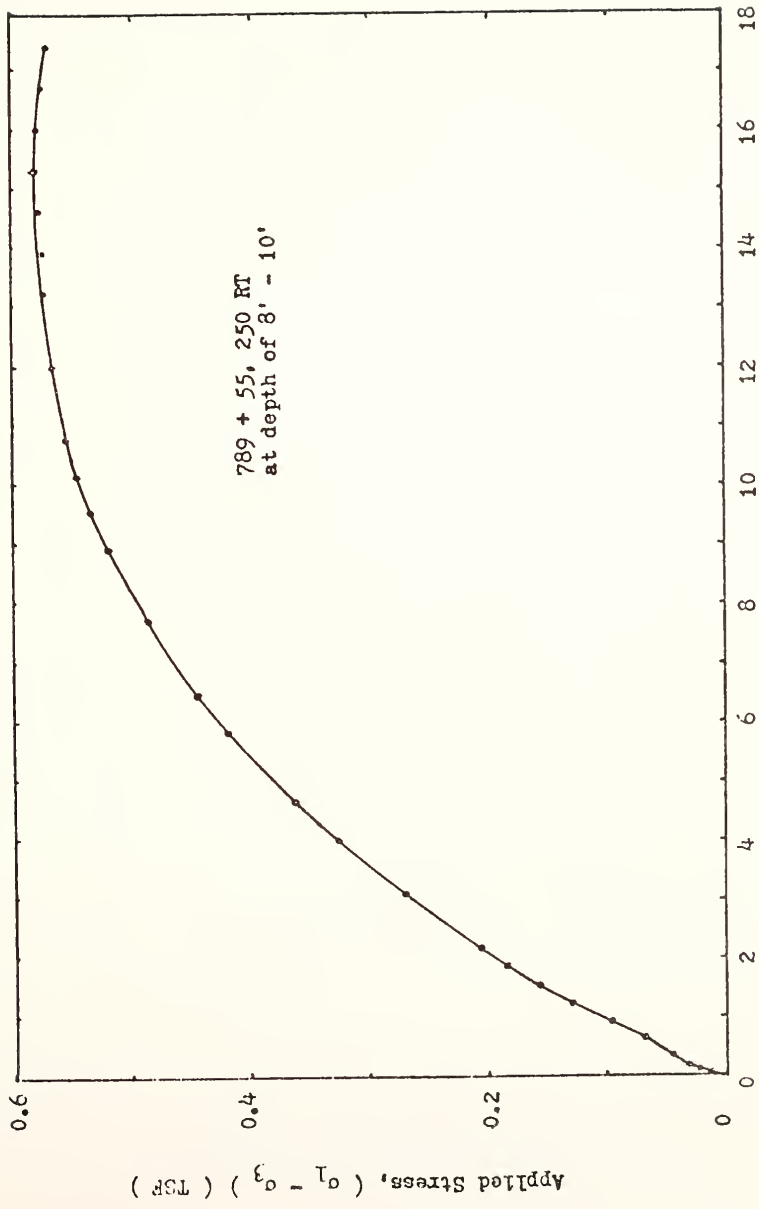


Figure 3.16, Unconfined Compression Test for Foundation Soil

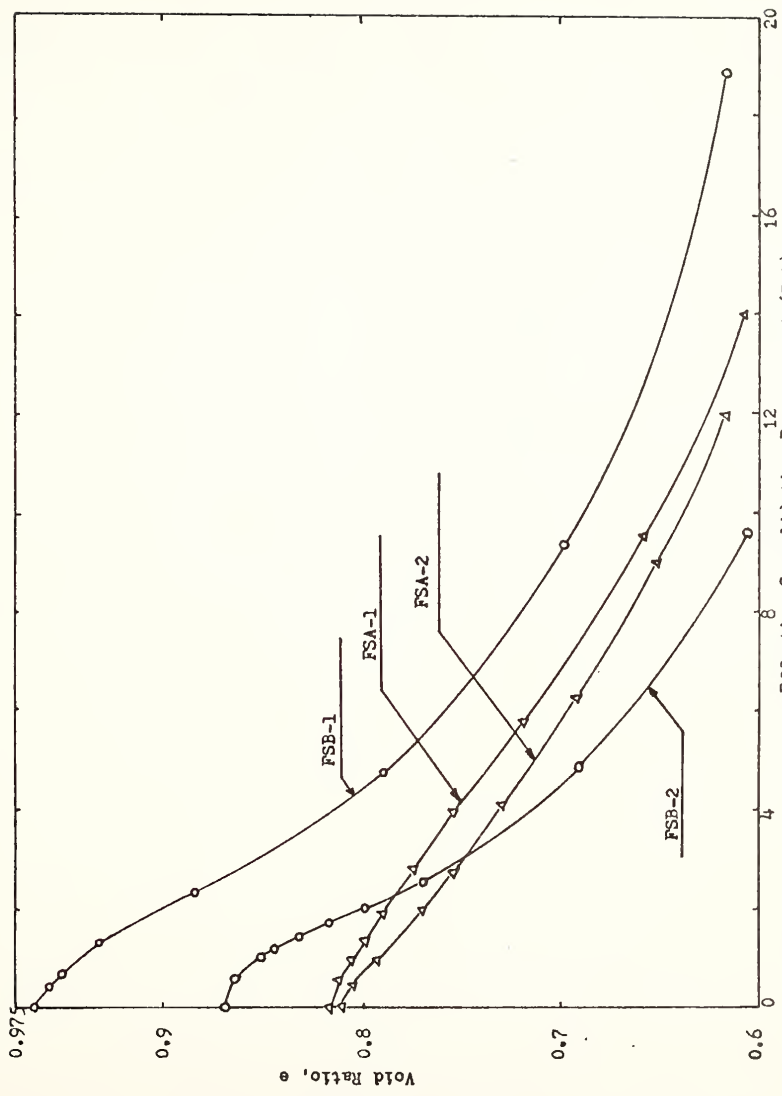


Figure 3.18. Relationship Between Effective Consolidation Pressure and Void Ratio

These data suggest that the constrained modulus can be obtained from the test results, independent of load increment, for specimens taken before embankment construction. Figure 3.19 shows the relationship between the effective stress and axial strain. The slope of this curve at each point is the constrained modulus. Figure 3.20 shows the relation between effective stress and constrained modulus for the soft clay.

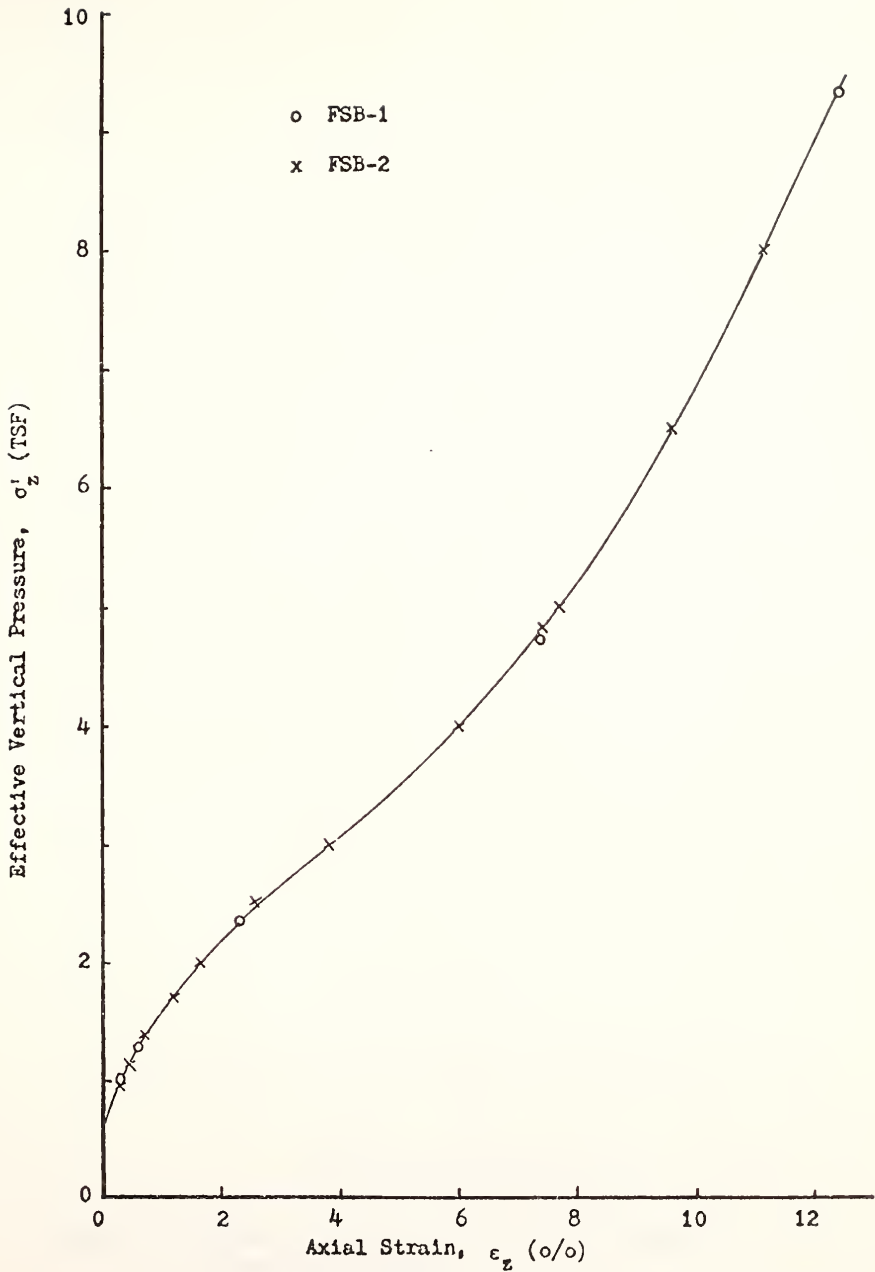


Figure 3.19 . Relationship Between Effective Vertical Pressure and Axial Strain

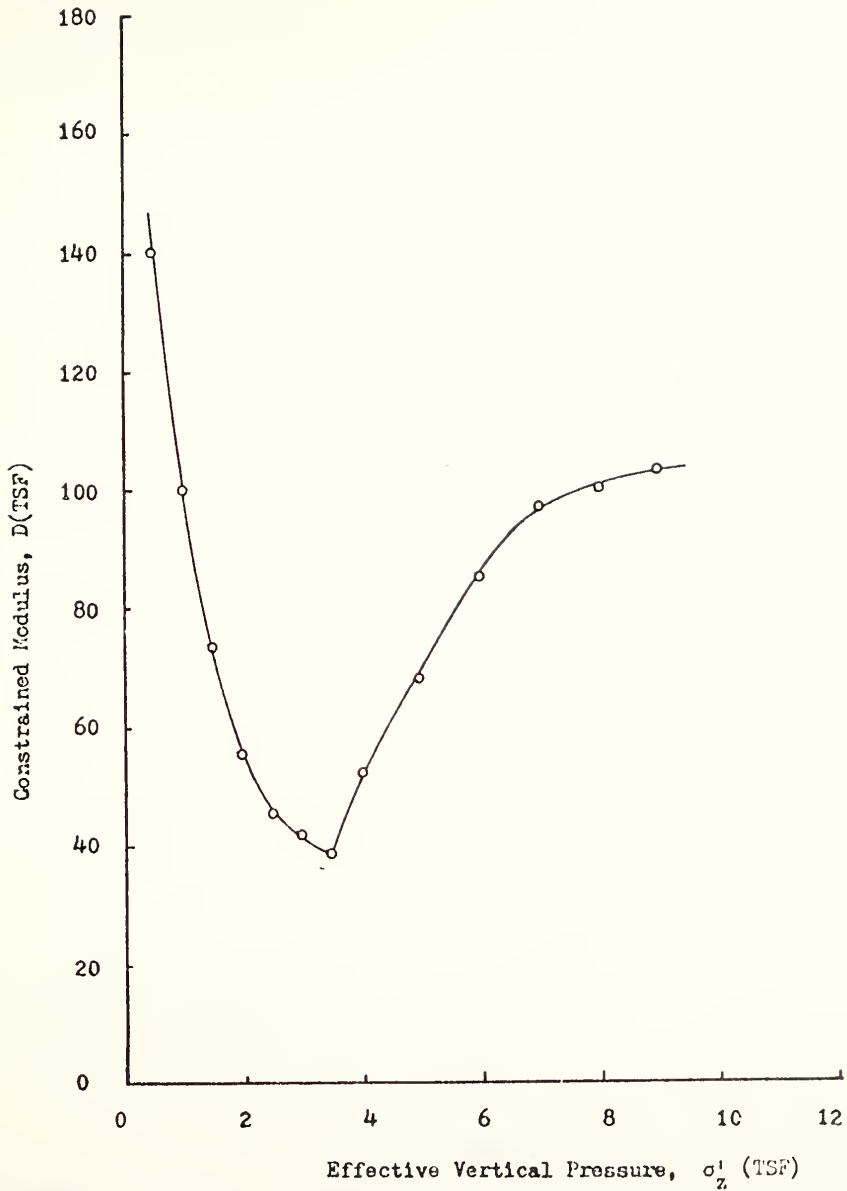


Figure 3.20. Effect of Effective Vertical Pressure on Constrained Modulus

CHAPTER IV
MEASURED PERFORMANCE OF THE TEST SECTION

4.1 Field Instrumentation

The test section studied herein begins at Station 789 + 00 and ends at Station 790 + 00. The test embankment is approximately 100 feet long by 310 feet left and right of the center line in cross section. It rises 40 feet above the original ground surface, which is roughly at elevation 504.50 feet, with a 12-foot thick berm. The embankment was constructed out of an available residual silty clay within the test section during a four and half month period starting on April 5, 1971. Outside the test section, the embankment was constructed of a locally blasted rock. Total unit weights of the fill were obtained during construction by the field engineers of ISHC, and from the relatively undisturbed block samples taken on August 2, 1972. Representative data are given in Table II (page 67). The average of all measured moist unit weights was close to 120 pcf. The saturated unit weight of foundation soft soils was also approximately 120 pcf. The factor of safety for completely undrained condition would be approximately close to unity.

The descriptions of detailed features in design, installation and operation of field instrumentation were given by DeGroof (1973). Figure 4.1 shows the fill elevation-time curve. The starting day in this figure was on April 5, 1971. In this figure, each curve is identified by a symbol. The curve for the test section is indicated by the symbol Δ .

FILL ELEVATION-TIME CURVE

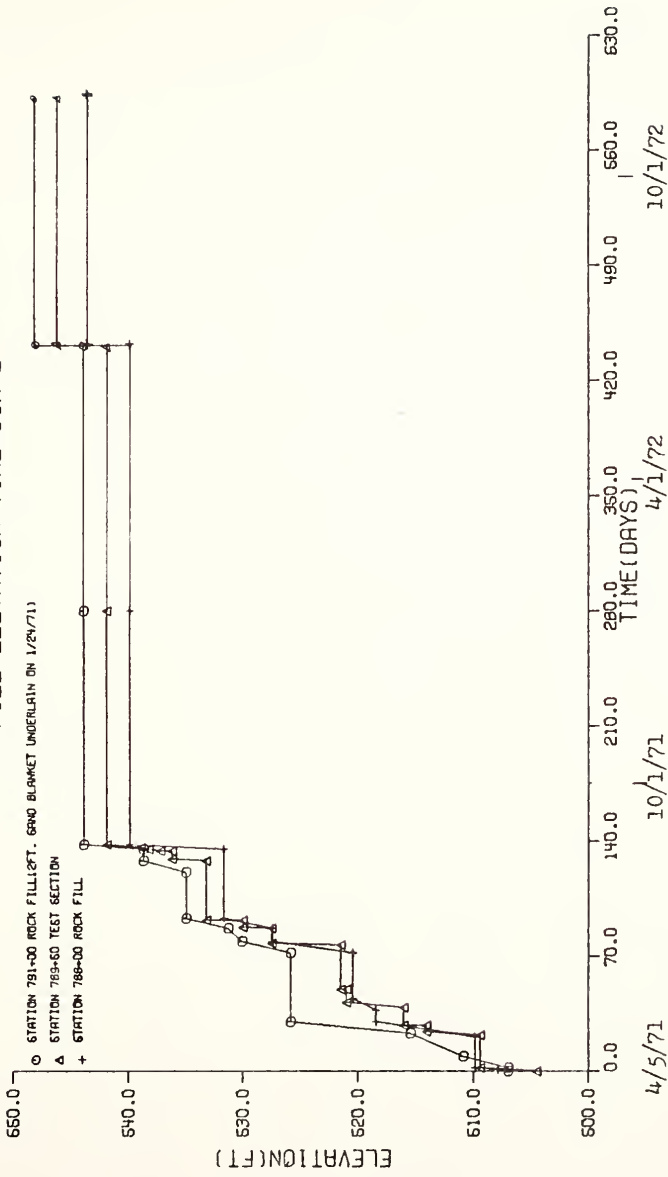


Figure 4.1. Fill Elevation-Time Curve

The fill in the test section was placed on April 5, 1971, at the original ground elevation of 504.5 feet. After two days, on April 7, the fill reached an elevation of 509.38 feet. There was no work during the next twenty days, up to April 27. Two days later, on April 29, the fill was added to elevation 514.06 feet, and remained at the same elevation until May 3. On that day, the fill reached elevation 516.00 feet. There was no work again till May 14. Another 4.94 feet, up to elevation 520.94 feet, was added gradually to the fill in the three days between May 14 and May 17. There was then no work till May 25. On that day, the fill was raised the elevation of 521.44 feet. No fill was added up to June 21. The fill reached elevation 533.15 feet on July 6. There was again no work done up to August 11. The final fill was placed gradually to the elevation of 541.8 feet on August 21, 1971. During June, 1972, the surface of the embankment was trimmed. The pavement was constructed on June 17, 1972. The pattern of the fill elevation against time curve for both the south and the north ends of the test section was similar to that for the test section. Before May 14, 1971, the fill in the south end was a little higher than that in the test section; after May 14, 1971, the fill in the south end was lower than that in the test section. At the north end of the test section, there was a two-foot sand blanket placed on January 24, 1971; and the fill was 4.38 feet higher than the test section during the period from May 5, 1971 to June 16, 1971.

Figures 4.2 to 4.5 show the instrumentation locations in the embankment and the foundation: 7 slope indicators, 12 spiral-foot settlement gauges, 4 hydraulic settlement gauges, 9 groups of three pressure plates and two bench marks. Figure 4.5a is a plan of boring and instruments.

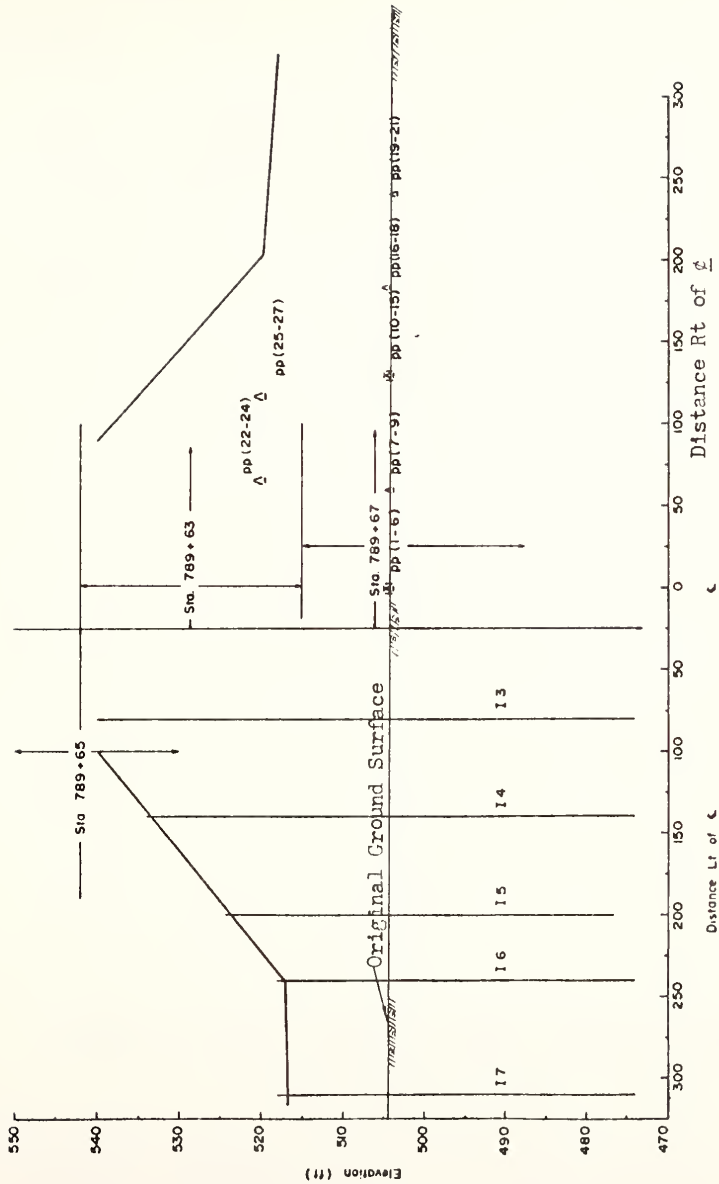


Figure 4.2. Slope Indicator 3-7 Locations and Pressure Plate Locations

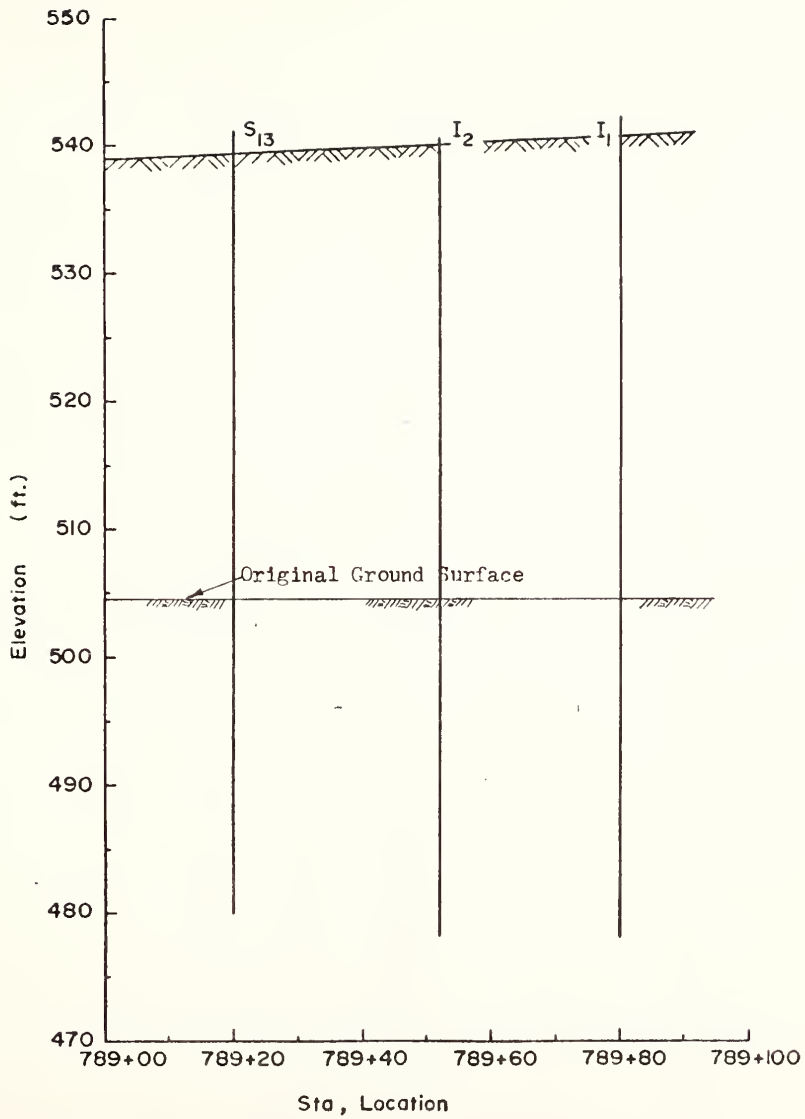


Figure 4.3. Spiral-Foot Number 13 and Slope Indicators Number 1 and 2

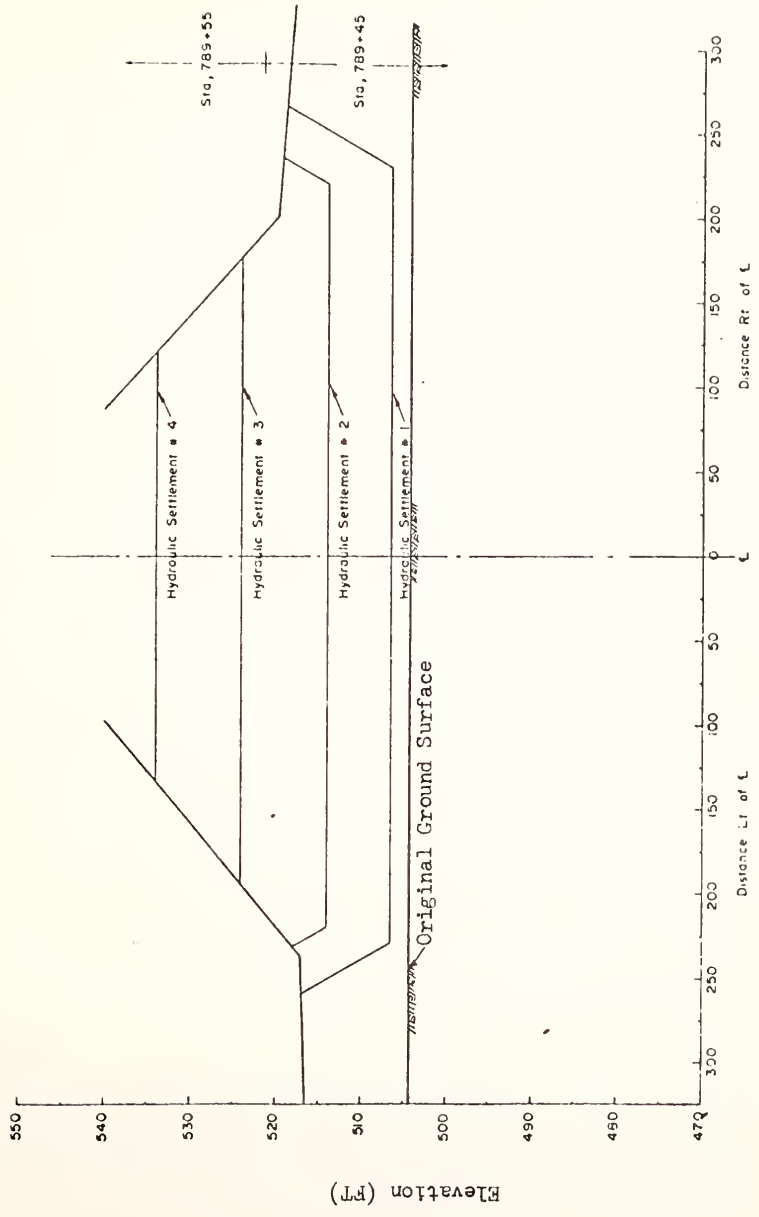


Figure 4.4. Hydraulic Settlement Gauge Locations

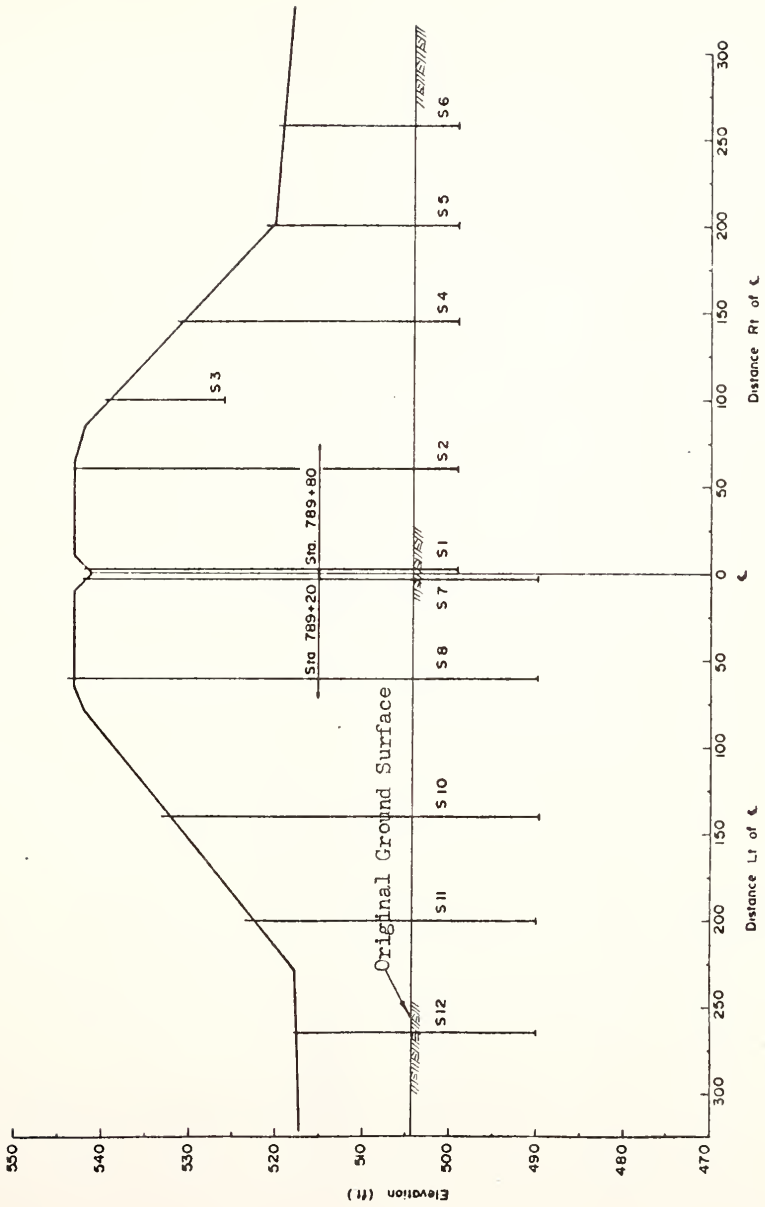


Figure 4.5. Spiral-Foot Locations

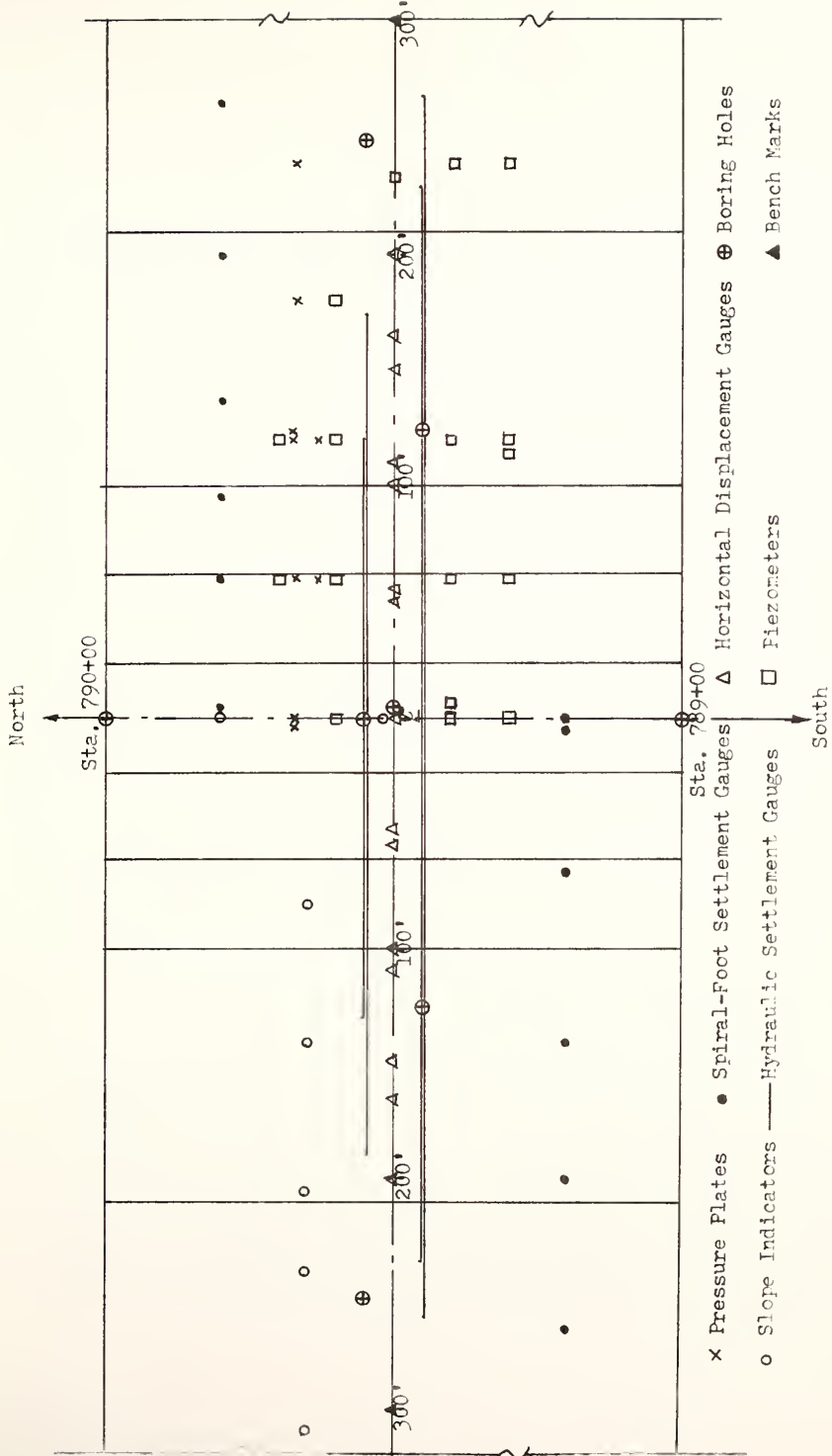


Figure 4.5a. Plan of Boring and Instruments

An instrument house was placed on the berm with the outside center of its west wall at Station 789 + 50, 232 feet right of the center line of the embankment.

4-2. Measured Stresses in the Embankment Fill

Gloetzl type pressure plates were used to measure the average normal pressure acting on a plate in a small region within the embankment. The plate which is 6 in. in diameter and $\frac{1}{4}$ in. thick, manufactured by Terrametrics, Inc., consisted of a double diaphragm cell filled with oil. There were two lines, an input and return, connected from each plate to the instrument house. When the input line pressure equaled that within the pressure plate, a small diaphragm valve would open permitting flow to the return line. Thus, the maximum pressure in the input line was the pressure in the plate. Further details are given by DeGroff (1973).

The stress state in the plane transverse to the embankment axis was computed from the average normal stresses on three plates oriented horizontally, 45° clockwise and counterclockwise, respectively, at one location.

The embedment procedure for the pressure plates was as follows. The soil was compacted to a height of 2-foot above the desired installation level and then a pit was dug to 6-inch below the desired elevation of the horizontal plate. A trench was cut leading from the pits to the instrument house. The bottom of the pit was carefully covered with damp sand formed so that the plates could be located by a template. The sand was replaced around the plates, and was compacted.

The template was removed; additional sand was placed and compacted to a depth of 18-inch above the horizontal plate. The pit was sealed by a plug consisting of a mixture of clay fill and bentonite. The tubes were connected to the manifold in the instrument house for a zero reading. The remaining portion of the pit was backfilled with the fill material. The trench was backfilled with the sand.

The state of stress for groups of three plates gives in Figure 4.6. By using a three-point stress rosette solution, the principal stresses may be obtained by the following equations [Terrametrics]:

$$\sigma_{\max} = \frac{\sigma_{ES} + \sigma_{WN}}{2} + \frac{\sqrt{2}}{2} \sqrt{(\sigma_{ES} - \sigma_v)^2 + (\sigma_v - \sigma_{WN})^2}, \quad (4-1)$$

$$\sigma_{\min} = \frac{\sigma_{ES} + \sigma_{WN}}{2} - \frac{\sqrt{2}}{2} \sqrt{(\sigma_{ES} - \sigma_v)^2 + (\sigma_v - \sigma_{WN})^2}, \quad (4-2)$$

and the angle between σ_{ES} and σ_{\max} is

$$\tan(2\alpha) = \frac{\sigma_v - \frac{1}{2}(\sigma_{ES} + \sigma_{WN})}{\sigma_{ES} - \frac{1}{2}(\sigma_{ES} + \sigma_{WN})} \quad (4-3)$$

where

σ_{ES} = stress acting on the plate inclined 45° with the horizontal line in the east or south directions,

σ_{WN} = stress acting on the plate inclined 45° with the horizontal line in the west or north directions,

σ_v = stress acting on the horizontal plate.

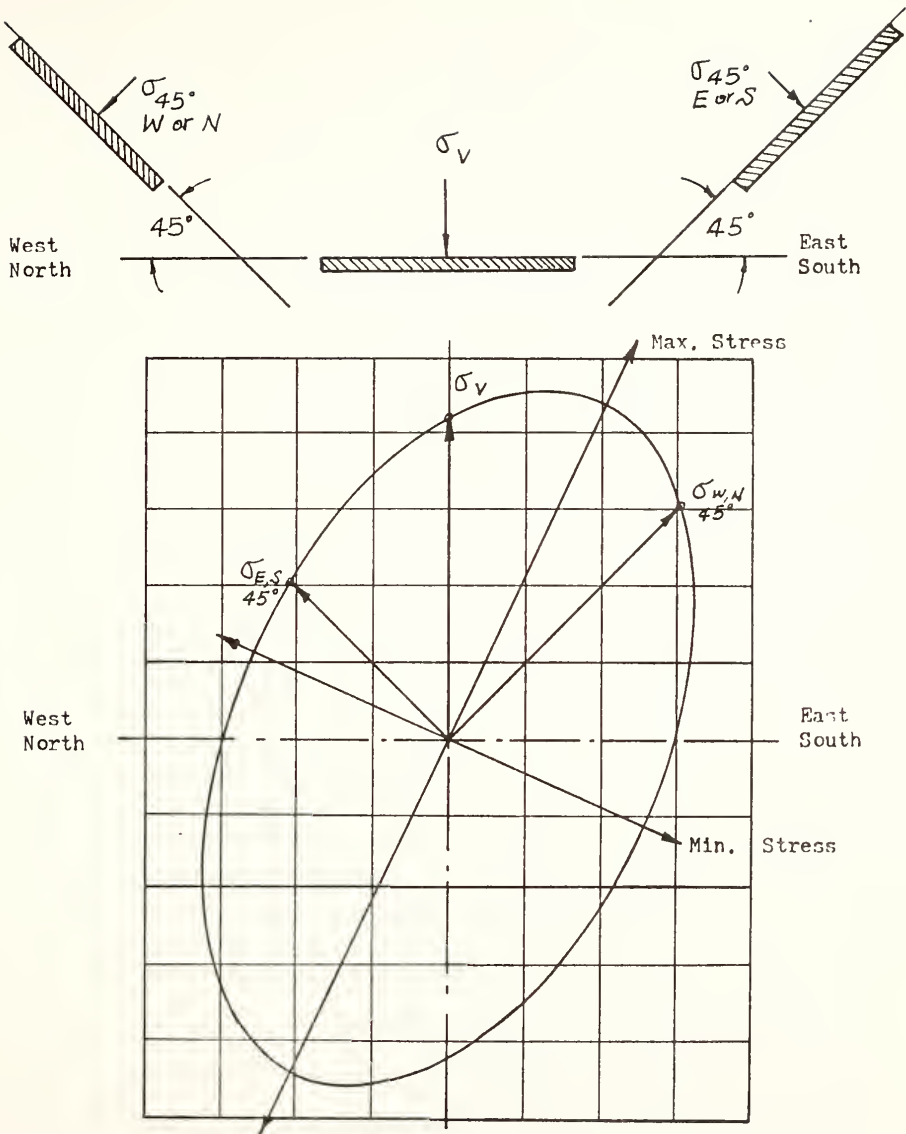


Figure 4.6. The State of Stress for a Group of Plates

Figure 4.7 shows a summary of the total stresses measured within the embankment fill. The initial reading for each plate was determined at the time of installation, and was corrected for elevation difference between the readout device and the plate. For the determination of total pressure at a given time, it was simple to subtract the reading at that time from the initial reading. It should be noted that the time scale is not the same as that shown in the fill elevation-time curve (Figure 4.1). Zero time shown in the figure was the day of installation.

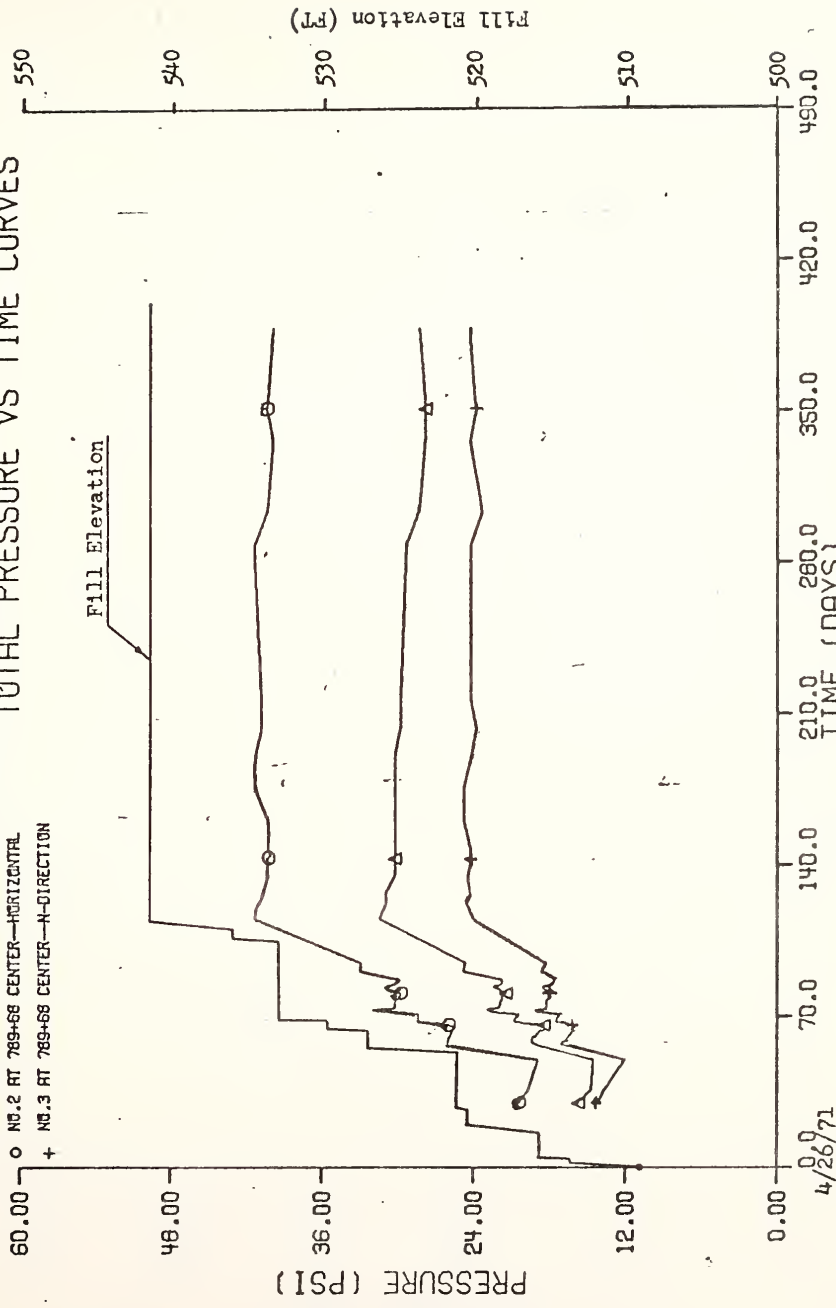
Each curve is identified by a symbol. For clarity only a few data points are indicated by symbols. Each curve also shows the maximum and minimum stresses calculated by equations (4-1) and (4-2).

Total pressure plates No. 1 to No. 21 were located at the base of the embankment; No. 22 to No. 27 were at elevation 519.00 feet, the mid-height of the embankment.

After the end of embankment construction, stresses at points close to the center line along the base of the embankment remained almost constant. At points away from the center line of the embankment near the original ground surface, stresses decreased with time after construction. The effect is especially pronounced for plates No. 16 to No. 18 and No. 19 to No. 21. By contrast, stresses at the points along elevation 519.00 feet remained almost constant. The probable explanation for this apparent anomaly can be deduced from the detailed examination of events indicated in Figure 4.8. The figure shows the elevation of the top of the test fill, the top of the rock fill just north of the test section, the ground water table at the north end of rock fill and

TOTAL PRESSURE VS TIME CURVES

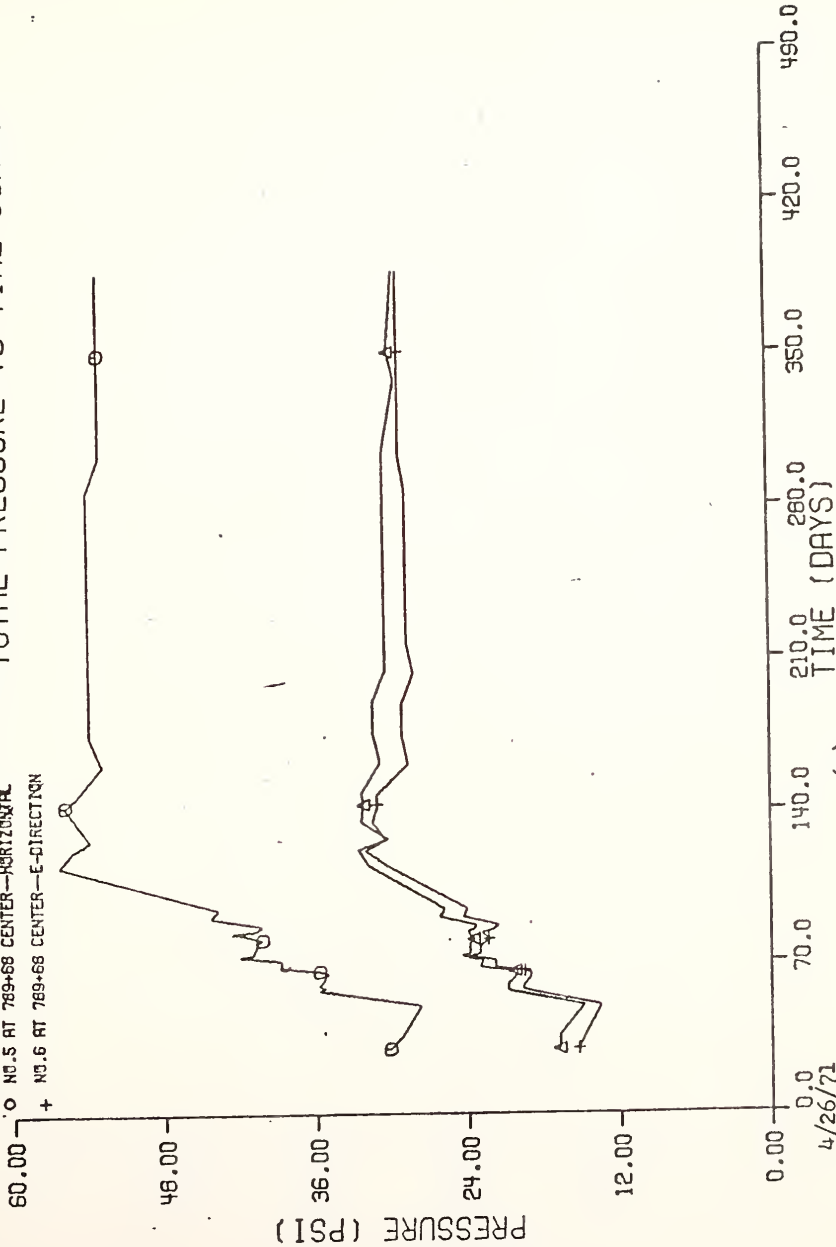
Δ NO.1 AT 789+68 CENTER—S-DIRECTION, ELEV.=505.50, INST.DRY=4/20/71
 ○ NO.2 AT 789+68 CENTER—HORIZONTAL
 + NO.3 AT 789+68 CENTER—N-DIRECTION



(a) Figure 4.7. Total Stresses

TOTAL PRESSURE VS TIME CURVES

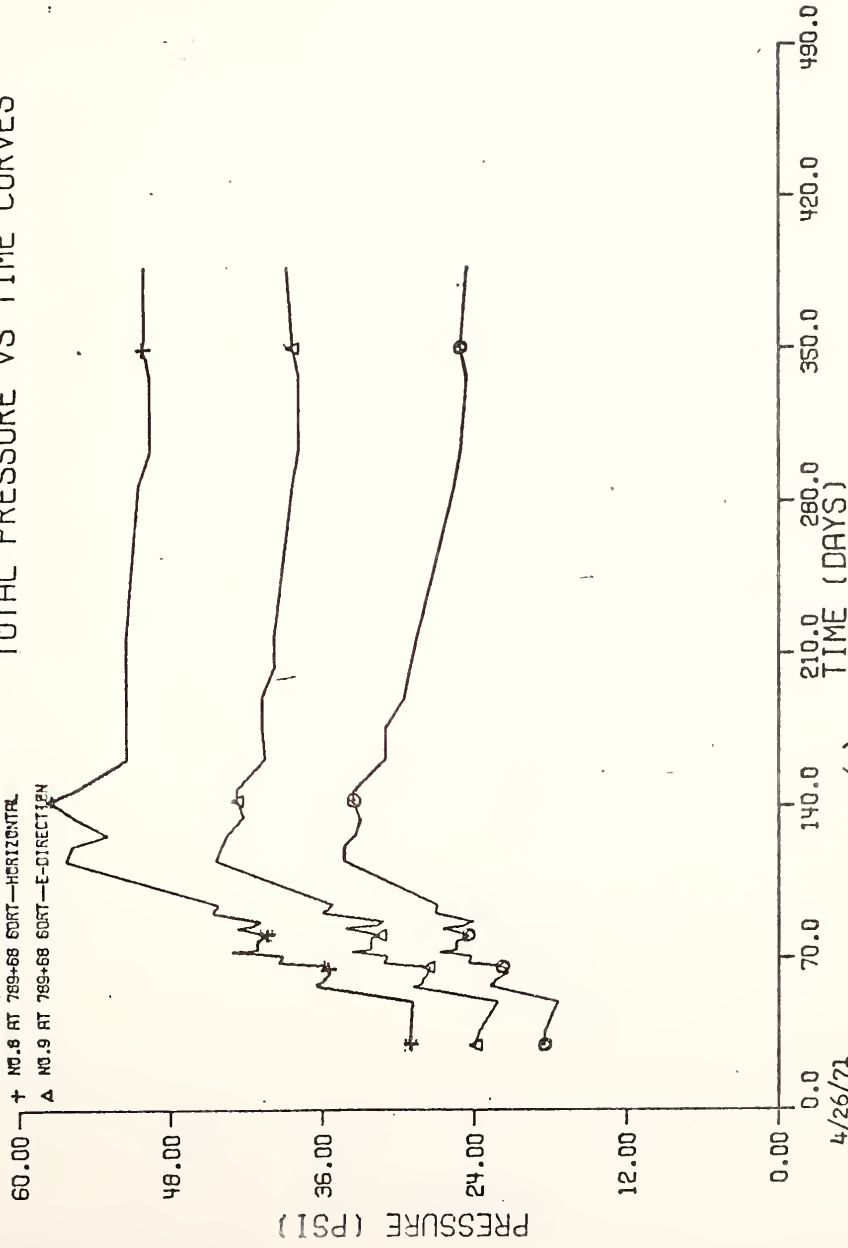
▲ NO. 4 AT 789+68 CENTER—W-DIRECTION, ELEV.=505.50, INST. DAY=4/20/71
 ○ NO. 5 AT 789+68 CENTER—HORIZONTAL
 + NO. 6 AT 789+68 CENTER—E-DIRECTION



(b).

Figure 4.7. Total Stresses

NO. 7 AT 789+66 SORT—H-DIRECTION. ELEV.=505.50. INST. DRAY=4/22/71
TOTAL PRESSURE VS TIME CURVES

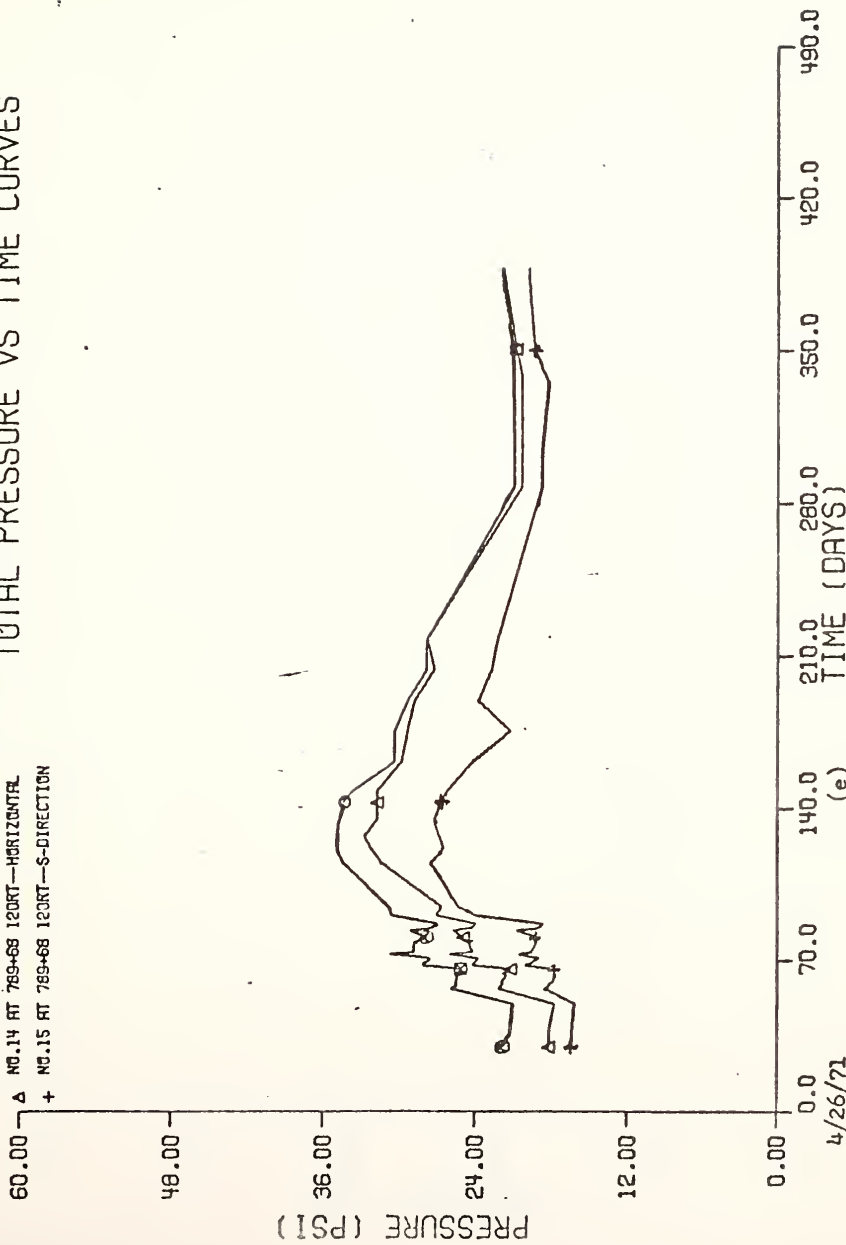


(c)

Figure 4.7. Total Stresses

TOTAL PRESSURE VS TIME CURVES

O NO.13 AT 789+68 120RT—N-DIRECTION, ELEV.=505.50, INST.DRY=4/23/71
 A NO.14 AT 789+68 120RT—HORIZONTAL
 + NO.15 AT 789+68 120RT—S-DIRECTION



4/26/71
(e)
Figure 4.7. Total Stresses

○ NO.16 AT 769+68 160RT→H-DIRECTION, ELEV.=505.50, INST.DRY=4/23/71
 TOTAL PRESSURE VS TIME CURVES
 ▲ NO.17 AT 769+68 160RT→HORIZONTAL
 + NO.18 AT 769+68 160RT→E-DIRECTION

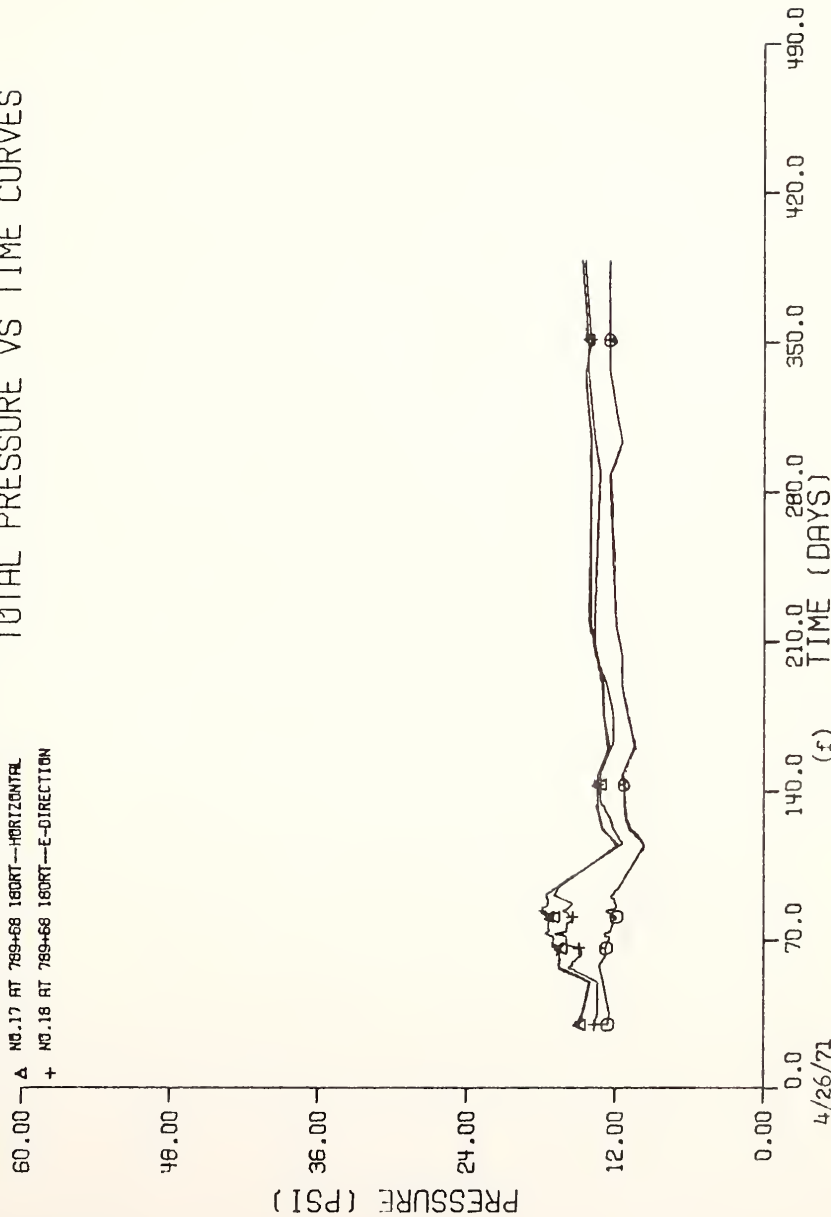


Figure 4.7. Total Stresses

4/26/71

○ NO.19 RT 789-65 2VORT-H-DIRECTION, ELEV.=504.50, INST.DRY=4/26/71
 △ NO.20 RT 789-65 2VORTE-HORIZONTAL
 + NO.21 RT 789-65 2VORTE-H-DIRECTION

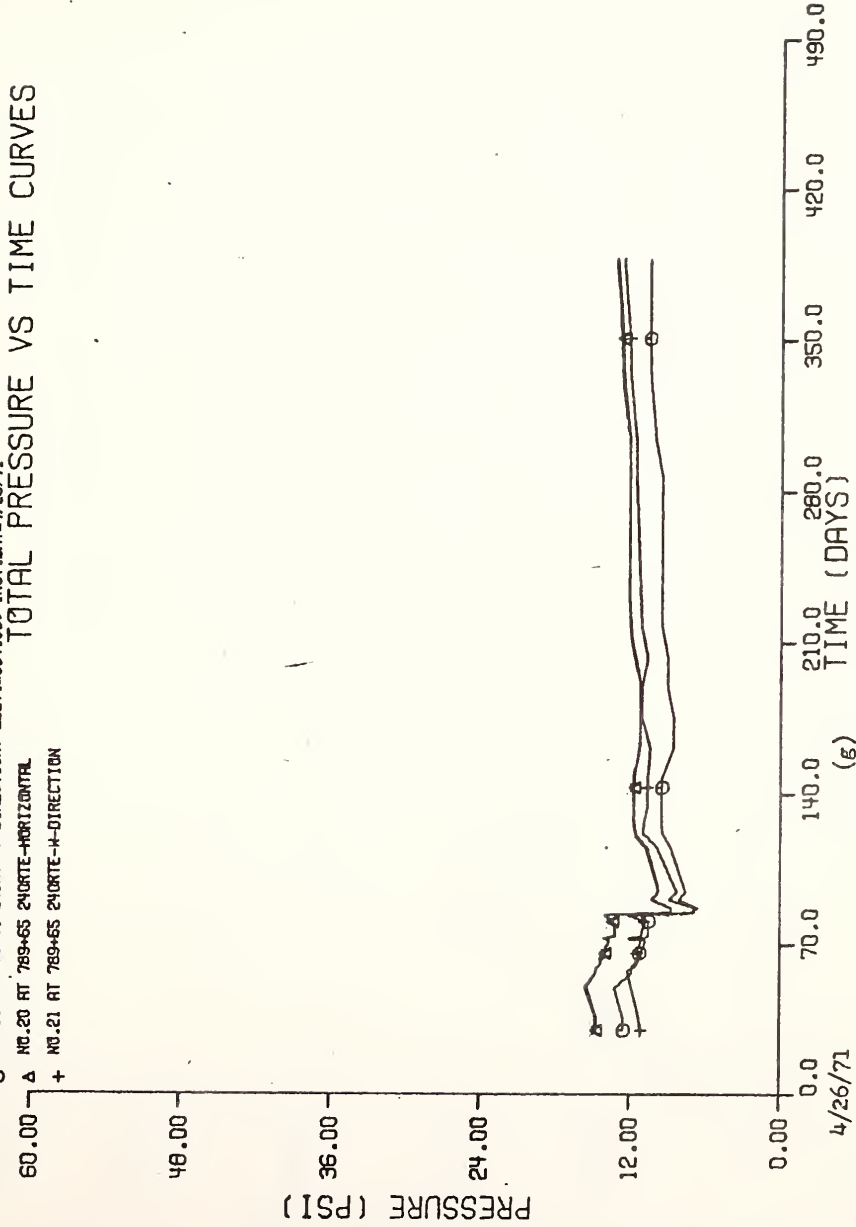


Figure 4.7. Total Stresses

O NO. 22 AT 789+62 60RT—H-DIRECTION. ELEY.=519.00. INST. DAY=6/08/71
 A NO. 23 AT 789+62 60RT—HORIZONTAL
 + NO. 24 AT 789+62 60RT—E-DIRECTION

TOTAL PRESSURE VS TIME CURVES

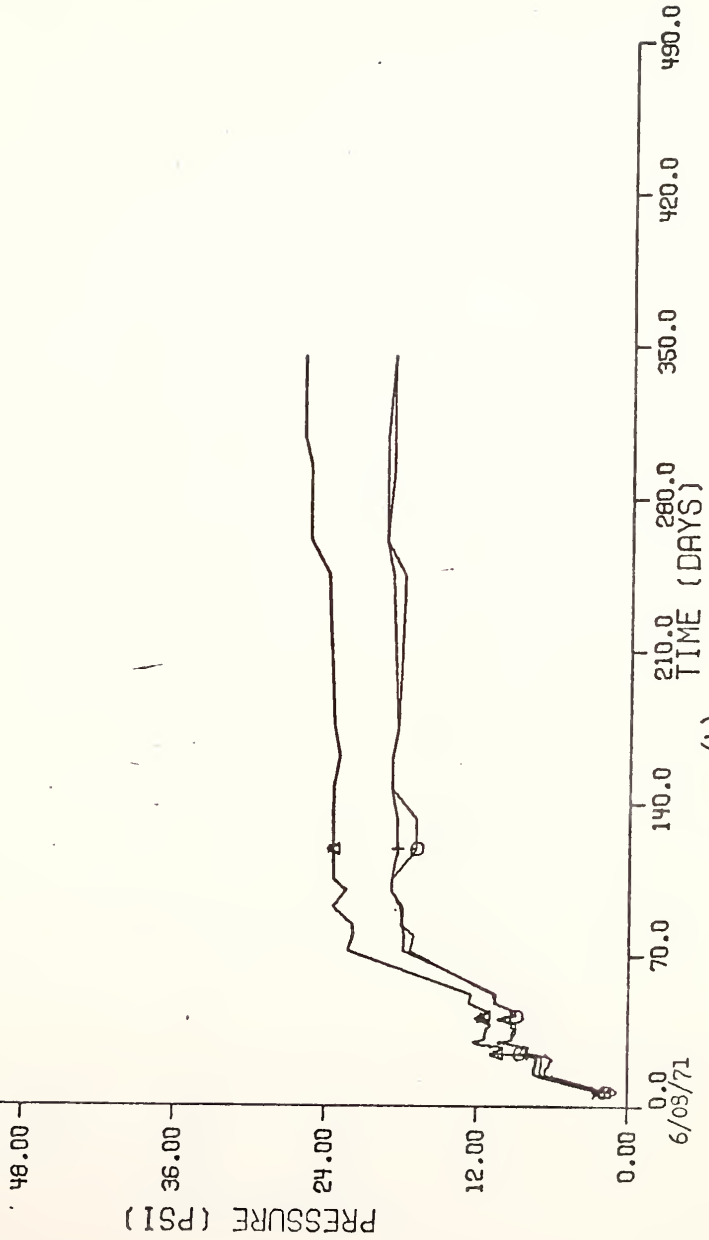
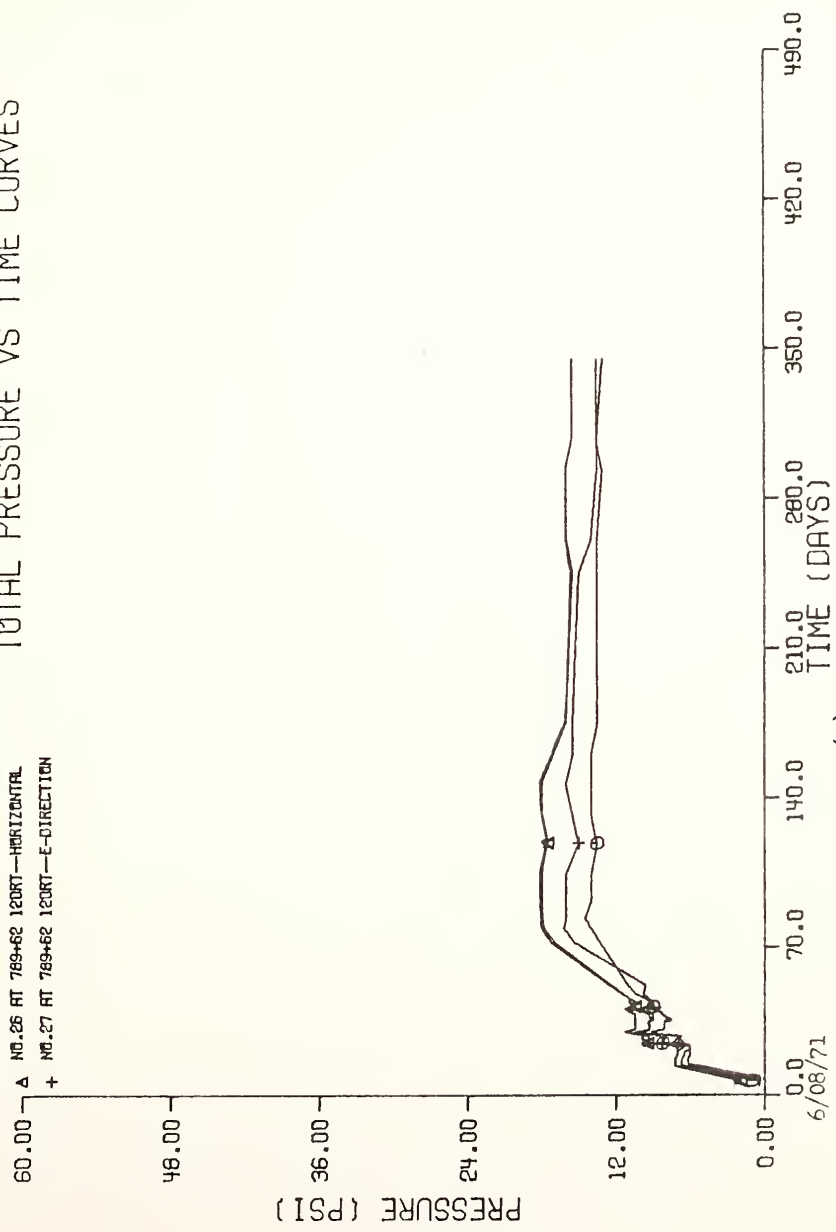


Figure 4.7. Total Stresses (h)

TOTAL PRESSURE VS TIME CURVES

O NO.25 AT 769+62 120RT—H-DIRECTION. ELEV.=519.00. INST. DAY=6/08/71
 A NO.26 AT 769+62 120RT—HORIZONTAL
 + NO.27 AT 769+62 120RT—E-DIRECTION



(1)
Figure 4.7. Total Stresses

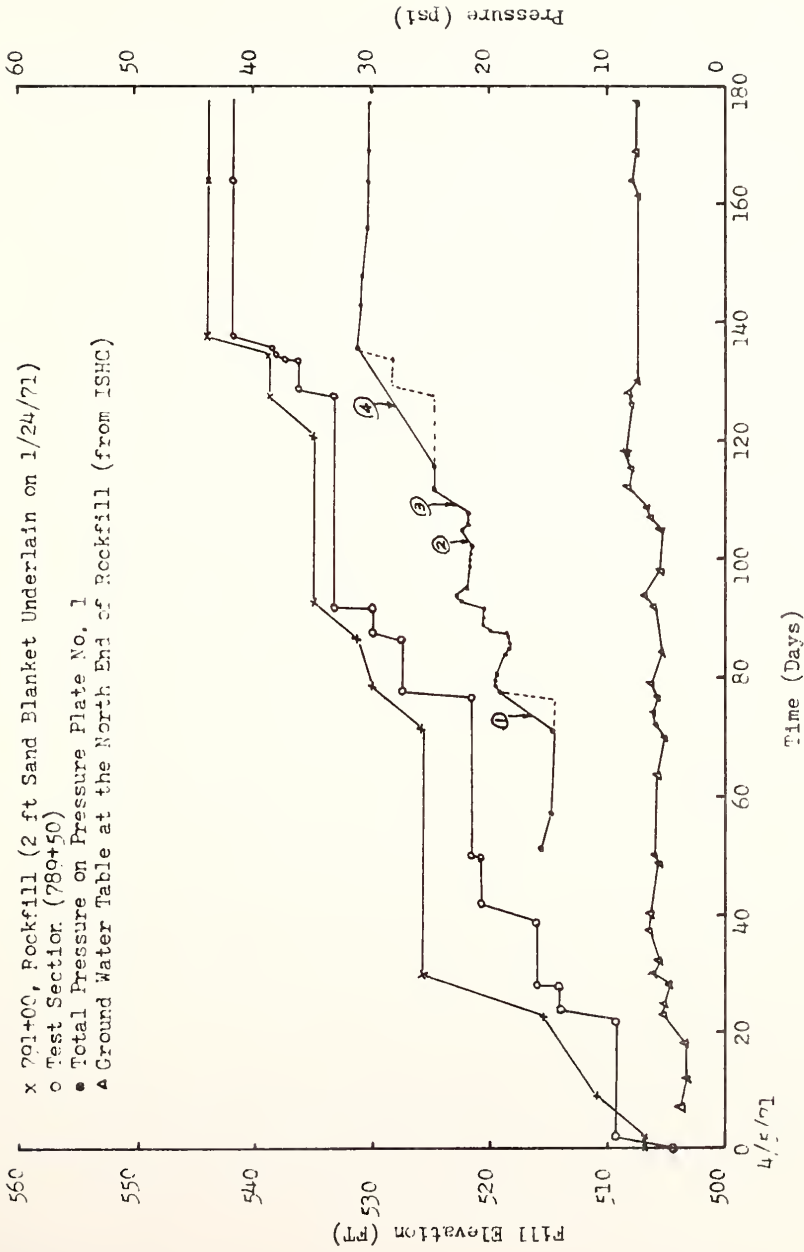


Figure 4.8. Total Pressure and Fill Elevation Diagrams

the measured vertical pressure near the center line at elevation 505.50 feet as a function of time.

The vertical pressure increases, as expected, as the test fill elevation increases. In general, however, the vertical pressure decreases when the fill height remains constant. This appears to occur because of two related factors:

- (1) The rockfill outside the test section was thicker during most of the construction period than the fill in the test section. Thus consolidation just outside the test fill occurred earlier than beneath the test fill. This effect was augmented by the relatively rapid consolidation due to the free draining rockfill to the south, and sand drains installed under the rockfill to the north.
- (2) The test fill is relatively thin compared to its 100-foot length. This is illustrated in Figure 4.9, which shows the rockfill and test fill elevations at 70 and 90 days after construction. Thus the tendency for differential settlement induces the test fill to act as a beam with restrained ends. The consequence of this beam action is a reduction in vertical stress as the foundation deforms.

The magnitude of the stress reduction would be expected to depend on the tendency for differential settlement between the midplane of the fill and its north and south boundaries. This tendency is greatest at the base of the fill below the left and right slopes and smaller near the centerline, as well as at higher elevations in the fill. This rationale is borne out by the observations, as indicated in Figure 4.7.

—— 70 Days
- - - 90 Days

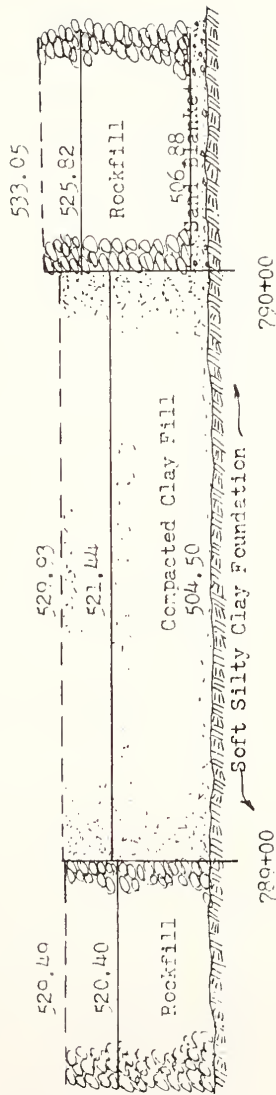


Figure 4.0. Fill Elevation For N-S Direction At 70 Days (June 14, 1971) and 90 Days (July 4, 1971)

There are four times shown in Figure 4.8 during which the measured vertical pressure does not follow the pattern described above, but rather appears to increase for some time, even though the fill height remains constant. These are labelled points ① - ④ in Figure 4.8. In the case of points ① and ④, it appears that the absence of readings at the times when the fill heights were changing is the reasonable explanation. Thus the probable actual stress have been sketched on the diagram as dashed lines.

In the case of points ② and ③, an increase in vertical pressure under constant external load was actually observed. This likely arose from the increase in ground water table elevation which occurred at these times. The tendency for greater rebound beneath the midplane of the embankment than at the north and south boundaries was counteracted by the beam action of the fill along its longitudinal axis. This probably led to the temporary increase in measured stress.

The field data for total pressure plates are listed in Appendix G-1.

4-3. Measured Vertical Movements

Two types of instruments were used to measure the vertical settlements: spiral-foot settlement gauges for points within and below the embankment, and hydraulic settlement gauges for points along horizontal lines within the embankment.

The spiral-foot gauge developed by Bozozuk (1968) consists of a spiral-foot attached to a datum rod. The gauge was installed by drilling a hole to within six inches of the desired measurement depth. The gauge was then screwed into the soil for the remaining six inches. Other

installation details are given by DeGroff (1973). During the embankment construction, the datum rod and protective casing were extended with the fill. There are eleven gauges in the foundation and only one in the embankment.

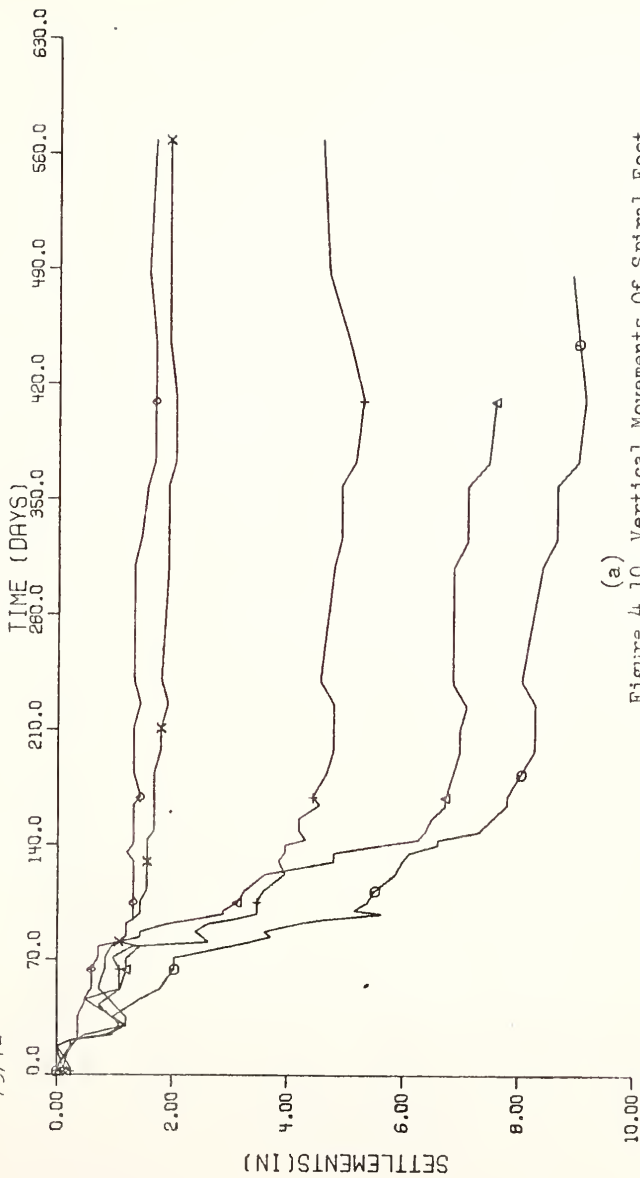
After the installation of each gauge, initial elevations were taken by a level to 0.01 ft from bench marks placed each on either side of the test section. At various time intervals, elevation readings were taken and subtracted from the initial reading to get the settlement at that time.

Vertical movements of the spiral-foot settlement gauges are summarized in Figure 4.10. The Purdue University's CDC 6500 computer and CALCOMP plotting system were used to produce all the curves. Each curve is identified by a symbol. For clarity, only a few data points are indicated by symbols. Each figure gives settlements at a specific elevation. Figure 4.10(a) shows the vertical movements at elevation 499.00 feet at the upper one-third of the soft silty clay layer, Figure 4.10(b) at elevation 490.00 feet at the bottom of the soft silty clay layer, Figure 4.10(c) at the center of elevation 481.00 feet at the thin medium silty clay layer, Figure 4.10(d) at the point, 95-foot right of the center at elevation 526.50 feet, within the embankment. At the end of the embankment construction, August 21, 1971, a total of 6.60 inches of settlement was measured at the upper one-third of soft silty clay layer of the center line (S-1). During the next one year another 2.28 inches of settlement took place, given a total vertical displacement of 8.88 inches by August 2, 1972 (last reading in this gauge). The embankment settled quite uniformly within a 70-foot distance left and

TIME-SETTLEMENT CURVE

O SPIRAL FOOT SETTLEMENT GAUGE NO. 1 RT 789+60 3RT(499.01)
 A SPIRAL FOOT SETTLEMENT GAUGE NO. 2 RT 789+60 1BRT(499.01)
 □ SPIRAL FOOT SETTLEMENT GAUGE NO. 3 RT 789+60 2BRT(499.01)
 △ SPIRAL FOOT SETTLEMENT GAUGE NO. 5 RT 789+60 2BRT(499.01)
 X SPIRAL FOOT SETTLEMENT GAUGE NO. 6 RT 789+60 2BRT(499.01)

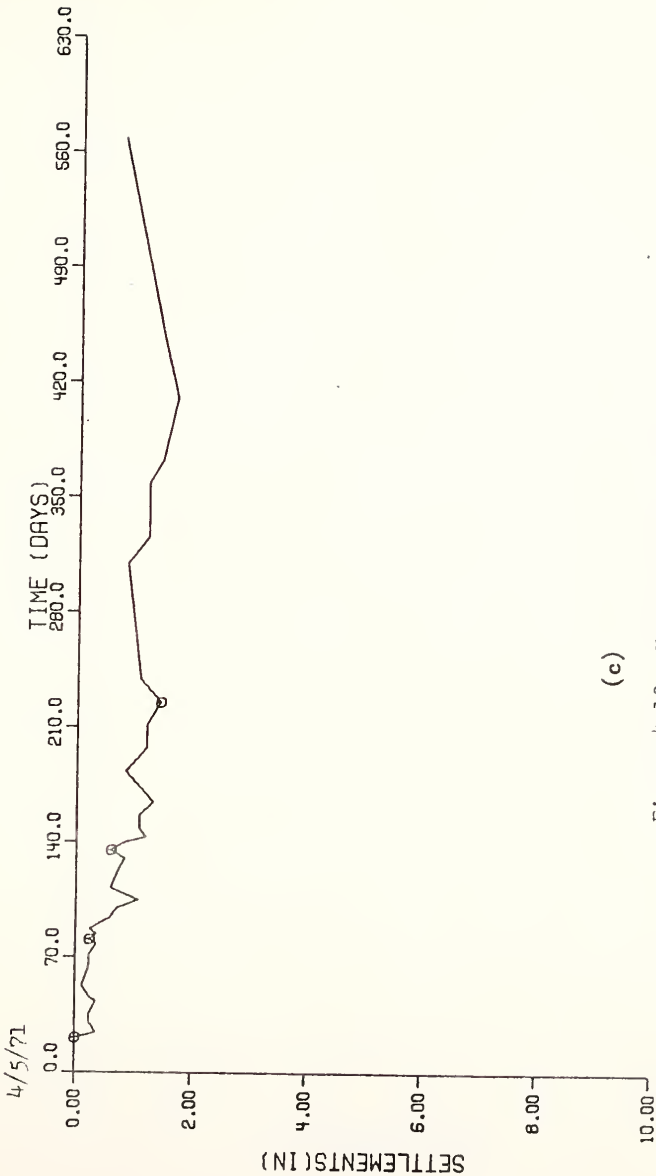
4/5/71



(a) Figure 4.10. Vertical Movements Of Spiral-Foot

o SPIRAL FOOT SETTLEMENT GAUGE NO.13 AT 789+20 CENTER (481.0)

TIME-SETTLEMENT CURVE

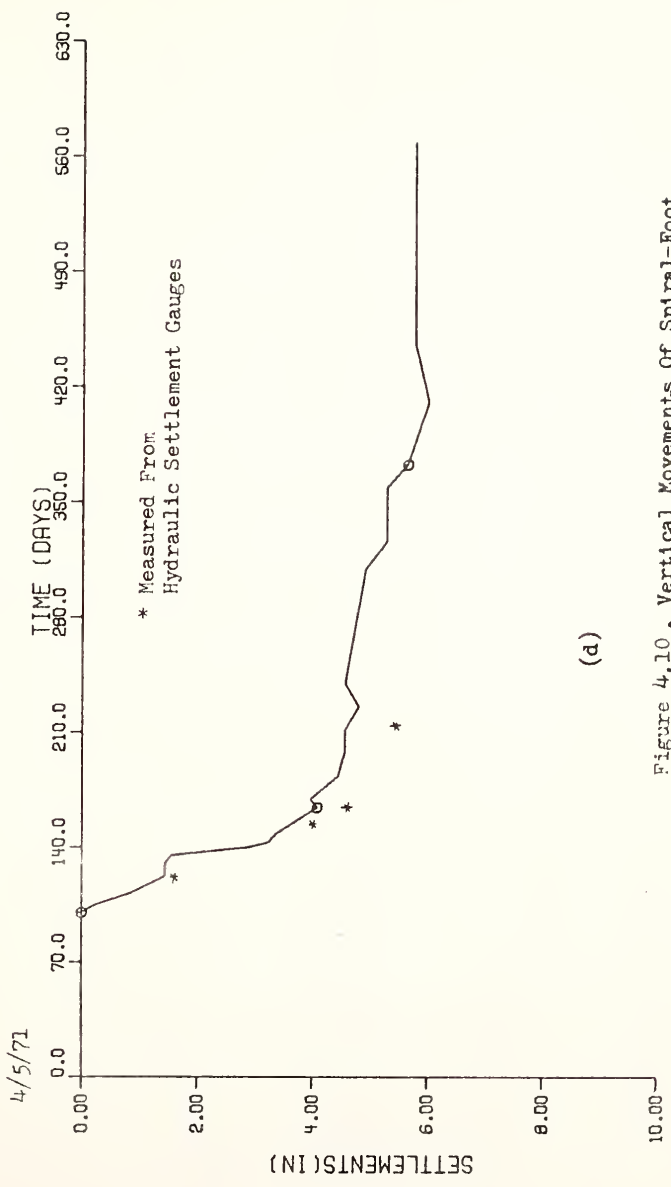


(c)

Figure 4.10 . Vertical Movements of Spiral-Foot

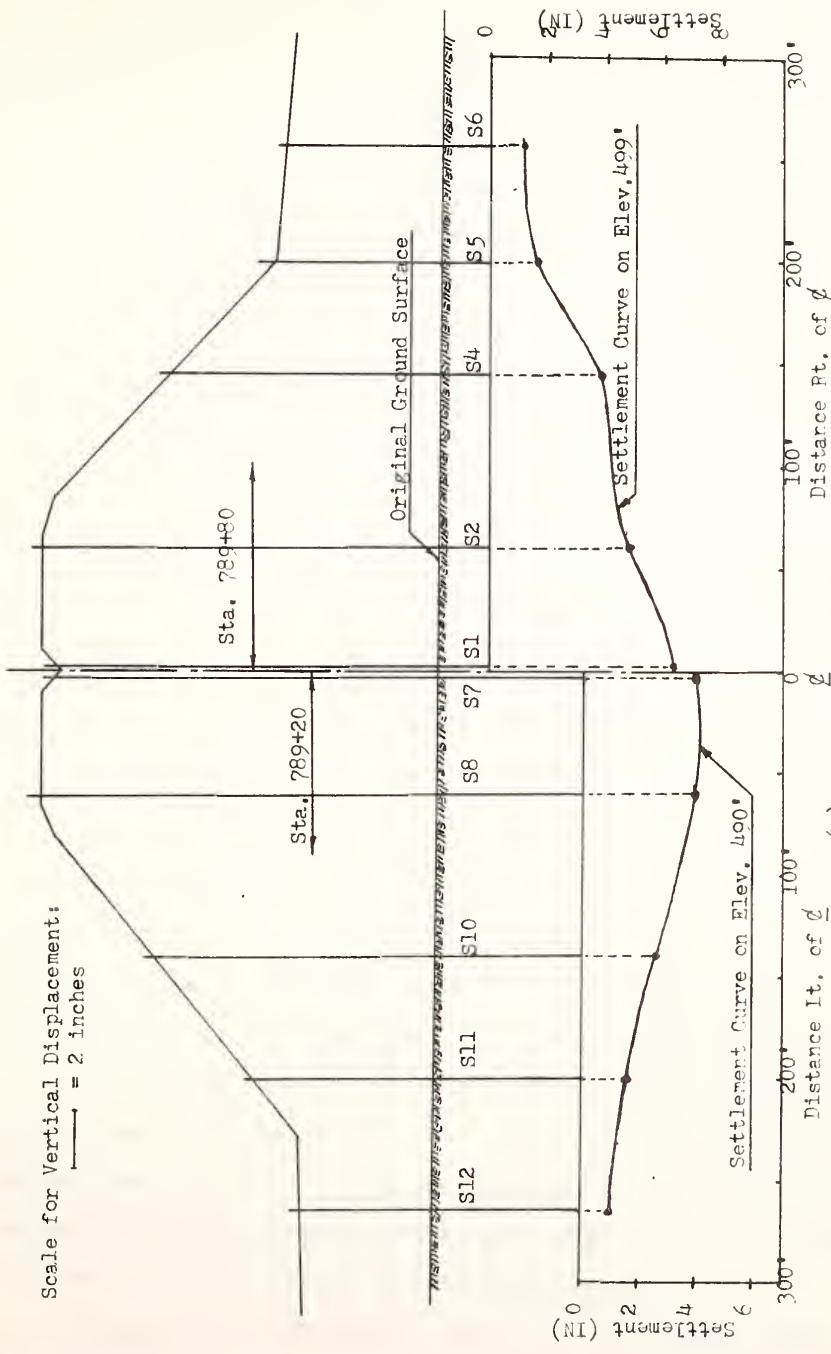
0 SPIRAL FOOT SETTLEMENT GAUGE NO. 3 AT 789+00 55811(226.5)

TIME-SETTLEMENT CURVE



(d)

Figure 4.10 . Vertical Movements Of Spiral-Foot



(e) Settlement on Elev. 400' and 400'
 Figure 4.10. Vertical Movements of Spiral-Foot

right of the center line, which can be seen by comparing movements of S-1, S-2, S-7, and S-8. Similar uniformity is apparent for the portion outside the toe. The settlements decreased from about 140 feet off the center line towards the toe of the embankment, where the vertical settlements were only 22% of that of center line at elevation 499 feet and 45% of that of center line at elevation 490 feet by the end of embankment construction. The evidence can be seen in Figure 4.10(e).

S-13, which was located at the thin clay layer, already settled almost 100% at the end of embankment construction. There were about 75% of settlements occurred at the end of embankment construction in the soft clay layer.

It is observed that the whole layer of soft clay settled only a little from about 200 feet off the center line to the outside of the embankment.

S-3, which was located in the embankment fill, has the same pattern and slope as those of S-1 and S-7 after the placement of embankment fill.

A few spiral-foot settlement gauge data are replotted on the semi-logarithmic diagram shown in Figure 4.11. In this figure, all data points for each curve are indicated by symbols. Figure 4.11 shows the vertical settlements beneath the center line of the embankment within different strata in the foundation. The curves suggested by these data imply that consolidation was completed at various depths in the two strata at approximately the same time. Thus it appears that the effective drainage path length was the same for those two layers. This observation suggested that there be short drainage path in the field and consolidation settlement be largely complete at the end of construction.

A complete listing of data for the spiral-foot settlement gauges is given in Appendix G-2.

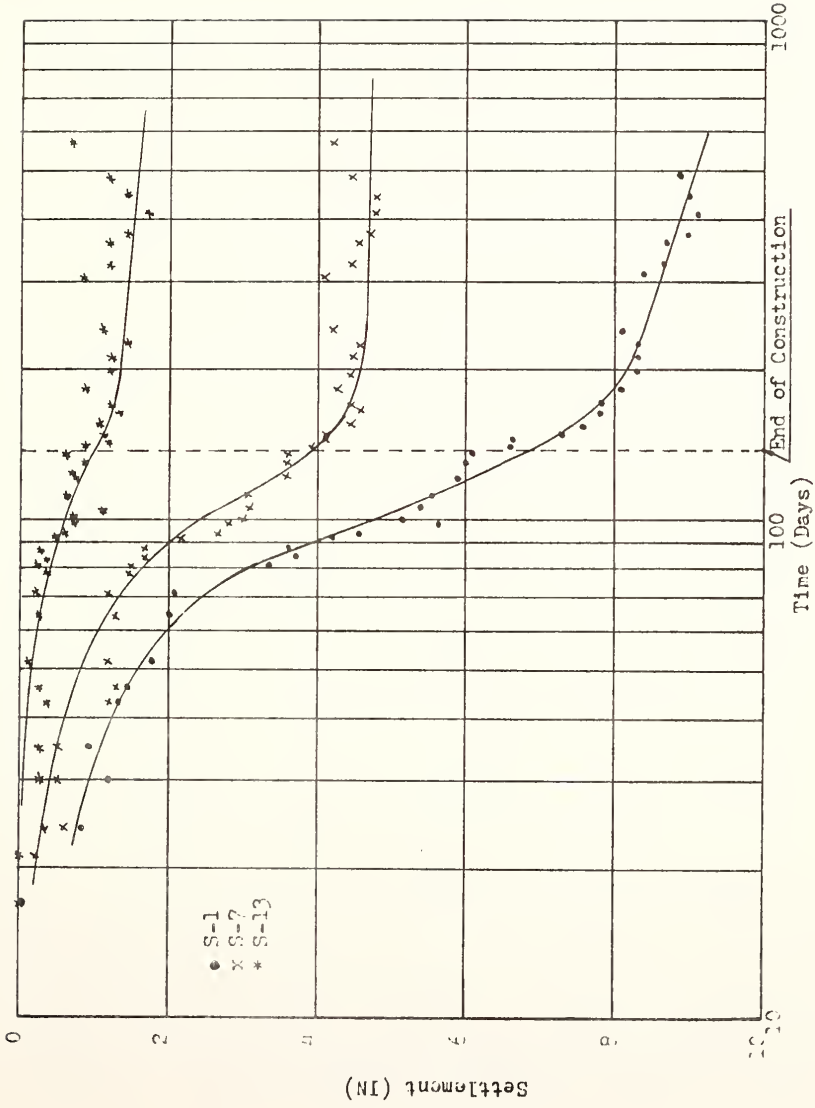


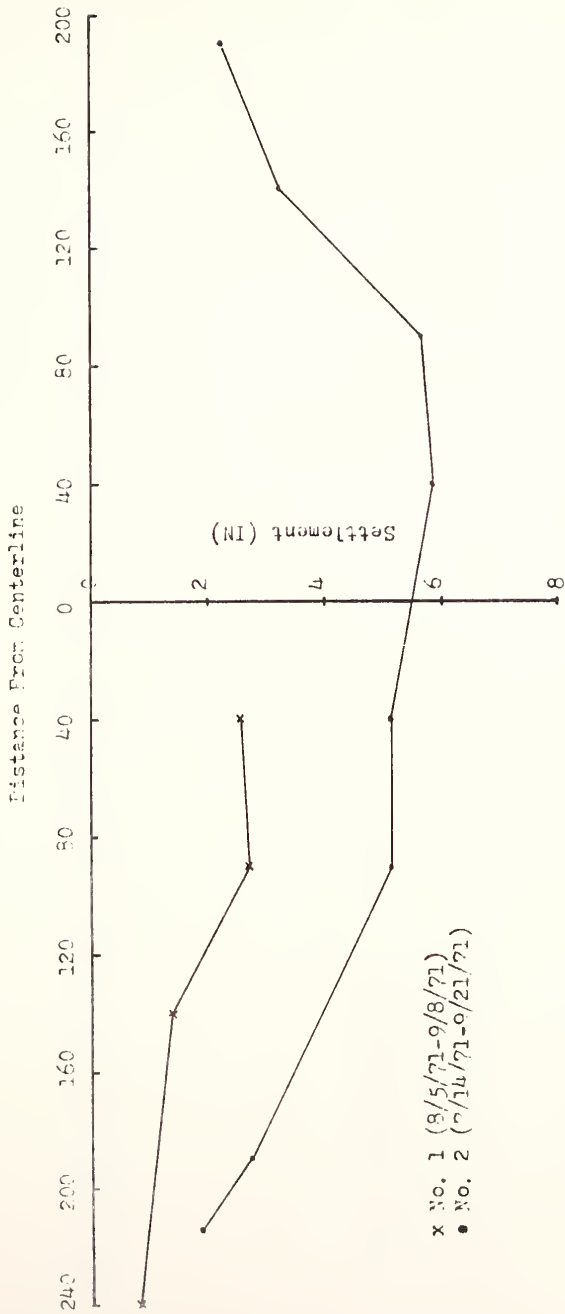
Figure 4.11. Vertical Settlements of S-1, S-7 and S-13

The hydraulic settlement gauge was used to measure vertical settlements along a horizontal line within the embankment. The system employed is similar to that described by Bozozuk (1969). One inch diameter tubes were installed in trenches through the embankment at four desired elevations. Each tube was filled with ethylene glycol and allowed to overflow reservoirs at both ends of the tube. A pressure transducer was pulled through the tube to measure the head relative to the reservoir elevation. From the pressure measurements, elevations at the points of the tube can be calculated.

A few available field data for the hydraulic settlement gauges are plotted in Figure 4.12. Shown are data taken between August 5, 1971 to September 8, 1971 for tube No. 1, from July 14, 1971 to September 21, 1971 for tubes No. 2 and No. 3, and from August 23, 1971 to September 21, 1971 for tube No. 4. These curves indicate that settlements were largest, and relatively uniform, near the center line, diminishing near the outside of the fill.

A check on the accuracy of this method can be made by comparing the measurements with those from spiral-foot settlement gauge No. 3. These are listed in Table V and shown in Figure 4.10(d). It is apparent from this table that the vertical settlements determined by these two methods are in substantial agreement during the summer season.

Unfortunately more extended useful data from the hydraulic settlement gauges could not be obtained. This occurred due to the temperature sensitivity of the pressure transducer. The transducer experienced a thermal zero shift equal to $0.01\%FS/^{\circ}F$ and thermal sensitivity shift of $0.01\%FS/^{\circ}F$. The large temperature fluctuations during the winter



(a)
 Figure 4.12. Settlements for Hydraulic Settlement Gauges

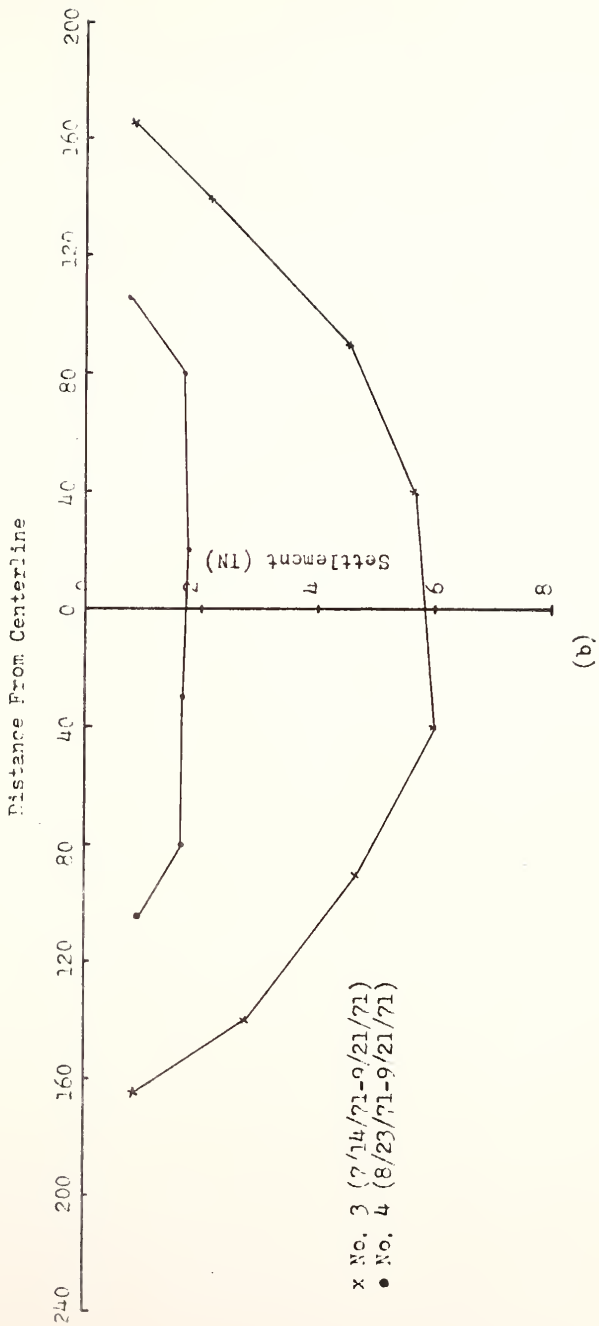


Figure 4.12. Settlements for Hydraulic Settlement Gauges

Table V

Comparison of Hydraulic Settlement Gauges and S-3
Measured Settlements Relative to Datum of 7/14/71

| Date | Vertical Settlements (IN) | |
|---------|-----------------------------|------|
| | Hydraulic Settlement Gauges | S-3 |
| 7/14/71 | 0 | 0 |
| 8/ 5/71 | 1.56 | 1.44 |
| 9/ 8/71 | 3.96 | 3.72 |
| 9/21/71 | 4.56 | 4.08 |
| 11/2/71 | 5.40 | 4.56 |

season limited useful readings to summer and fall. By spring 1972, the tubes had crushed and were no longer operable.

The time-settlement data (Figure 4.10) show small oscillations superimposed on the larger settlement pattern. This may be due to the effect of ground water table fluctuations. When the position of the ground water table is plotted as function of time (Figure 4.13), these movements exhibit a similar pattern to the variability in the measured settlements. In addition the pressure measurements appear to reflect the water table movements similarly, as discussed above.

4-4. Measured Horizontal Movements

Horizontal movements were measured by slope indicators, manufactured by the Slope Indicator Company. The slope indicator consists of an inclination sensing torpedo, readout device and grooved tubing. Prior to construction, the grooved tubing was installed vertically from the surface to the bedrock, and socketed three feet into the rock. Five-foot long sections were added during construction by 12-inch coupling to extend the tubing above the surface of the embankment. Additional details of installation are given by DeGroff (1973).

The instrument has two sets of guide wheels: fixed guide wheels, aligned in a vertical plane parallel to the axis of the instrument one side; on the opposite side is a corresponding pair of spring-mounted guide wheels. The orientation of the readings is controlled by the direction of the fixed pair of wheels.

The slope indicator measures the inclination of the tubing along two mutually perpendicular pair of guide grooves. Inclination readings

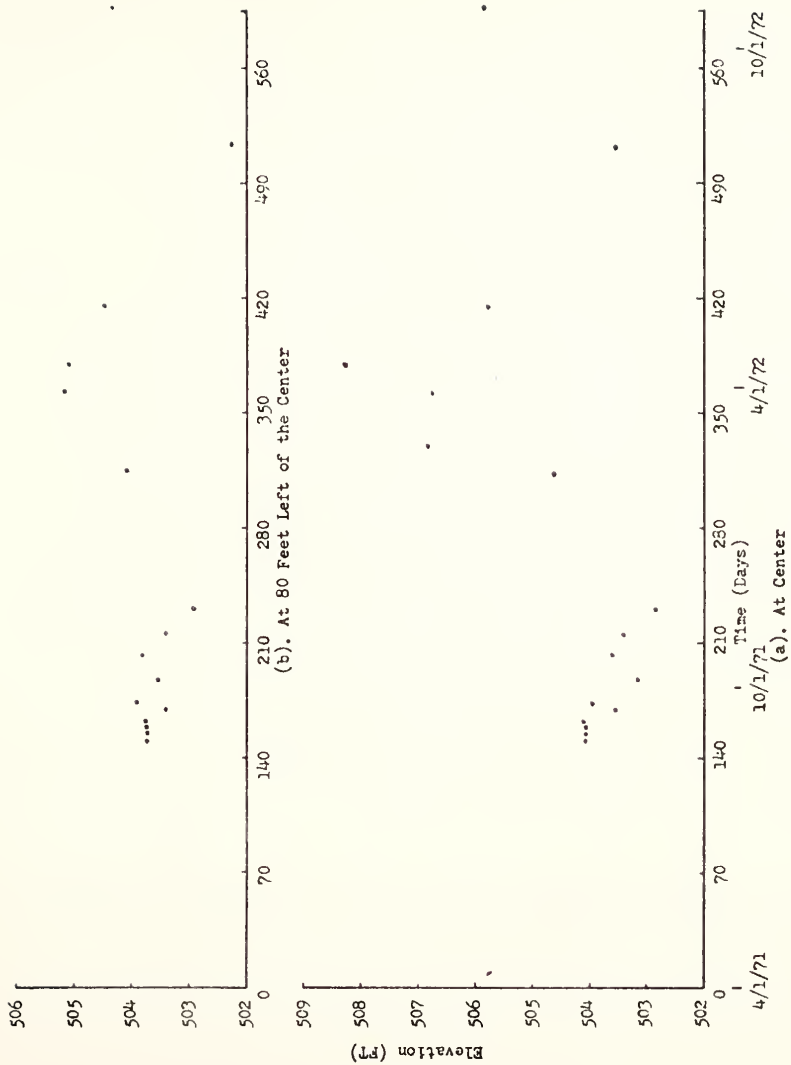


Figure 4.13. Ground Water Table Change With Time

relative to a plumb line were taken at different elevations, one set parallel and another normal to the center line of the highway (N-S direction), at various time intervals. The instrument is adjusted so that the inclination (δ) of the casing from the vertical plane can be calculated by the following equation (SINCO):

$$\tan \delta = \frac{D_1 - D_2}{2k'} \quad (4-4)$$

where

D_1 = dial reading in north or east groove,

D_2 = dial reading in south or west groove,

k' = constant = 2000 for the Series 200-B instrument used

in this study.

A change in dial differences due to any change in inclination at a given depth is given as

$$\Delta D = (D_1 - D_2)_{\text{new}} - (D_1 - D_2)_{\text{initial}} \quad (4-5)$$

Then, the change in inclination is

$$\Delta \tan \delta = \frac{\Delta D}{2k'} \quad (4-6)$$

The horizontal movements at each interval of depth can be determined by

$$\Delta H = l(\Delta \tan \delta) \quad (4-7a)$$

or

$$\Delta H = C \cdot \Delta D \quad (4-7b)$$

where

ΔH = horizontal movement at each interval of depth,

l = vertical distance in two consecutive readings,

$$C = \frac{l}{2k'} \quad (4-8)$$

If the vertical distance in two consecutive readings is constant, then the total horizontal movement at any point with respect to the bottom is

$$\begin{aligned} H &= \Sigma \Delta H \\ &= C \Sigma (\Delta D) \end{aligned} \quad (4-9)$$

The system used to make the inclination measurements can distinguish inclination changes which correspond to less than 1/160 inch horizontal movement over the two-foot length of the torpedo.

A field check for correct dial readings can be made. The sum of corresponding pairs of readings at identical depths should be equal to a constant. The sum of the readings for each depth should not vary more than three to five dial units from their mean.

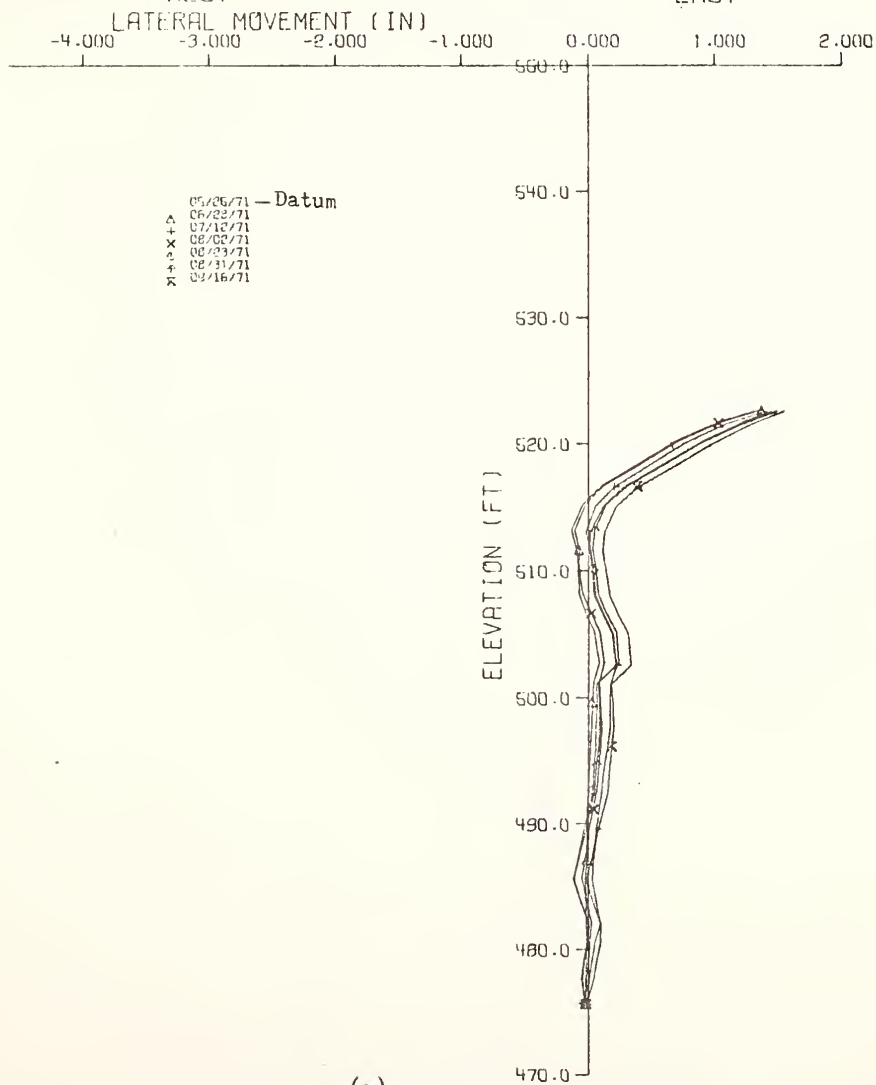
The horizontal E-W movements detected by the slope indicators are plotted in Figure 4.14. In each part of the figure, slope indicator movements are given relative to the date shown at the top of the figure. Thus in Figure 4.14a, the position of the tubing is shown relative to that on 5/25/71. As the embankment was raised, more casing was added, and a new datum, 9/16/71, is used in Figure 4.14b. Purdue University's CDC 6500 computer and CALCOMP plotting system were used to produce all the plots. A computer program for evaluating lateral movement is listed in Appendix C.

SLOPE INDICATOR NO. 1 --E-W(05/25/71)

AT LOCATION = 789 + 80 CENTER

WEST

EAST



(a)

Figure 4.14 . Slope Indicator Movements

SLOPE INDICATOR NO. 2 -- E-W (9/16/71)

AT LOCATION = 789 + 52 CENTER

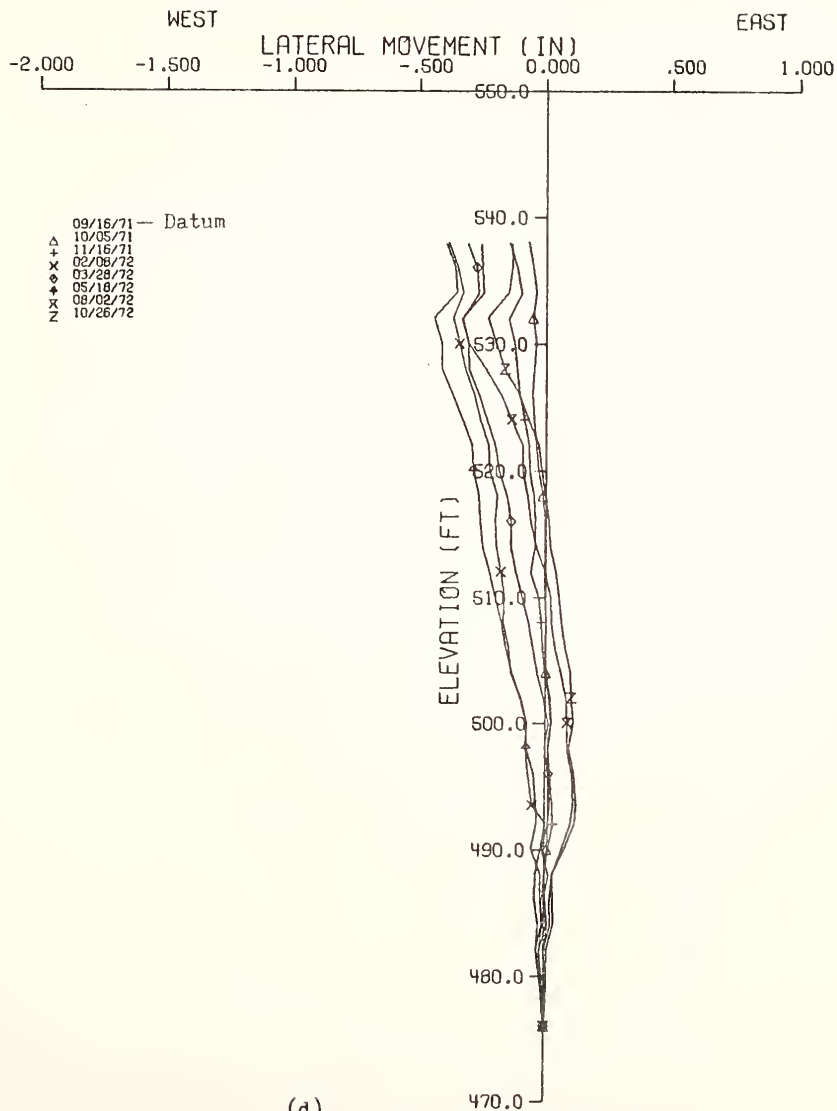


Figure 4.14. Slope Indicator Movements

SLOPE INDICATOR NO. 3 --E-W(02/05/71)

AT LOCATION = 789 + 65 80 LT

WEST

EAST

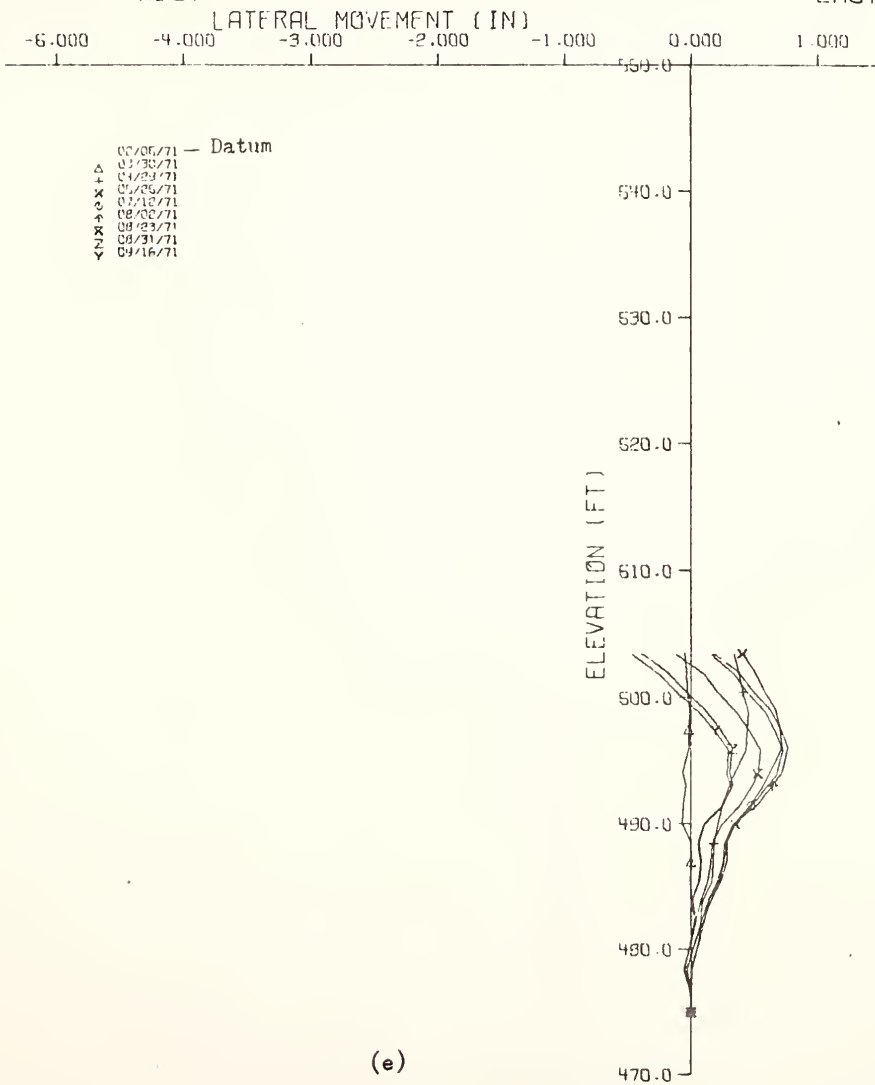


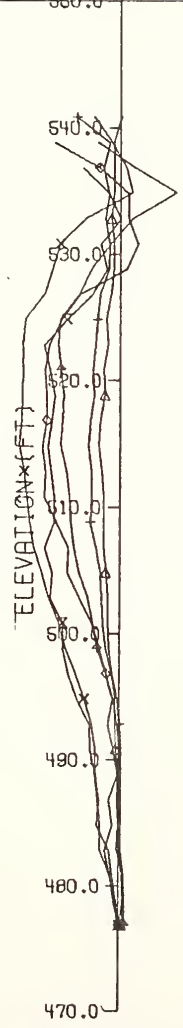
Figure 4.14. Slope Indicator Movements

SLOPE INDICATOR NO. 3 --E-W (9/16/71)

AT LOCATION = 789 + 65 80 LT



- 09/16/71 — Datum
- △ 10/05/71
- + 11/16/71
- × 02/08/72
- ◇ 03/28/72
- ↑ 05/18/72
- × 06/22/72



(f)

Figure 4.14. Slope Indicator Movements

SLOPE INDICATOR NO. 4 --E-W(04/29/71)

AT LOCATION = 789 + 65 140 LT

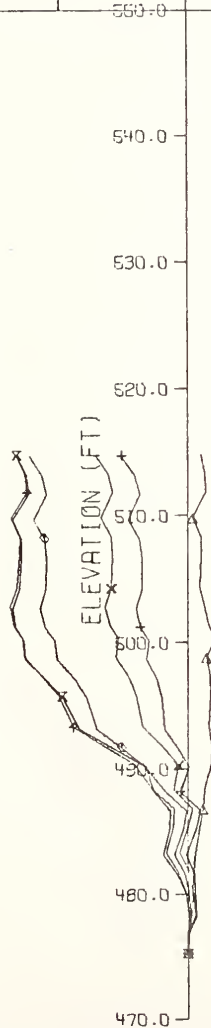
WEST

EAST

LATERAL MOVEMENT (IN)

-4.000 -3.000 -2.000 -1.000 0.000 1.000 2.000

01/23/71 — Datum
 ▲ 05/25/71
 + 07/12/71
 x 08/08/71
 o 08/23/71
 △ 08/31/71
 x 09/16/71



(g)

Figure 4.14 . Slope Indicator Movements

SLOPE INDICATOR NO. 5 --E-W(05/25/71)

AT LOCATION = 789 + 65 205 LT

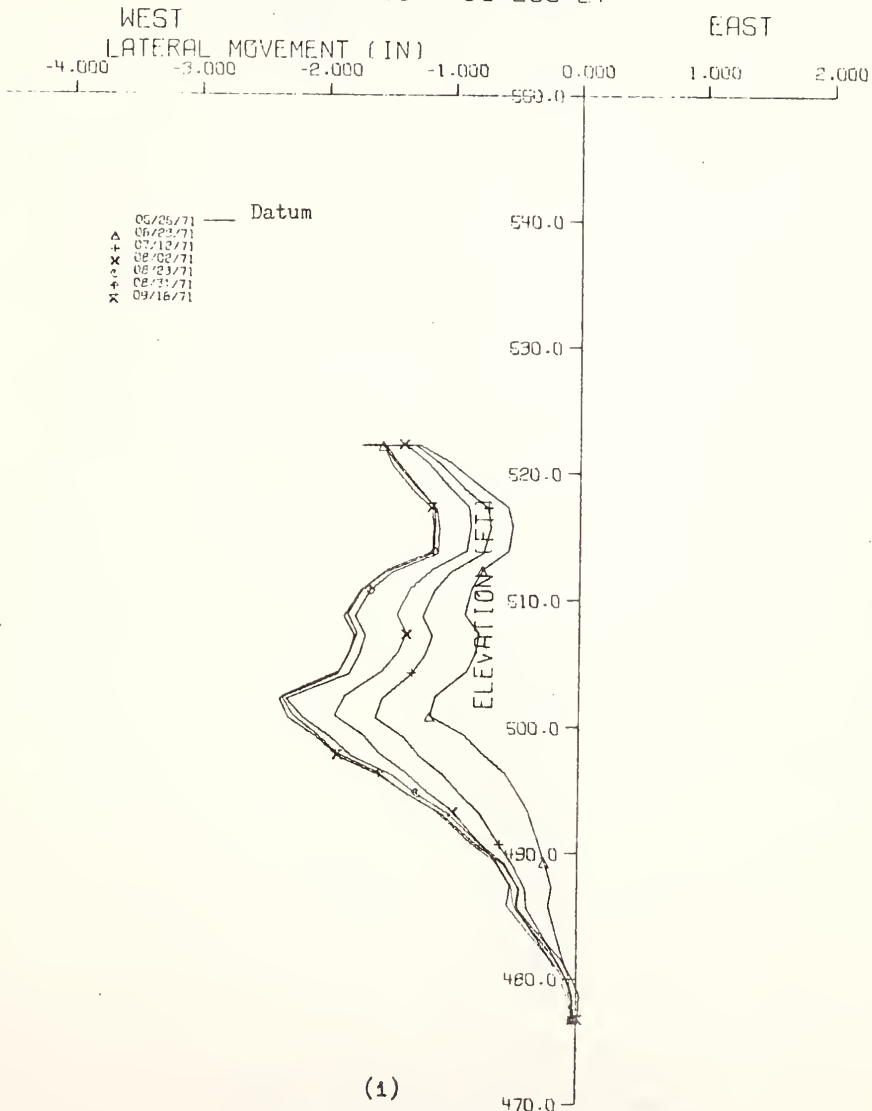
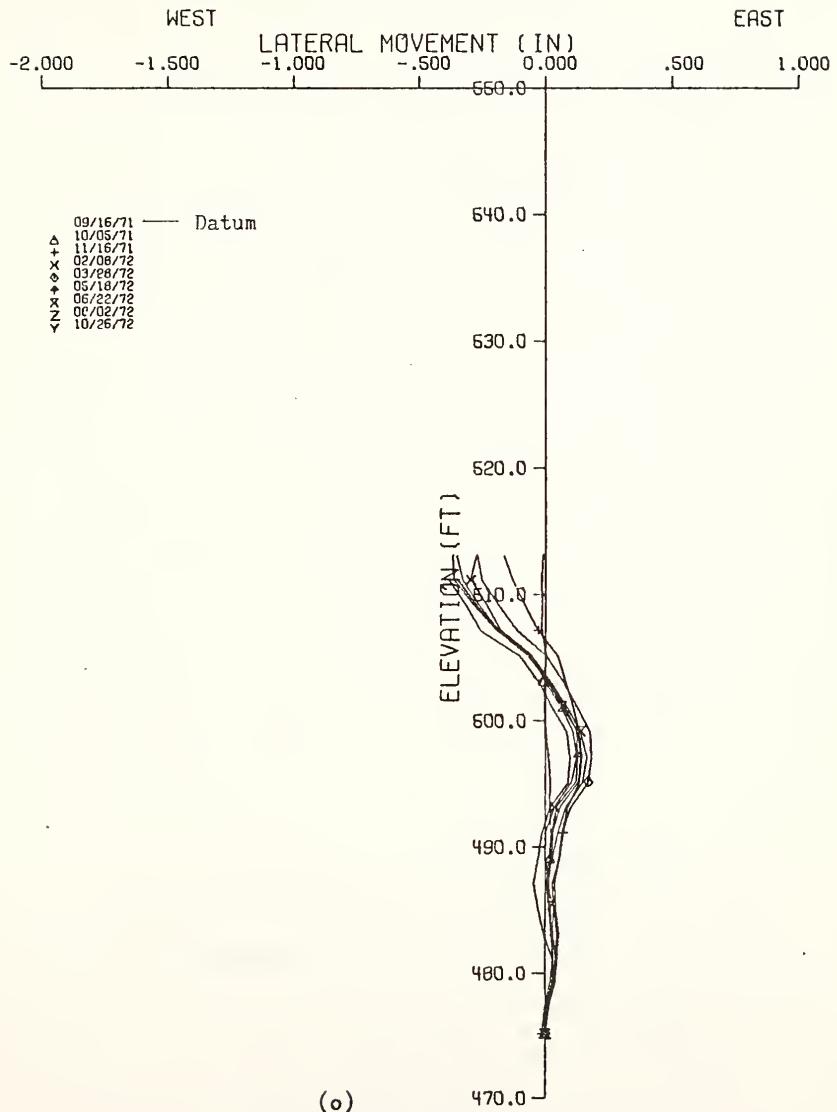


Figure 4.14. Slope Indicator Movements

SLOPE INDICATOR NO. 7 --E-W (9/16/71)
AT LOCATION = 789 + 65 310 LT



(o)

Figure 4.14 , Slope Indicator Movements

Movements in the N-S direction are not shown, but they were of small magnitude (< 0.25 -inch toward south within embankment after the construction).

Horizontal deformations in the E-W direction within the foundation increased from the center line towards the toe of the embankment and then decrease again beyond the toe. The maximum movement of slope indicator No. 5, near the toe, was 3.35 inches by October 26, 1972. There is a distinct difference in the pattern of horizontal movements that took place within and away from the toe of the embankment. Movements of I-3, I-4, and I-5 tapered off gradually from the original ground surface, whereas movements of I-6, I-7 showed a peak in the upper one-third of the soft clay layer. As evidenced by the movements of I-1 and I-2, the embankment as a whole seems to have displaced slightly eastward.

The deformation patterns for drained and undrained cases differ markedly near the center line. Specifically, slope indicator No. 3 moved horizontally toward the east up to August 2, 1971, and then moved back toward the west. Similarly, I-4 moved horizontally toward east until May 25, 1971, and then moved back toward west. I-5 and I-6 always moved west.

Horizontal movements at two points near the original ground surface (Elevation 504.00 feet) are shown as a function of time in Figure 4.15. The figure shows movements for points below the top and toe of the sideslope. The majority of the movement occurred during the construction period, with the rate of subsequent movements diminishing with time.

As indicated in Figure 4.14(0), westward movement of slope indicator No. 7 ceased after November 16, 1971. This was probably due to the

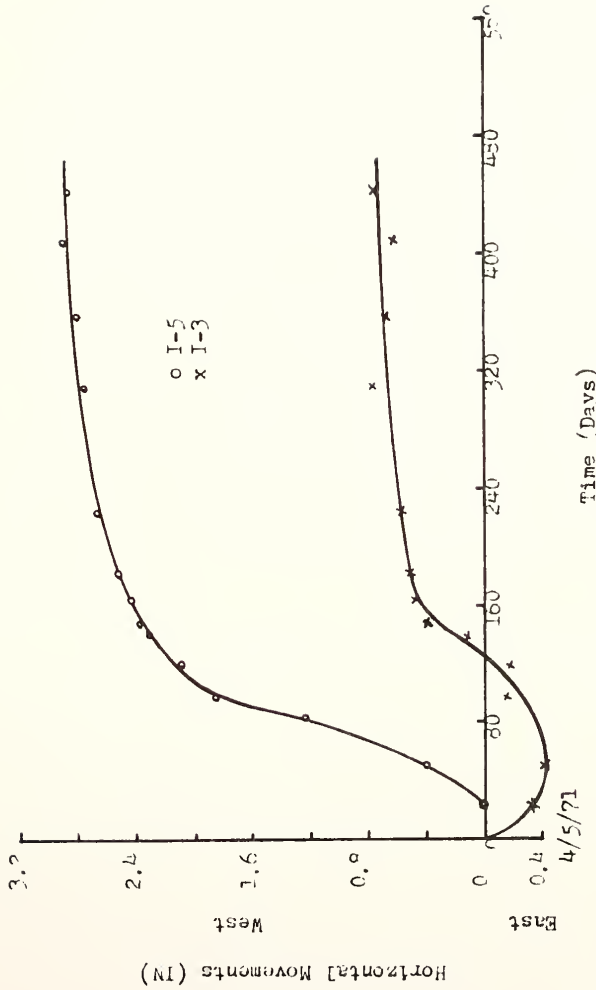


Figure 4.15. Horizontal Movements at Elevation 504.00 feet For I-3 & I-5

placement of an additional 3.72 feet of rockfill on the west side of the slope indicator on October 19, 1971, to bring the berm thickness to a total of 12 feet.

The field data for the slope indicators are listed in Appendix G-3.

CHAPTER V

PREDICTION OF THE TEST SECTION PERFORMANCE

5-1. Method of Analysis and Material Parameters

This investigation is concerned primarily with predicting creep deformations of the compacted clay embankment. Because of the importance of the interaction between the embankment and its foundation, deformations of the soft foundation soils are also considered. This complex boundary value problem was solved using the finite element method. The program used for the calculations of displacements and stresses in this study is a modified version of one developed originally at the University of California (Wilson, 1965 and 1967), and adapted by Ramaswamy (1971) to nonlinear viscoelastic problems. The program, which is listed in Appendix A, utilizes the CDC 6500 computer available at The Computing Center, Purdue University.

The idealized scheme for plane strain finite element analysis of the test embankment is illustrated in Figure 5.1. This was drawn by an automated mesh plotting program listed in Appendix B. Purdue University's CDC 6500 computer and CALCOMP plotting system were used to produce the plot. The CALCOMP system at Purdue consists of a set of subroutines that produce a file on a disk that is copied on to a plot tape. This tape is then run on a Model 563 CALCOMP Digital Incremental Plotter, producing an X-Y plot of digital data. The mesh plotting program was developed originally by Reingold (Costantino, 1968).

MESH FOR COMPACTED CLAY EMBANKMENT OVER SOFT FOUNDATION

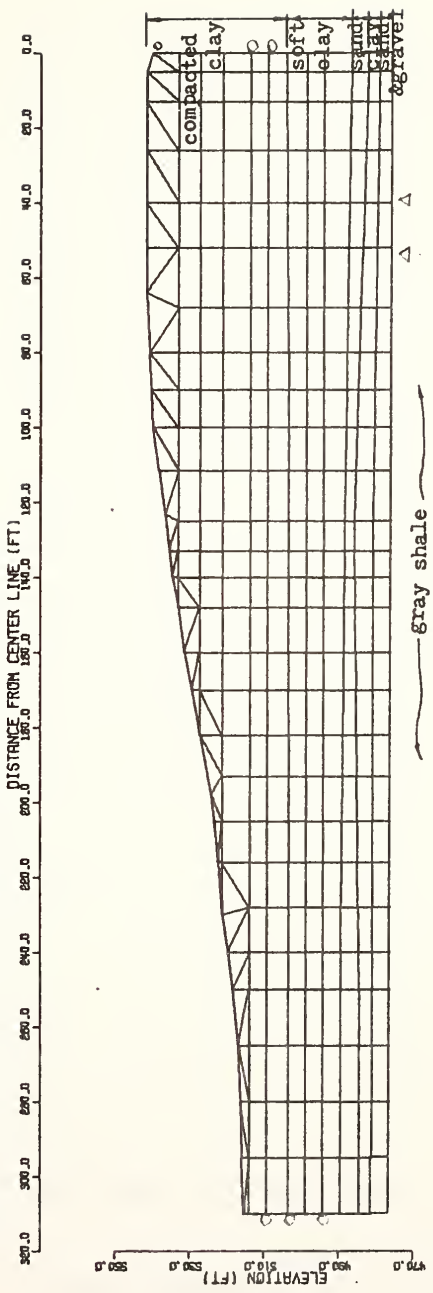


Figure 5.1. Idealized Scheme for Two Dimensional Finite Element Analysis

For the analysis of the test section performance, embankment construction is divided into six stages in accordance with the fill elevation-time curve as shown in Figure 4.1. The elevations of the embankment top surface at stage of construction were 509.38 ft, 514.06 ft, 521.44 ft, 527.44 ft, 533.15 ft, and 541.80 ft. The corresponding starting dates for each stage construction were April 7, April 29, May 25, June 22, July 6, and August 21, 1971 respectively.

The assumed boundary conditions for the finite element analysis are based on the field conditions. In Figure 5.1, the bottom of the system is assumed to be a fixed boundary equivalent to a pinned connection at the bottom nodal points, because of gray shale existing at the site. The right hand side wall which is located at the centerline of the embankment, is assumed to move vertically only due to the almost symmetrical loading; the left hand side wall is also assumed to move vertically only since the horizontal movement at the left boundary is small and can be ignored as discussed in section 4-4. Thus the lateral boundary nodes are assumed to be attached to rollers which can move only in a vertical plane.

The material for the embankment-layered foundation system is assumed homogeneous for each layer before the embankment load is applied. After loading, the properties of each element (except those in sandy gravel layers) are changed in response to the state of stress and time of loading in the element. Thus, each element is assumed to be a different material for each incremental stress and time.

The numerical values of soil parameters for each layer are obtained as summarized below :

(a) Compacted clay. The material properties for this layer are

expressed by the nonlinear viscoelastic parameters discussed in section 2-5. The equivalent incremental elastic constants E and ν are obtained from equations (2-88) and (2-84) respectively. All parameters related to the elastic constants are evaluated from the compression creep test results by the procedures described in section 2-5. An average total unit weight of 120 pcf is assumed.

(b) Soft silty clay. Although this study was concerned primarily with the long term deformation of the compacted cohesive fill, the interaction between the embankment and the foundation soils depends upon time-dependent movements of the foundation. To avoid the necessity of an elaborate consideration of the clay behavior, as for example carried out by Davidson (1973), and still permit incorporation of consolidation effects, the following approach was adopted:

(1) Flow of water from the clay was assumed to occur according to one-dimensional consolidation theory. Thus at each time interval an average degree of consolidation was calculated for each element.

(2) Based on this result, the change in effective stress in each element within the clay was determined. The new value of effective stress was then used to estimate equivalent incremental values for E and ν as described in section 2-8. These equivalent elastic parameters were obtained from equations (2-82) and (2-83) respectively.

(3) These equivalent elastic parameters were then used in the finite element program to calculate foundation deformations during the time increment considered. An average saturated unit weight of 120 pcf was assumed for the determination of the initial vertical effective stress.

(c) Medium silty-sandy gravel. Elastic constants E and ν assumed for this layer in the analysis are (Lambe & Whitman, 1969):

$$E = 2,000 \text{ psi}$$

$$\nu = 0.35$$

(d) Medium silty clay. Due to the small thickness of this layer undisturbed samples were not obtained. From classification and field vane data, it seemed reasonable to use the same material parameters as the soft silty clay layer discussed in item (b) above.

(e) Dense silty sand and gravel. The elastic constants were assumed as follows (Lambe and Whitman, 1969):

$$E = 8,000 \text{ psi}$$

$$\nu = 0.30$$

5-2. Stresses in the Embankment Fill

For a homogeneous linear elastic semi-infinite soil mass only stress boundary conditions exist. For this case, vertical stresses at least, are independent of the elastic constants. But when the foundation is of finite depth, boundary conditions are both stress and displacement types, and all stresses are affected by the magnitude of the elastic parameters.

A comparison of the measured and computed stresses at the end of embankment construction is given in Table VI. In addition to the measured stresses, the table shows stresses computed by the finite element program and those corresponding to a homogeneous linear elastic embankment and foundation given by Perloff, et al. (1967). For vertical stresses, the unit weight times the depth below the embankment surface, γz , is also shown. By using the assumed unit weight of 120 pcf as a reference, the following observations can be drawn concerning the vertical stresses that were measured at the end of embankment construction, August 21, 1971: in general, the average vertical stresses correspond closely to the computed

Table VI
Comparison of Measured and Computed Stresses at the End of Embankment Construction

| Group | Location | Elevation (ft) | Orientation | Vertical Stresses (psi) | | | Horizontal Stresses (psi) | | | |
|-------|-----------------|-------------------|-------------|-------------------------|------|----------|---------------------------|----------|----------|-------------------|
| | | | | Measured | yz | Computed | Perloff et al. | Measured | Computed | Perloff et al. |
| 1-3 | 789+68 g | 505.50 | N-S | 37.0 | 30.2 | 29.1 | 30.30 | - | - | - |
| 4-6 | " | " | W-E | 44.0 | 30.2 | 29.1 | 30.30 | 16.0 | 3.3 | 14.2 |
| 7-9 | 789+68 60RT | " | " | 46.7 | 30.2 | 29.1 | 30.30 | 30.2 | 2.9 | 14.2 |
| 10-12 | 789+68 120RT | " | " | 34.8 | 26.1 | 25.9 | 25.10 | 18.8 | 2.5 | 12.8 |
| 13-15 | " | " | N-S | 31.5 | 26.1 | 25.9 | 25.10 | - | - | - |
| 16-18 | 789+68 180RT | " | W-E | 17.9 | 18.7 | 18.3 | 19.80 | 10.6 | 2.6 | 11.5 |
| 19-21 | 789+65 240RT | 504.50 | " | 11.0 | 12.7 | 11.1 | 10.90 | 7.9 | 1.9 | 5.8 |
| 22-24 | 789+62 60RT | 519.00 | " | 21.8 | 19.0 | 18.7 | 18.80 | 12.9 | 1.3 | 15.0 |
| 25-27 | 789+62 120RT | " | " | 15.5 | 15.0 | 15.3 | 15.0 | 11.30 | 1.0 | 11.0 |

values which, in turn, are nearly the same as those for an elastic embankment as well as the weight of soil directly above the pressure plates. The exception was groups¹⁻⁹ in which the measured stress exceeded that calculated by nearly 50 percent. This is illustrated in Figure 5.2, which shows the comparison for vertical stresses at elevation 505.50 feet.

These results indicate that for the type of geometry considered herein, the computed vertical stress is insensitive to the material characteristics and boundary condition assumptions. This suggests that the data from groups¹⁻⁹ were in error.

Comparison of measured and predicted horizontal stresses given in Table VI indicates major discrepancies. Among the factors which may be involved are the following:

(1) Computed horizontal stresses are sensitive to the material characteristics assumed. The values from Perloff, et al. (1967) are based on a Poisson's ratio of 0.3. For smaller values of ν , much smaller horizontal stresses result. The equivalent ν of the embankment material following wetting by an elevated ground water table is not known, but is probably higher than that measured in the laboratory on specimens compacted near optimum water content.

(2) The relative stiffness of the embankment and foundation influence the calculated horizontal stress markedly. This is illustrated in Figure 5.3, which shows the vertical distribution of horizontal stress within an elastic embankment on an elastic foundation for varying ratios of embankment modulus to foundation modulus. With a modular ratio of 10, the analysis indicates horizontal tensile stress in the embankment. Because the ratio of the equivalent moduli used for the embankment and foundation at the end of construction is of the order of about 10 at the

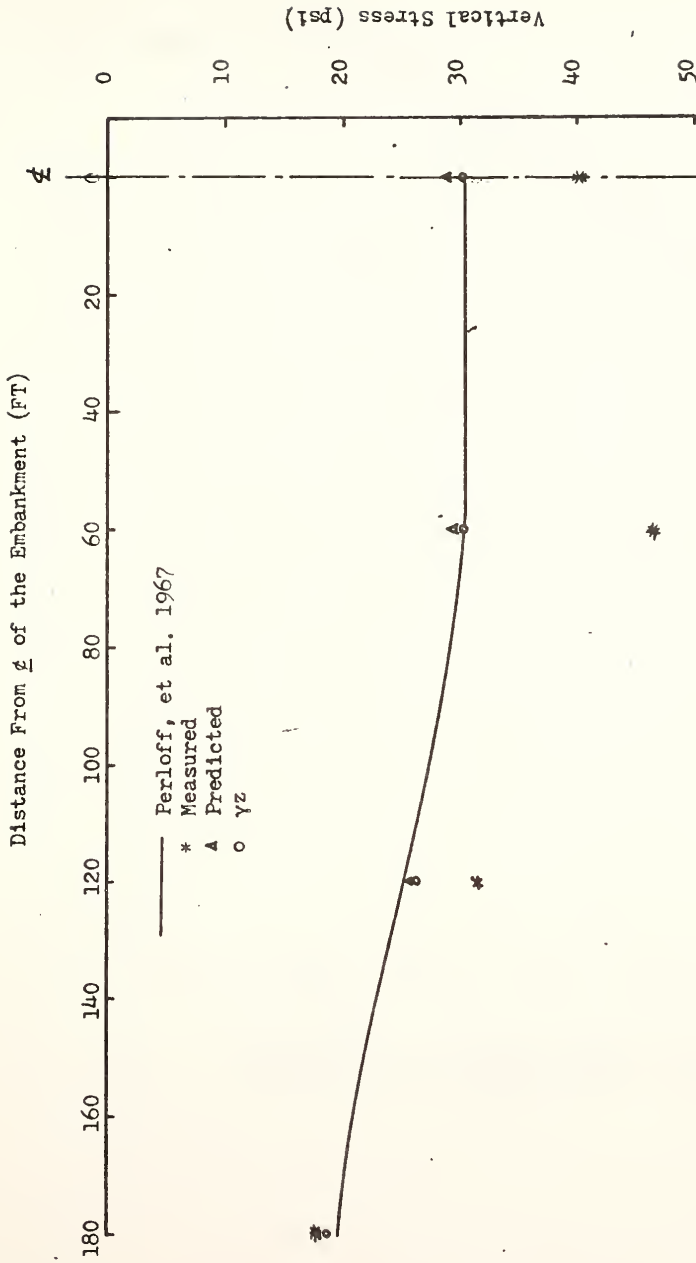


Figure 5.2. Vertical Stress At Elevation 505.50 Feet

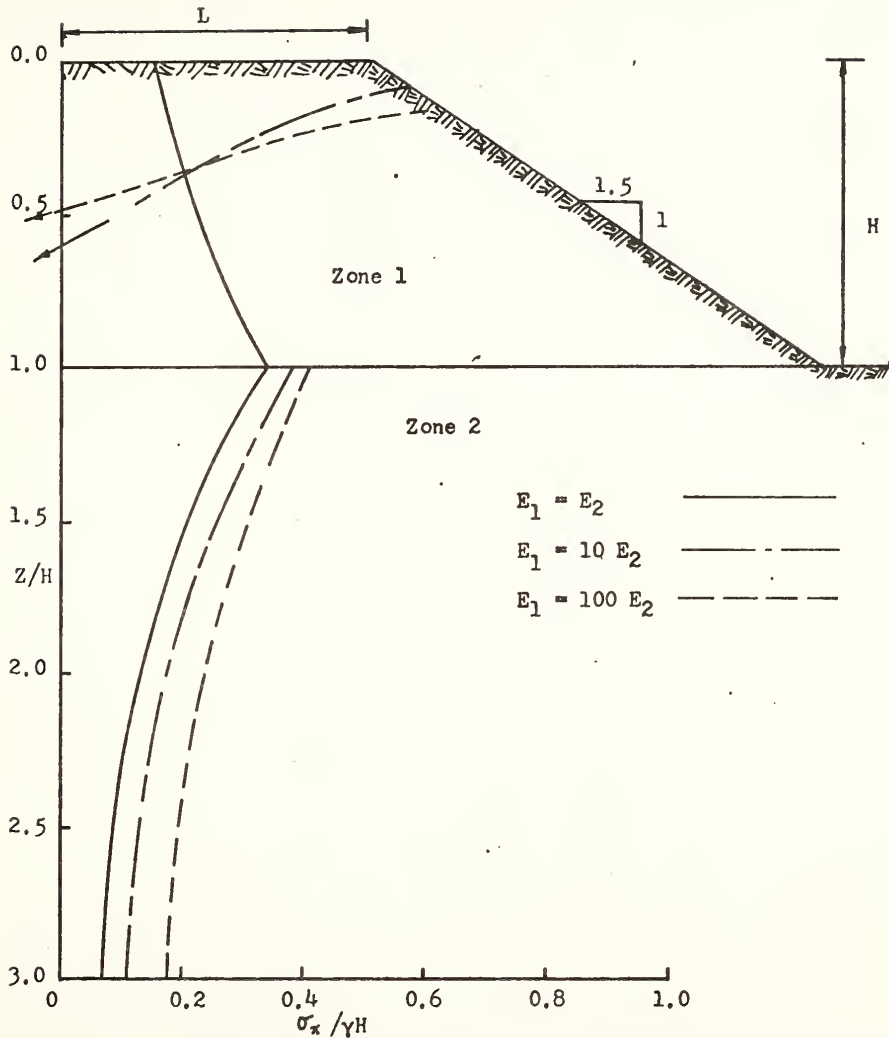


Figure 5.3. Distribution of Horizontal Stress Due to Embankment Along Vertical Section (Perloff, 1974)

center line and about 4 at the outside of the toe, the predicted horizontal stress near the base of the embankment is small. The moduli for the compacted clay were based upon the laboratory tests on compacted specimens near optimum moisture content. This analysis does not consider, however, the effect of potential plastic yielding in the foundation soil, or as mentioned above, saturation of the embankment soil at elevations near the original ground level.

The question arises also whether the discrepancies are due to erroneous measurements resulting from placing a foreign body. Selig (1964) reported that the most important factor affecting stress gauge response is the difference in stiffness between the gauge and the soil. The influence of this factor is significantly affected by placement conditions, and is not a constant because the soil stiffness is variable. The installation of the plates usually requires disturbance of the immediate surrounding soil so that this soil does not behave like the remainder of the soil body. It seems likely that this is not a major factor in view of the fact that the measured vertical stresses correspond so closely to the calculated values. The softening effect on the fill of the groundwater table change appears to be a more plausible explanation. This is supported by the agreement between measured horizontal stresses and those calculated for a homogeneous system at the outer portions of the embankment where groundwater movements are likely most pronounced.

It should be noted that the "measured" horizontal stresses were actually calculated from the measured inclined and vertical normal stresses.

5-3. Vertical Movements

Only one of the spiral-foot settlement gauges, S-3, was installed within the embankment. In order to compare predicted and measured settlement for S-3 due to deformation within the embankment, the settlement of the original ground surface directly under S-3 must be known. This was estimated by extrapolating from other spiral-foot gauges located at appropriate points relative to S-3 in geometry. From Figure 4.5, it is seen that the measured values at the original ground surface directly below S-3 would be computed from the settlements of S-2, S-4, S-8, and S-10. However, the vertical measured movements shown in Figure 4.10 (b) indicates that the vertical movements for S-8 are larger than S-7 after the embankment construction (constant load). This probably occurred due to a soft pocket under S-8. Thus for purpose of extrapolation, the field measurements for S-7 was used instead that for S-8.

Figure 5.4 shows predicted and measured time-settlement curves for S-7 and S-10; Figure 5.5 shows the time-settlement curves for S-2 and S-4. In view of the simplified procedure for calculating these movements, the agreement between prediction and observation is considered satisfactory. The method for estimating vertical settlement at the original ground surface under the S-3 is outlined below. The average settlement of S-7 and S-10, located at elevation 490.00 feet, and that for S-2 and S-4, located at elevation 499.00 feet were determined. The settlement for the layer between elevations 490.00 feet and 499.00 feet was calculated from these figures. Linear interpolation was used to estimate the settlement for the soft clay layer above elevation 490.00 feet. This settlement was added to the average settlement of S-7 and S-10 to determine

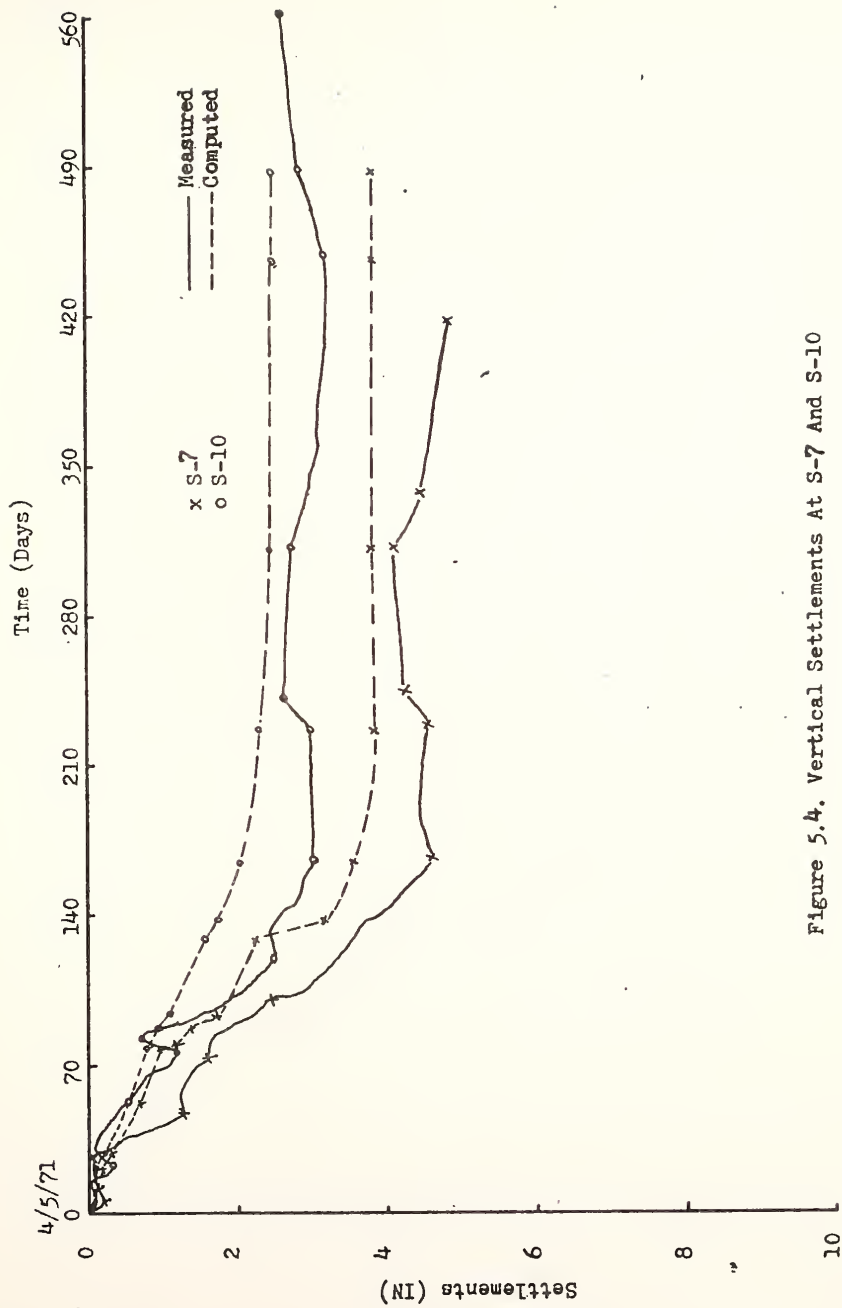


Figure 5.4. Vertical Settlements At S-7 And S-10

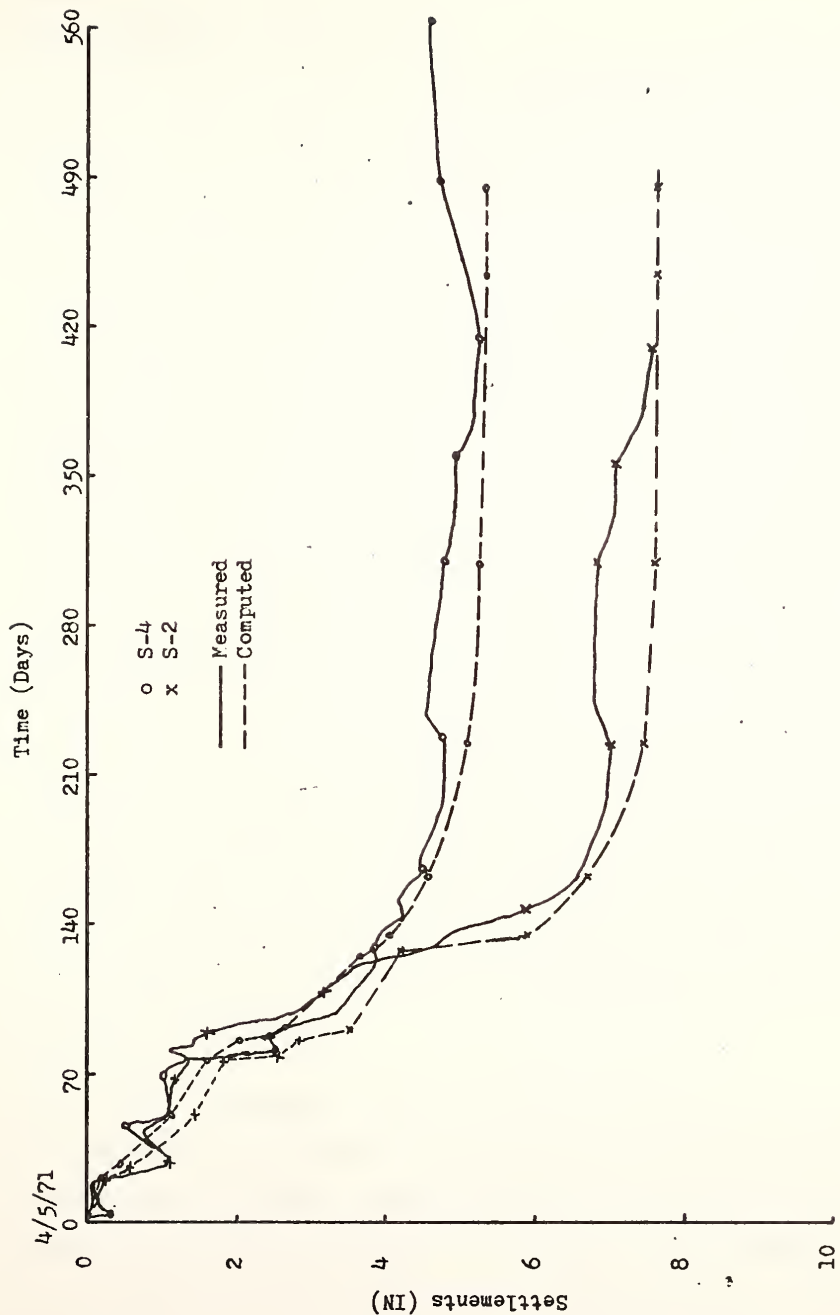


Figure 5.5. Vertical Settlements At S-2 And S-4

the settlement of the ground surface.

The lower curves in Figure 5.6 show the predicted and measured vertical settlement for S-3, located within the embankment. The solid line indicates the direct measurement of S-3 settlement; the starred points show settlement measured in hydraulic settlement gauge 3 which was about at the same elevation.

The upper curves in Figure 5.6 show the predicted settlement of S-3 due solely to deformations of the embankment, compared to the values estimated from the field measurements as described above. In both cases, the predicted settlements in Figure 5.6 correspond quite well to the measured values.

The hydraulic settlement gauge results permit comparison of predicted and measured settlement profiles during the period when the gauges functioned satisfactorily. This comparison is shown for four elevations in Figure 5.7. The relevant time period is shown in the figure. The measured settlements for No. 1 were available only on the left hand side half section. The predicted values are very close to the field measurements for No. 3 and No. 4. The predicted settlements for No. 1 and No. 2 are underpredicted on both sides outside of about 120 feet from the center line of the embankment. Otherwise, the predicted values are close to those measured.

5-4. Horizontal Movements

A comparison of measured and predicted lateral movements at the end of embankment construction is shown in Figure 5.8. It can be seen that, except for slope indicator number 3 which is close to the center line of the embankment, the calculated pattern of horizontal movements resembles

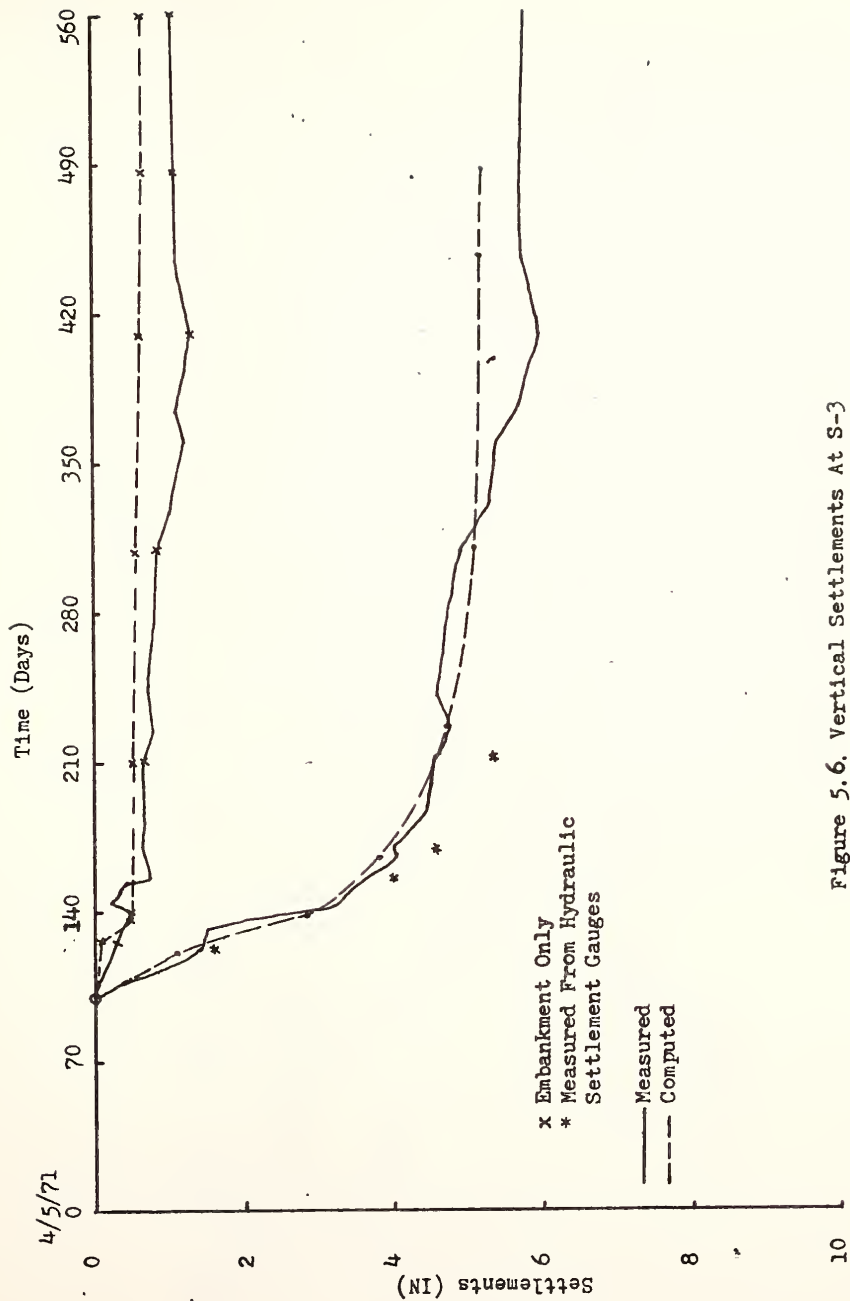


Figure 5.6. Vertical Settlements At S-3

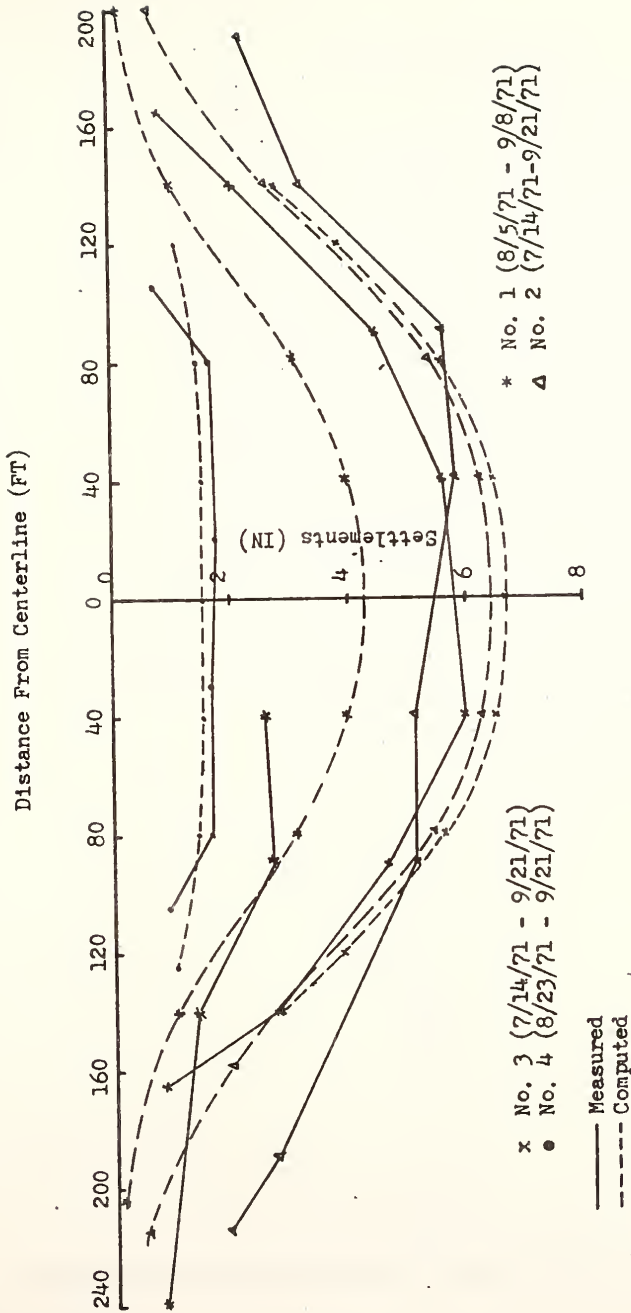


Figure 5.7. Vertical Settlements For Hydraulic Settlements Gauges

the measured pattern, though the magnitudes differ. The major discrepancy appears to result from large lateral movement concentrated in the soft upper clay layer near the original ground surface. This was probably due to plastic deformations which were not considered in the approximate analysis of the foundation materials. Because the emphasis in this investigation was on the performance of the compacted clay fill, the computed lateral movements were "corrected" by shifting the predicted curve to coincide with the measured movement at the ground surface (Figure 5.8). By this means the observed lateral movements within the embankment at the end of construction correspond reasonably well to the predicted values.

Figure 5.9 shows a comparison between measured and calculated lateral movements of the slope indicators after the embankment construction was complete, i.e., at constant total load. The measurements all show movements away from the center line in the soft clay layer. These were probably associated with creep deformations due to the large shearing effects mentioned above which were considered in the analysis for the foundation soils. This view is supported by the small horizontal movement of I-3 which is near the center line of the embankment. The predicted values were "corrected" for these movements as described above and shown in Figure 5.9. Within the embankment, the predicted pattern and magnitude of movements occurring due to embankment deformations following construction correspond well to the observations, except for the top portion of slope indicator number 4. The displacement pattern for this indicator suggests that it was struck by construction equipment and that the observed large movement near the top is an artifact.

5-5. Combined Movements Within the Embankment

In order to assess the capability of the approach taken to predict movements due to deformations within the embankment, combined vertical and horizontal movements within the embankment are shown in Figure 5.10. Vectors showing the movements of a few available points are given on the half cross section. The section has been divided into layers according to the locations of the hydraulic settlement gauges. The vertical position of the points correspond to the locations of the slope indicators. The measured movements are plotted with a symbol "x" and the predicted movements are shown by a solid circle. The time span illustrated is that from 8/5/71 to 9/8/71. All movements for the points are referred to the line D-D', at elevation 506.00 feet, which is close to the original ground surface (elevation 504.50 feet). In general, the agreement between predicted and observed movements is considered satisfactory, although there is somewhat more compression occurring along elevation B-B' than predicted.

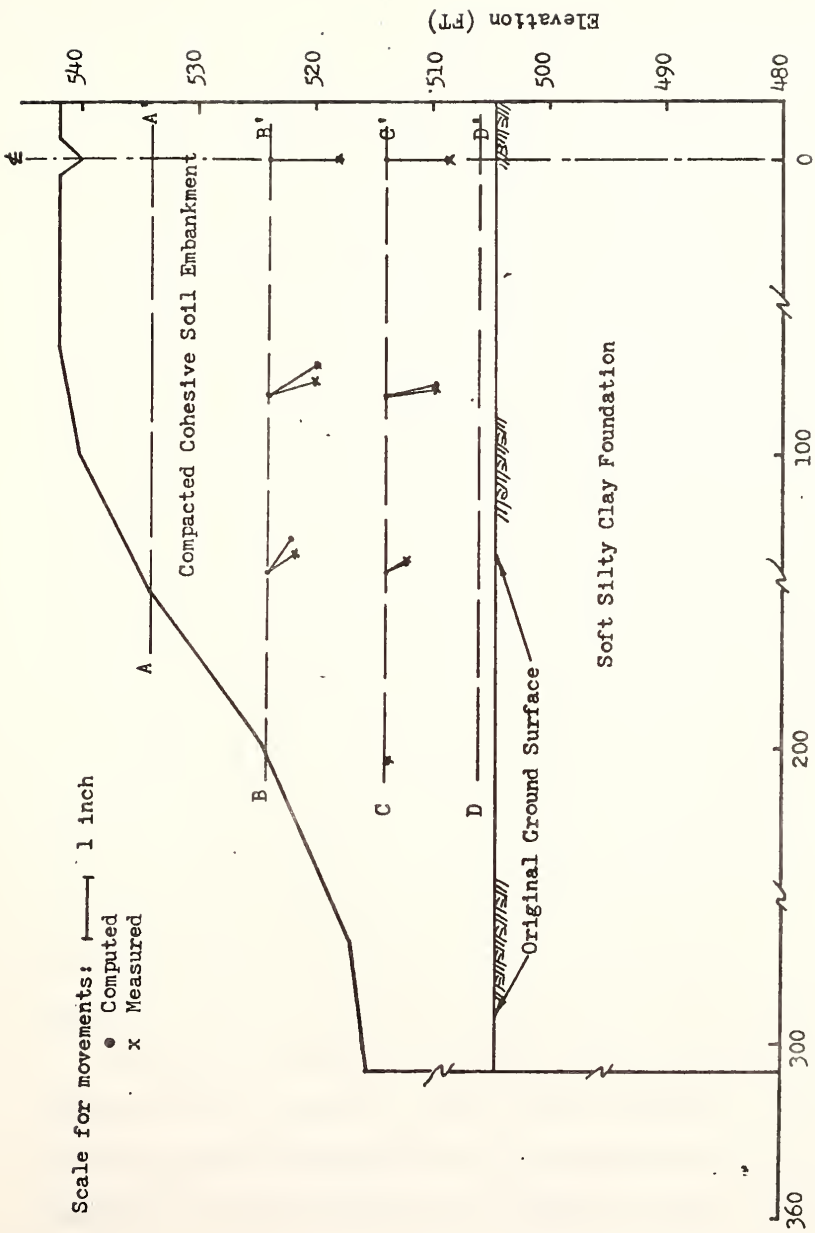


Figure 5.10. Comparison Of Computed And Measured Movements(8/5/71-9/8/71)

CHAPTER VI
SUMMARY, CONCLUSIONS AND RECOMMENDATION

6-1. Summary

The study is concerned with prediction of the long-term deformation of a compacted cohesive soil embankment over a soft foundation. The prediction of embankment performance was made using the finite element method of analysis incorporating a nonlinear viscoelastic model of the fill behavior and a quasi-elastic representation of the foundation. A full-scale test embankment was constructed and instrumented to permit evaluation of the predictive approach. Samples of the subsurface and the embankment material were tested in the laboratory to determine numerical values of desired material parameters. The performance of the test embankment was monitored both during and after its construction.

Instrumentation included spiral-foot settlement gauges, slope indicators and total pressure plates. These functioned satisfactorily, and the measurements obtained were of sufficient accuracy except for a few instruments. Hydraulic settlement gauges were also used. They have many advantageous features, but these were outweighed by the temperature sensitivity which was a significant problem during cold weather.

The observed results were compared with the theoretical predictions. Variations from the predicted behavior were interpreted in light of the relation between the assumptions of the analysis and the real field conditions. Primary emphasis was on predicting those movements

resulting from long-term deformations of the compacted clay fill. The calculated results are fairly close to the field measurements.

6-2. Conclusion

On the basis of the analysis and observations of performance as described herein, the following conclusions are drawn:

(1) Field instruments can be used to monitor performance of earth structures with acceptable accuracy. As found by many others, simple instrumentation is desirable for field use. However, as we experienced, the pressure plates near the center line of the embankment along the original ground surface functioned not satisfactorily and over-registered about 50%. The readings of hydraulic settlement gauges were limited to summer and fall, due to large temperature fluctuations during the winter season.

(2) The nonlinear viscoelastic model for the compacted fill incorporated into the finite element analysis leads to satisfactory prediction of vertical stresses and vertical and horizontal displacements within the embankment except the horizontal movements at the upper part of the embankment. Horizontal stresses near the center line at elevations close to the original ground surface were underpredicted probably due to wetting of the embankment soil in this area by the elevated ground water table.

(3) The quasi-elastic model for the saturated foundation clays, combined with one-dimensional consolidation theory, and incorporated into the finite element analysis allowed an adequate accounting of the vertical displacements within the foundation. Horizontal displacements were underestimated, probably due to shearing effects not considered in the analysis.

6-3. Recommendations

Based on the present investigation, the following topics are recommended for further study:

(1) A more comprehensive model for the behavior of saturated clay-including drainage and nonlinear shearing effects, such as that developed by Davidson (1973) should be incorporated into the analysis.

(2) Since the movements of ground water table are important to the embankment performance, a modified model to include effects of wetting from the elevated ground water table, infiltration etc., should be investigated.

(3) Investigation of the applicability of the model to predict the field behavior of an earth dam is a logical extension of this work.

(4) The most difficult problem for the hydraulic settlement gauges was the effect of temperature fluctuation of the fluid. Because so much information can be gleaned from a continuous settlement profile, an attempt should be made either to control the temperature of the fluid, or to measure the temperature of the instrument while readings are being taken within the embankment.

LIST OF REFERENCES

LIST OF REFERENCES

- Alpan, I., (1961), "The Dissipation Function for Unsaturated Soils," Proceedings, Fifth International Conference of Soil Mechanics and Foundation Engineering, Vol. 1, Paris, pp. 3-5.
- Argyris, J. H., (1957), "The Matrix Theory of Statics," Ingenieur-Archiv, Vol. 25.
- Andresen, A., and Simons, N. E., (1960), "Norwegian Triaxial Equipment and Technique," Proceedings, ASCE Research Conference on Shear Strength of Soils, Boulder, Colorado, pp. 695-709.
- Barden, L., (1965), "Consolidation of Compacted and Unsaturated Clays," Geotechnique, Vol. 15, No. 3, pp. 267-286.
- Barden, L., and McDermott, R. J. W., (1965), "Use of Free Ends in Triaxial Testing of Clays," Journal of the Soil Mechanics and Foundations Division, ASCE, Vol. 91, No. SM6, November 1965.
- Bell, J. M., (1965), "Stress-Strain Characteristics of Cohesionless Granular Materials Subjected to Statically Applied Homogeneous Loads in an Open System," Ph.D. Dissertation, California Institute of Technology.
- Biot, M. A., (1941), "General Theory of Three Dimensional Consolidation," Journal of Applied Physics, Vol. 12, pp. 155-163.
- Biot, M. A., (1956), "General Solutions of the Equations of Elasticity and Consolidation for a Porous Material," Transaction, ASCE, Journal of Applied Mechanics, Vol. 23, No. 1, 1956, pp. 91-96.
- Biot, M. A., and Willis, D. G., (1957), "The Elastic Coefficients of the Theory of Consolidation," Transactions, ASCE, Journal of Applied Mechanics, Vol. 24, No. 4, 1957, pp. 594-601.
- Bishop, A. W., (1966), "The Strength of Soils as Engineering Materials," Geotechnique, 16, pp. 91-128, June 1966.
- Bishop, A. W., and Green, G. E., (1965), "The Influence of End Restraint on the Compression Strength of a Cohesionless Soil," Geotechnique, Vol. 15, No. 3, pp. 243-266.
- Bishop, A. W., and Henkel, D. J., (1962), The Measurement of Soil Properties in the Triaxial Test, Edwin Arnold, London.

- Blight, G. E., (1965), "Shear Stress and Pore Pressure in Triaxial Testing," Journal of the Soil Mechanics and Foundations Division, ASCE, Vol. 91, No. SM6, November, 1965.
- Boehmer, J. W., and Christian, J. T., (1969), "Plane Strain Consolidation by Finite Elements," Report by M.I.T. Dept. of Civil Eng. to U.S. Dept. of Transportation, Washington, D.C.
- Bozozuk, M., (1968), "The Spiral-foot Settlement Gauge," Canadian Geotechnical Journal, Vol. V., No. 2.
- Bozozuk, M., (1969), "A Fluid Settlement Gauge," Canadian Geotechnical Journal, Vol. VI, No. 3.
- Brown, C.B., and King, I.P., (1966), "Automatic Embankment Analysis: Equilibrium and Instability Conditions," Geotechnique, Vol. 16, No.3, 1966.
- Brooker, E.W., and Ireland, H.O., (1965), "Earth Pressure at Rest Related to Stress History," Canadian Geo. J., Vol. 2, No. 1, pp. 1-15.
- Casagrande, A., and Wilson, S.D., (1951), "Effect of Rate of Loading on Strength of Clays and Shales at Constant Water Content," Geotech., Vol. II, No. 3., June 1951.
- Chen, Y. N., (1970), "A Study of the Load-Sinkage Relationship of a Rectangular Loaded Area on Soft Soils Using the Finite Element Method," MS Thesis, Purdue University, West Lafayette, Indiana.
- Christian, J.T., and Boehmer, J.W., (1970), "Plane Strain Consolidation by Finite Elements," Journal of the Soil Mechanics and Foundations Div., ASCE, Vol. 96, No. SM4, pp.1435-1457.
- Christensen, R. W. and Wu, T.H., (1964), "Analysis of Clay Deformation as a Rate Process," Journal of Soil Mechanics and Found. Division, ASCE, Vol. 90, No. SM6, pp. 125-157.
- Clough, R. W., (1960), "The Finite Element Method in Plane Stress Analysis," 2nd Conference on Electronic Computation, ASCE.
- Clough, R. W., and Woodward, R. J., (1967), "Analysis of Embankment Stresses and Deformations," Journal SMFD, ASCE, July 1967.
- Costantino, C.J., (1968), "Stress Waves in Layered Arbitrary Media," Report No. SAMSO TR 68-181, for Space and Missile Systems Organization, Norton Air Force Base, California.
- Coulomb, C.A., (1776), "Essai sur une Application des Regles de Maximis et Minimis a quelques Problemes Relatifs a l'Architecture," Memoirs de l'Academie des Sciences, Savants Etrangers, Vol. 7, p. 343, Paris.
- Crawford, C.B., (1963), "Pore Pressure Within Soil Specimens in Triaxial Compression," ASTM Special Technical Publication No. 361, Sept. 1963.

- Davidson, J. L., (1973), "Effects of Quasi-Preconsolidation on Long Term Settlements," Ph.D. Thesis, Purdue University, West Lafayette, Indiana.
- DeGroof, W. L., (1973), "Compacted Cohesive Test Embankment-Design, Installation and Operation of Field Instrumentation," Progress Report, Joint Highway Research Project, Project: C-36-5F, File: 6-6-6, Purdue University, Lafayette, Indiana.
- Desai, C. S., and Abel, J. F., (1972), "Introduction to the Finite Element Method," Reinhold Company, New York, 1972.
- Drucker, D. C., Gibson, R. E., and Henkel, D. J., (1957), "Soil Mechanics and Work-Hardening Theories of Plasticity," Transactions ASCE, No. 122.
- Duncan, J. M., Monismith, C. L., and Wilson, E. L., (1968), "Finite Element Analysis of Pavements," Highway Research Record No. 228.
- Duncan, J. M., and Dunlop, P., (1968), "The Significance of Cap and Base Restraint," Journal of Soil Mechanics and Foundations Division, ASCE, Vol. 94, No. SMI, pp. 271-290.
- Duncan, J. M., and Dunlop, P., (1969), "Slopes in Stiff-Fissured Clays and Shales," Journal SMFD, ASCE, March 1969.
- Finn, W. D. L., (1967), "Static and Dynamic Behavior of an Earth Dam," Canadian Geotechnique Journal, Vol. 4, No. 1, 1967.
- Folque, J., (1961), "Rheological Properties of Compacted Unsaturated Soils," Proceedings of the Fifth International Conference on Soil Mechanics and Foundation Engineering, Vol. I, p. 113.
- Girijavallabhan, C. V., and Reese, L. C., (1968), "Finite-Element Method for Problems in Soil Mechanics," Journal SMFD, ASCE, March 1968.
- Glasstone, S., Laidler, K., and Zyring, H., (1941), "The Theory of Rate Process," McGraw-Hill Book Co., Inc., New York.
- Habib, M. P., (1953), "Influence de la Variation de la Contrainte Principale Moyenne sur la Resistance au Cisaillement des Sols," Proceedings, Third International Conference on Soil Mechanics, Vol. 1.
- Haythornthwaite, R. W., (1960), "Mechanics of the Triaxial Test for Soils," Proceedings, ASCE, SMFD, Vol 86, No. SM5, pp. 35-61.
- Hvorslev, M. J., (1936), "Conditions of Failure for Remolded Cohesive Soil," Proceedings of the First International Conference on Soil Mechanics and Foundation Engineering, Vol. III, pp. 51-53.
- Hvorslev, M. J., (1937), "Ueber die Festigkeitseigenschaften gestorter bindiger Boden," (On the Strength Properties of Remolded Cohesive Soils), Thesis, 159 pages, published by Danmarks Naturvidenskabelige samfund, Ingeniorvidenskabelige Skrifter, Series A, Nr. 45, Copenhagen.

Hvorslev, M. J., (1960), "Physical Components of the Shear Strength of Saturated Clays," Proc. ASCE Research Conf. on Shear Strength of Cohesive Soils, Boulder, 1960.

Januskevicius, C. K., and Vey, E., (1965), "Stresses and Strains in Triaxial Specimens Using Embedded Gauges," ASTM Special Technical Publication No. 392.

Jones, R. E., (1964), "A Generalization of The Direct-Stiffness Method of Structural Analysis," Journal of the A.I.A.A., Vol. 2.

Kirkpatrick, M. W., (1957), "The Condition of Failure for Sands," Proceedings, Fourth International Conference on Soil Mechanics, Vol. 1.

Kirkpatrick, M. W., and Belshaw, D. J., (1968), "On the Interpretation of the Triaxial Test," Geotechnique, Vol. XVIII, No. 3, September 1968.

Ko, H. Y., and Scott, R. F., (1968), "Deformation of Sand at Failure," Journal, SMFD, ASCE, July 1968.

Lambe, T. W., and Whitman, R. V., (1969), "Soil Mechanics," John Wiley & Sons, Inc., New York.

LaraTomas, M., (1962), "Time-Dependent Deformation of Clay Soils Under Shear Stress," Proceedings, First International Conference on the Structural Design of Asphalt Pavements, Ann Arbor, Michigan.

Leonards, G. A., and Altschaeffl, A. G., (1964), "Compressibility of Clay," Journal of the Soil Mechanics and Foundations Division, ASCE, Vol. 90, No. SM5, pp. 133-155. Also Published in Proceedings, Conference on Design of Foundations for Control of Settlement, ASCE, Evanston, Ill. pp. 163-185.

Leonards, G. A., and Ramiah, B. K., (1959), "Time Effects in The Consolidation of Clay," Special Technical Publication No. 254, ASTM pp. 116-130.

Love, A. E. H., (1944), Treatise on the Mathematical Theory of Elasticity, 4th Edition, Dover.

Melosh, R., (1963), "Basis for Derivation of Matrices for the Direct Stiffness Method," Journal of the A.I.A.A., Vol. 1.

Mikhlin, S. G., (1965), "The Problem of the Minimum of a Quadratic Functional," Translated from Russian, Holden-Day.

Mitchell, J. K., (1964), "Shearing Resistance of Soil as a Rate Process," Journal, SMFD, ASCE, Vol. 90, No. SM1, pp. 29-61.

Mitchell, J. K., and Campanella, R. G., (1963), "Creep Studies on Saturated Clays," ASTM Special Technical Publication No. 361, pp. 90-103.

- Mitchell, J. K., Campanella, R. G., and Singh, A., (1968), "Soil Creep as a Rate Process," Journal of Soil Mechanics and Foundations Division, ASCE, Vol. 94, No. SMI, pp. 231-254.
- Mohr, O., (1914), "Abhandlungen aus dem Gebiete der technischen Mechanik," 2nd ed., pp. 192-235, Wilhelm Ernst & Son KG, Berlin.
- Murayama, S., and Shibata, T., (1961), "Rheological Properties of Clays," Proceedings, Fifth International Conference on Soil Mechanics and Foundation Engineering, Paris, Vol. 1, pp. 269-273.
- Newmark, N. M., (1960), "Failure Hypotheses for Soils," Res. Conf. Shear Strength of Cohesive Soils, ASCE.
- Oden, J. T., (1967), "Numerical Formulation of Nonlinear Elasticity Problems," Journal of the Structural Division, ASCE, June 1967.
- Oliveira, E. R., (1968), "Theoretical Foundations of the Finite Element Method," Int. J. Solids Structures, October 1968.
- Osterberg, J. O., and Perloff, W. H., Jr., (1960), "Stress-Strain Characteristics of Compacted Clay Under Varied Rates of Strain," Proceedings of the Highway Research Board, Vol. 39, p. 605.
- Pagen, C. A., and Jagannath, B. N., (1967), "Evaluation of Soil Compaction by Rheological Techniques," Highway Research Record 177, Highway Research Board, pp. 22-42.
- Pagen, C. A., and Jagannath, B. N., (1968), "Mechanical Properties of Compacted Soils," Highway Research Record 235, Highway Research Board, pp. 12-26.
- Parker, H. W., and Miller, D. G., (1970), "Operation Manual for Model A Anteus Back Pressure Consolidometers," Internal Report, Lehigh University.
- Parry, R. H. G., (1960), "Triaxial Compression and Extension Tests on Remolded Saturated Clays," Geotechnique, Vol. 10, 1960.
- Peltier, M. R., (1957), "Recherches Experimentales sur-la Courbe Intrinsique de Rupture des Sols Pulverulents," Proceedings, Fourth International Conference on Soil Mechanics, Vol. 1.
- Perloff, W. H., (1965), "Study of Long-Term Deformation of Compacted Cohesive Soils," Research Project EES 260, First Quarterly Report, Transportation Engineering Center, The Ohio State University.
- Perloff, W. H., (1966), "Study of Long Term Deformation of Compacted Cohesive Soil Embankments," Plan of Study, Joint Highway Research Project, Project No. C-36-5F, File No. 6-6-6, Purdue University, Lafayette, Indiana.

- Perloff, W. H., (1974), "Pressure Distribution and Settlement," Chapter 4 in Foundation Engineering Handbook, edited by H. F. Winterkorn and H. Y. Fong, Van Nostrand, New York.
- Perloff, W. H., Baladi, G. Y., and Harr, M. E., (1967), "Stress Distribution Within and Under Long Elastic Embankments," Highway Research Record 181, Highway Research Board, Washington, D. C.
- Perloff, W. H., and Pombo, L. E., (1969), "End Restraint Effects in the Triaxial Test," Proceedings, Seventh-International Conference on Soil Mechanics and Foundation Engineering, Mexico, pp. 327-334.
- Przemieniecki, J. S., (1968), "Theory of Matrix Structural Analysis," McGraw-Hill, New York.
- Ramaswamy, S. V., (1971), "Creep of Compacted Clays," Ph.D. Thesis, Purdue University, West Lafayette, Indiana.
- Roscoe, K. H., and Burland, J. B., (1968), "On the Generalized Stress-Strain Behavior of 'Wet' Clay," from Engineering Plasticity, Papers for a Conference held in Cambridge, March, 1968, Cambridge University Press, 1968.
- Roscoe, K. H., Schofield, A. N., and Thurairajah, A. C., (1963), "An Evaluation of Test Data for Selecting a Yield Criterion for Soils," ASTM Special Technical Publication 361, Ottawa, pp. 111-128.
- Rowe, P. W., and Barden, L., (1964), "Importance of Free Ends in Triaxial Testing," Journal of the Soil Mechanics and Foundations Division, ASCE, Vol. 90, No. SMI, pp. 1-28.
- Samsioe, A. F., (1936), "Report on the Investigation of the Compressibility of the Ground of the Hydro-Electric Power Plant Svir 3," Proceedings, First Internat. Conf. on Soil Mech. and Found. Engineering, Vol. 1, pp. 41-47.
- Sankaran, K. S., (1966), "Time Dependent Deformation of Partially Saturated Cohesive Soils," Unpublished Ph.D. Thesis, Indian Institute of Technology, Madras, India.
- Schapery, R. A., (1966), "A Theory of Non-Linear Thermoviscoelasticity Based on Irreversible Thermodynamics," Proceedings, Fifth U. S. National Congress of Applied Mechanics, ASME, pp. 511-530.
- Schapery, R. A., (1969), "Further Development of a Thermodynamic Constitutive Theory: Stress Formulation," A&ES Report No. 69-2, Purdue University, Lafayette, Indiana.
- Seed, H. B., Mitchell, J. K., and Chan, C. K., (1960), "The Strength of Compacted Cohesive Soils," Proceedings, ASCE Research Conference on Shear Strength of Cohesive Soils, Boulder, Colorado, pp. 877-964.

Selig, E. T., (1964), "A Review of Stress and Strain Measurement in Soil," Proceedings, of the Symposium on Soil-Structure Interaction, University of Arizona, Tucson, Arizona, Sept. 1964.

Sherif, M. A., and Koch, D. E., (1970), "Coefficient of Earth Pressure at Rest as Related to Soil Precompression Ratio and Liquid Limit," Highway Research Record No. 323, Highway Research Board, pp. 39-48.

Shockley, W. G., and Ahlvin, R. G., (1960), "Nonuniform Conditions in Triaxial Test Specimens," Proceedings, ASCE Research Conference on Shear Strength of Cohesive Soils, Boulder, Colorado, pp. 341-358.

Sinco, "Instruction Manual-Series 200-B Instrument," The Slope Indicator Co., Seattle, Washington.

Singh, A. and Mitchell, J. K., (1968), "General Stress-Strain Time Function for Soils," Journal of Soil Mechanics and Foundations Division, ASCE, Vol. 94, No. SMI, pp. 21-46.

Soydemir, C. & Schmid, W. E., (1967), "Stress and Displacement Fields in Viscoelastic Soil Media," Proceedings, Third Asian Conference, International Society of Soil Mechanics and Foundation Engineering, Vol. 1, 1967, pp. 312-317.

Soydemir, C., and Schmid, W. E., (1970), "Deformation and Stability of Viscoelastic Soil Media," JSMFD, ASCE, Nov. 1970, pp. 2081-2098.

Tan, T. K., (1961), "Consolidation and Secondary Time Effect of Homogeneous Anisotropic, Saturated Clay Strata," Proceedings, Fifth Conf. Soil Mech., Vol. 1, pp. 367-374.

Taylor, D. W., (1951), "Research on the Shearing Characteristics of Clays," Soil Mechanics Laboratory Report, Massachusetts Institute of Technology.

Terrametrics, (1969), "Instruction Manual - Gloetzl Equipment," Golden, Colorado.

Terzaghi, K., (1923), "Die Berechnung der Durchlässigkeitsziffer des Tones aus dem Verlauf der hydrodynamischen Spannungsercheinungen," Sitzber. Akad. Wiss. Wien, Abt IIa, Vol. 132.

Thorkildsen, R. L., (1964), "Mechanical Behavior," Chapter 5 in Engineering Design for Plastics, Edited by E. Baer, Reinhold, pp. 277-392.

Toriyama, K., and Sawada, T., (1968), "On the Consolidation of Partly Saturated Soils Compacted Wet of Optimum Moisture Content," Soils & Foundations, Vol. 8, No. 3, pp. 62-86.

Tsyrovich, N. A. Z., Ter-Martirosyan, Z. G., and Abelev, M. Y., (1965), "Discussions," Proc. 6th Int. Conf. Soil Mech. and Found. Eng., Vol. 3, pp. 368-370.

Tresca, H., (1868), "Mémoire sur L'Ecoulement des Corps Solids," Mém. Par. Div. Sav., Vol. 18.

Turner, M. J., Clough, R. W., Martin, H. C., and Topp, L. T., (1956), "Stiffness and Deflection Analysis of Complex Structures," Journal, Aerospace Science, 23, September 1956.

Vainberg, M. M., (1964), "Variational Methods for the Study of Nonlinear Operators," Translated from Russian, Holden-Day.

Von Mises, R., (1913), "Mechanik der festen Korper in plastisch deformablen Zustand," Gottinger Nachrichten, Math. Phys. Kl.

Walker, L. K., (1969), Discussion on "General Stress-Strain Time Function for Soils," Journal of Soil Mechanics and Foundations Division, ASCE, Vol. 95, No. SM 1, pp. 409-415.

Wang, C. T., (1953), Applied Elasticity, McGraw-Hill Book Company, Inc., New York.

Westmann, R. A., (1968), "Stress Analysis by Finite Elements," Highway Research Record No. 228.

Wilson, E. L., (1965), "Structural Analysis of Axisymmetric Solids," AIAA Journal, Vol. 3, No. 12, December 1965.

Wilson, E. L., (1967), "Analysis of Axisymmetric Solids," Computer Programming Series, University of California, February 1967.

Wu, T. H., Loh, A. K., and Malvern, L. E., (1963), "Study of Failure Envelope of Soils," Journal of the SMFD, ASCE February 1963.

Yoshimi, Y., and Osterberg, J. O., (1963), "Compression of Partially Saturated Soils," Journal of Soil Mechanics and Foundations Division, ASCE, Vol. 89, No. SM 4, pp.1-24.

Zienkiewicz, O. C., (1971), "The Finite Element Method in Engineering Science," McGraw-Hill, London.

Zienkiewicz, O. C., and Cheung, Y. K., (1965), "Finite Elements in the Solution of Field Problems," The Engineer, London, September, 1965.

Zienkiewicz, O. C., and Cheung, Y. K., (1967), The Finite Element Method in Structural and Continuum Mechanics, McGraw-Hill Publishing Company Limited.

Zienkiewicz, O. C., and Holister, G. H., (Editors), (1965), Stress Analysis, John Wiley & Sons.

APPENDICES

The several detailed and lengthy Appendices of this Report indicated in the Table of Contents are not included in this copy of the Report because of their length and lack of value to many.

A copy of the Appendix or Appendices desired will be supplied upon request from a recipient of this Report. Please state which Appendix or Appendices are desired.

| <u>Appendix</u> | <u>Title</u> | <u>No. of Pages</u> |
|-----------------|--|---------------------|
| A | Finite Element Computer Program | 16 |
| B | Mesh Plotter | 11 |
| C | Computer Program for Evaluating Lateral Movement | 3 |
| D | Creep Test Data | 11 |
| E | Consolidation Test Data | 1 |
| F | Field Records of Exploratory Borings | 9 |
| G-1 | Total Pressure Plates | 27 |
| G-2 | Spiral-Foot Settlement Gauges | 12 |
| G-3 | Slope Indicators | 69 |

COVER DESIGN BY ALDO GIORGINI